SUPPORTING INFORMATION

Generation of new sipanmycin analogues by combinatorial biosynthesis and mutasynthesis approaches relying on the substrate flexibility of key enzymes in the biosynthetic pathway.

Mónica G. Malmierca,[a,b,c] Ignacio Pérez-Victoria,[d] Jesús Martín,[d] Fernando Reyes,[d] Carmen Méndez,[a,b,c] José A. Salas,[a,b,c] and Carlos Olano,[a,b,c#]

[a] Departamento de Biología Funcional, Universidad de Oviedo, Oviedo (Asturias), Spain.

[b] Instituto Universitario de Oncología del Principado de Asturias (I.U.O.P.A), Universidad de Oviedo, Oviedo (Asturias), Spain.

[c] Instituto de Investigación Sanitaria del Principado de Asturias (ISPA), Oviedo, Spain

[d] Fundación MEDINA, Parque Tecnológico de Ciencias de la Salud, Granada, Spain

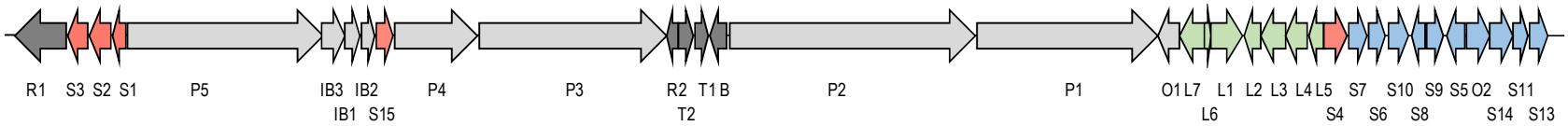

1. Starter unit biosynthesis pathway

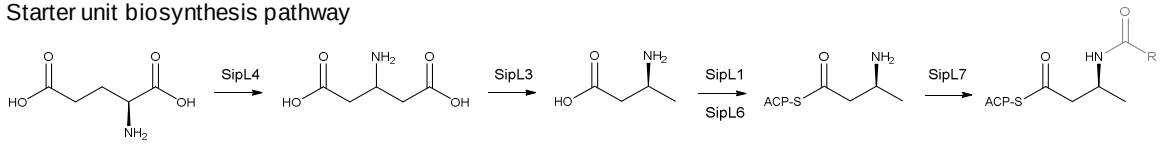

2. UDP-D-xylosamine biosynthesis pathway

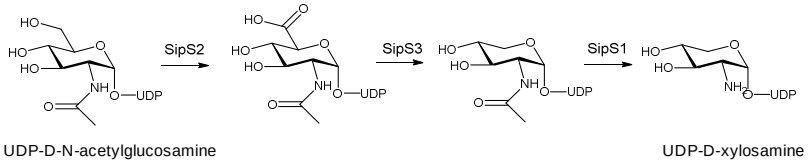

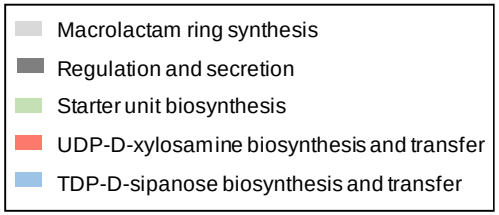

3. TPD-D-sipanose biosynthesis pathway

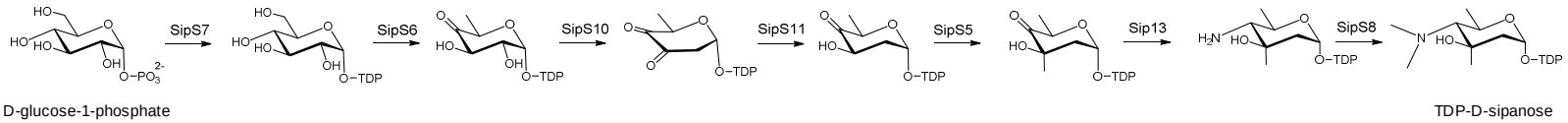

4. Glycosylation of macrolactam

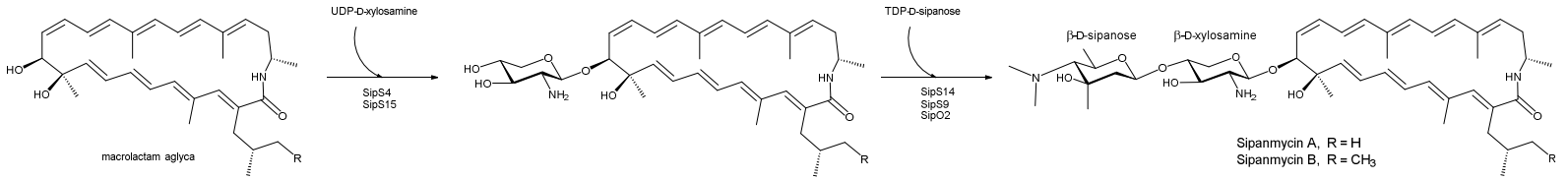

Fig. S1. Sipanmycin biosynthesis gene cluster. Biosynthetic pathways important for the understanding of this work are included. For more detailed information regarding the assembly of the macrolactam, please refer to Malmierca et al., 2018 [1].

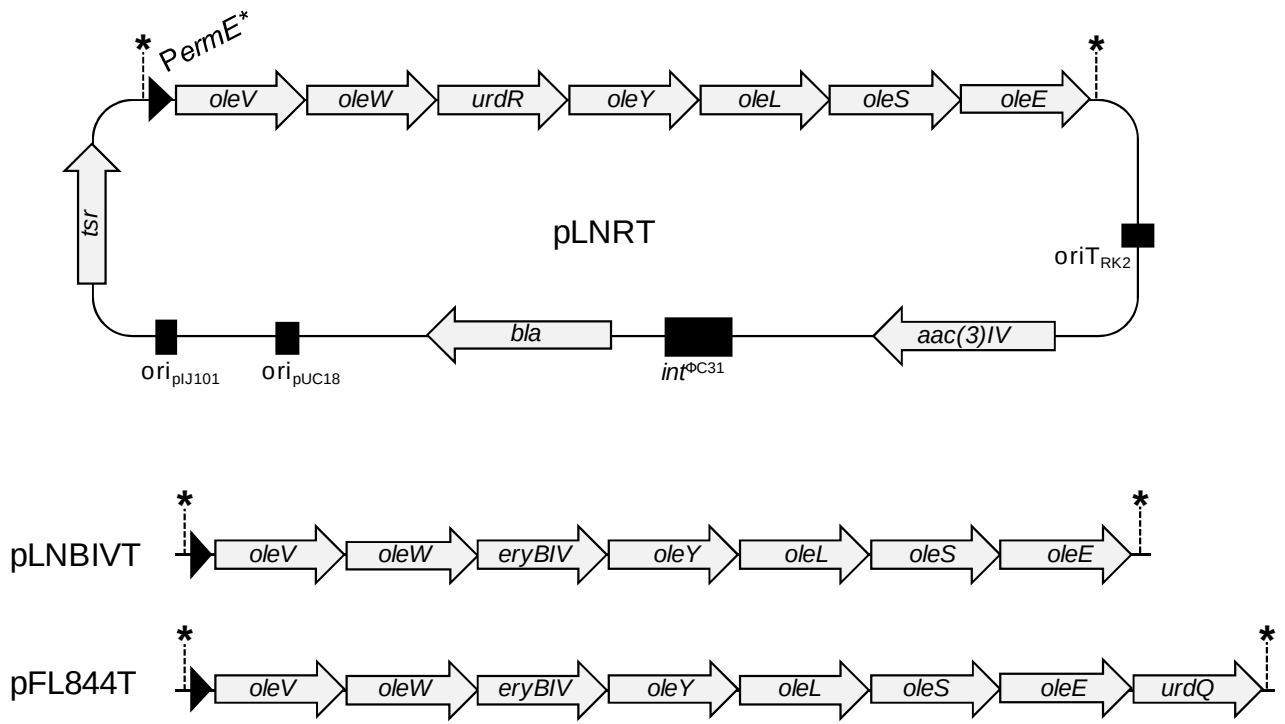

Fig. S2. Plasmids used in combinatorial biosynthesis experiments. pLNRT is completely represented. pLNBIV and pFL844 only differ from pLNRT in the region between asteriscs [2]. Backbone: *tsr*, thiostrepton resistance gene; *bla*, β-lactamase gene; *aac(3)IV*, apramycin resistance cassette; P*ermE**, promoter of the erythromycin resistance gene; ori$_{pIJ101}$, origin of replication of plasmid pIJ101; ori$_{pUC18}$, origin of replication of plasmid pUC18; *int*$^{\Phi C31}$, ΦC31 integrase; oriT$_{RK2}$, origin of transfer of plasmid RK2. Sugar biosynthetic genes: *oleV* (2,3-dehydratase), *oleW* (3-ketoreductase), *oleY* (3-O-methyltransferase), *oleL* (3,5-epimerase), *oleS* (synthase) and *oleE* (4,6-dehydratase) from the oleandomycin producer *Streptomyces antibioticus*; *urdR* (4-ketoreductase) and *urdQ* (3,4-dehydratase from the urdamycin A producer *Streptomyces fradiae*; *eryBIV* (4-ketoreductase) from the erythromycin producer *Saccharopolyspora erythraea.*

Structure elucidation of sipanmycin A1 (1).

The molecular formula of **1** was established as $C_{43}H_{64}N_2O_9$ based on the observed ion $[M+H]^+$ at *m/z* 753.4692 (calcd. for $C_{43}H_{65}N_2O_9^+$ = 753.4685, Δm = 0.9 ppm). Such formula confirmed its structural relationship with sipanmycin A (SIP-A) [3]. As expected, the UV (DAD) spectrum of **1** is identical to that of sipanmycins A and B, showing a maximum at 320 nm and a shoulder at 360 nm, due to the presence of the polyene moieties in the macrolactam aglycon [3]. Comparison of the in-source fragment ion at *m/z* = 131.0702 with the corresponding one from SIP-A (*m/z* =172.1332) suggested that **1** and SIP-A just differ in the terminal monosaccharide moiety. Substitution of the native terminal sipanose residue in SIP-A by digitoxose (the monosaccharide encoded by the introduced plasmid pLNBIVT) perfectly accounts for the molecular formula of **1**. Comparison of the NMR data of **1** and SIP-A revealed that the signals of the aglycon and its directly attached xylosamine residue are essentially identical for both compounds. As expected, the characteristic NMR signals of the D-sipanose residue of SIP-A do not appear in the spectra of **1**. Instead, a new set of signals is found which was revealed to correspond to the new terminal desoxysugar. The connectivity (based on COSY, TOCSY and HMBC correlations) and the relative configuration (based on coupling constants and NOE analysis) of this monosaccharide residue was established as the expected digitoxose, with an α anomeric configuration (axial glycosidic linkage). Bearing in mind that the glycosyl transferase pair SipS9/SipS14 acts as an inverting GT (see explanation in the main text of the article), according to Klyne's rule [4] the terminal digitoxose residue has an α-L absolute configuration. The absolute configuration of the D-xylose residue and the chiral centers at positions C-10, C-11 and C-23 in the macrolactam aglycon must be identical to that of SIP-A for obvious biosynthetic reasons [1]. Not surprisingly, for the macrolactam

and the xylosamine residue, the same key NOESY correlations and essentially identical chemical shifts are observed in the spectra of both SIP-A and **1**. Additionally, the only observed NOE correlation between both monosaccharides (H1'' and H4') agrees with the L absolute configuration for the digitoxose residue according to the minimized molecular model of the disaccharyl moiety.

Compound **1** thus corresponds to α-L-digitoxyl-(1→4')-3'-*O*-demethylsilvalactam and was trivially designated as sipanmycin A1 (SIP-A1).

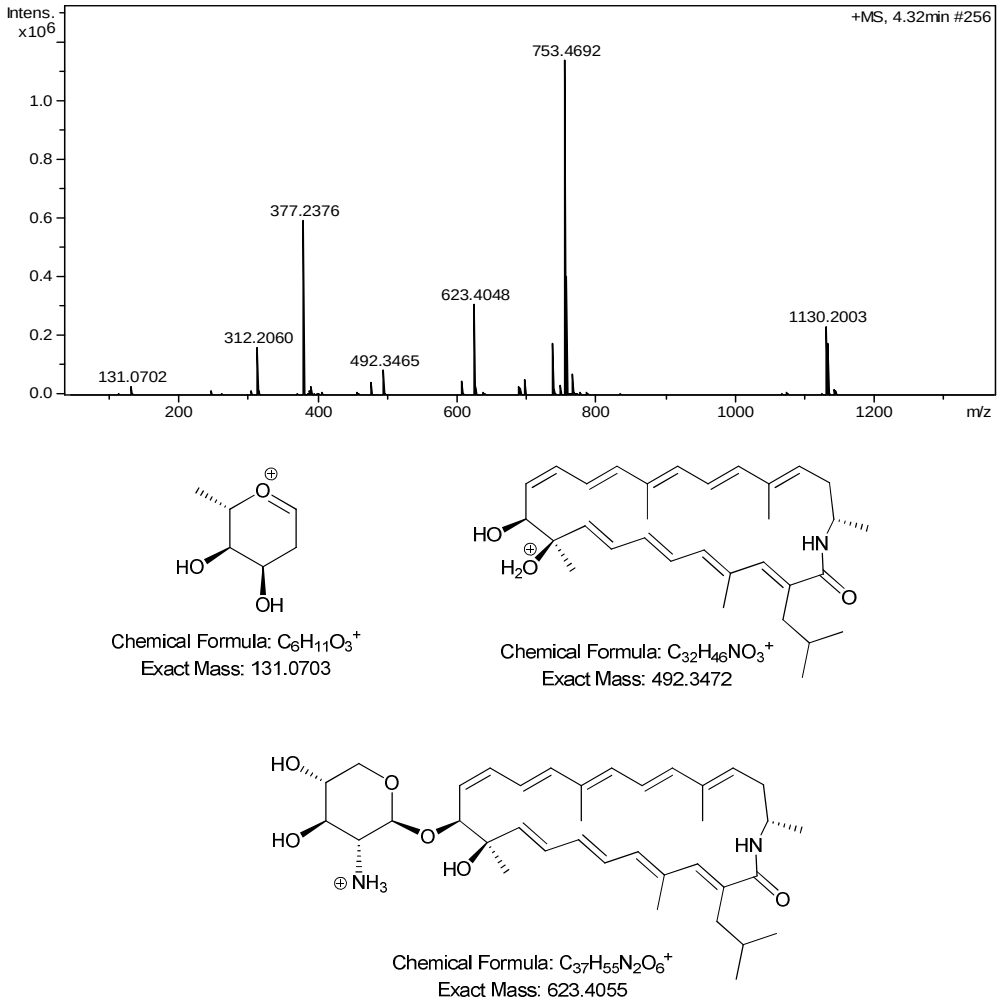

Fig. S3. HRMS spectrum of SIP-A1 (**1**) and identification of the key in-source fragment ions.

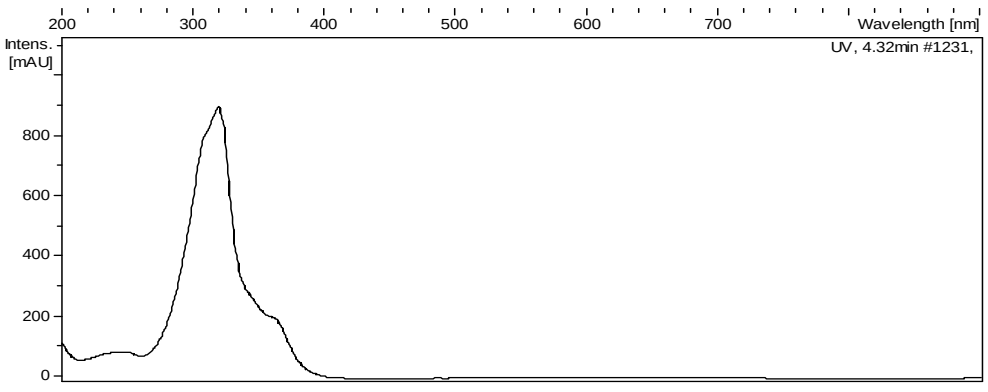

Fig. S4. UV-vis (DAD) spectrum of SIP-A1 (**1**).

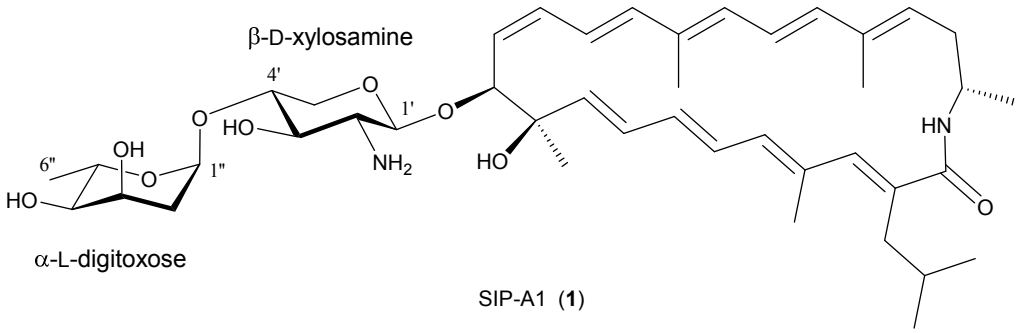

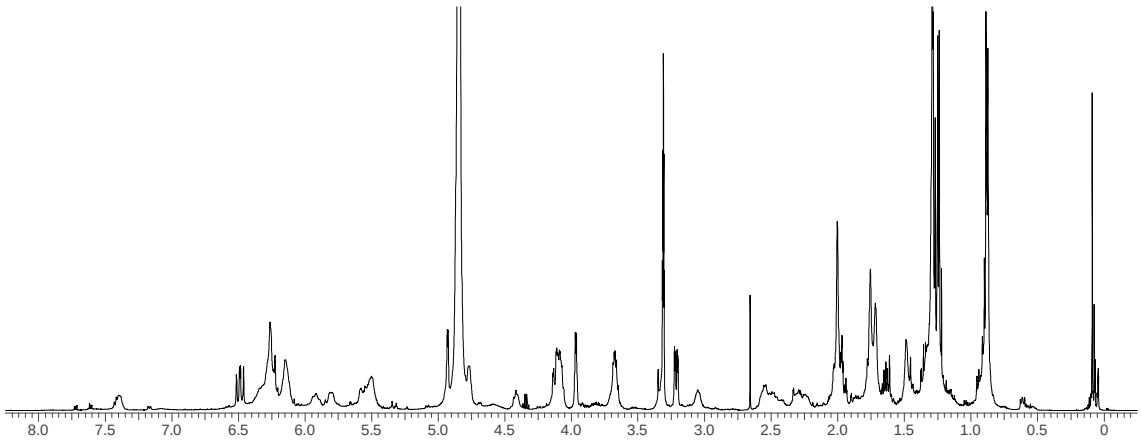

Fig. S5. ^{1}H NMR spectrum (CD_3OD, 500 MHz) of SIP-A1 (**1**).

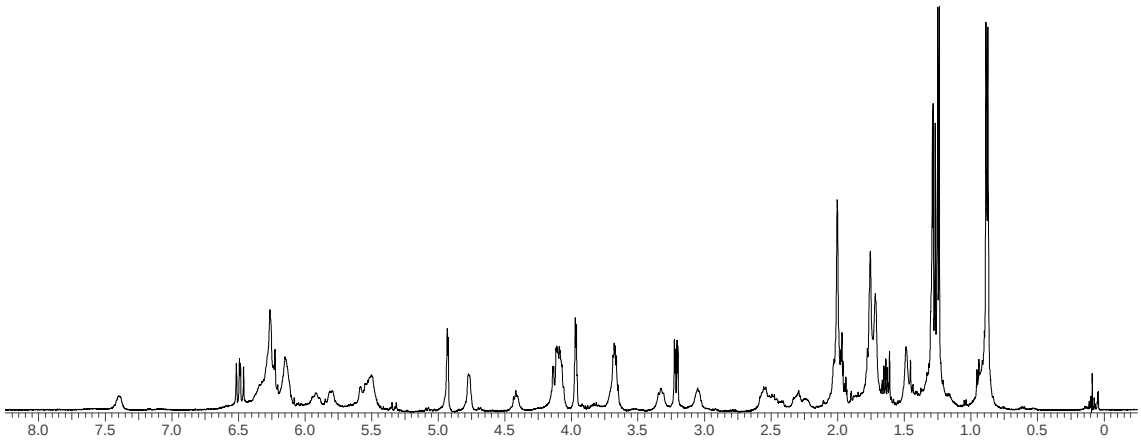

Fig. S6. Diffusion-filtered ^{1}H NMR spectrum of SIP-A1 (**1**).

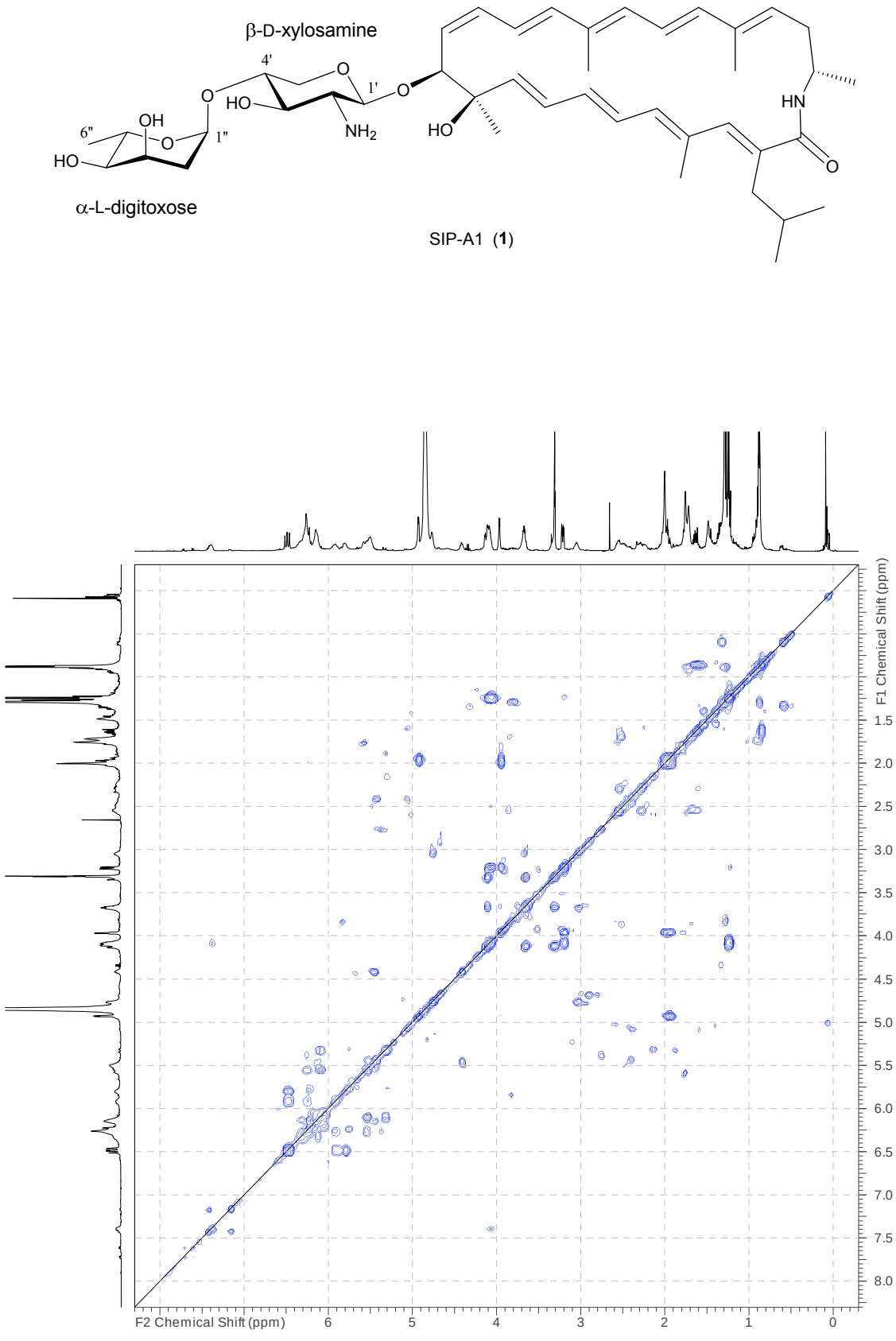

Fig. S7. COSY spectrum of SIP-A1 (**1**).

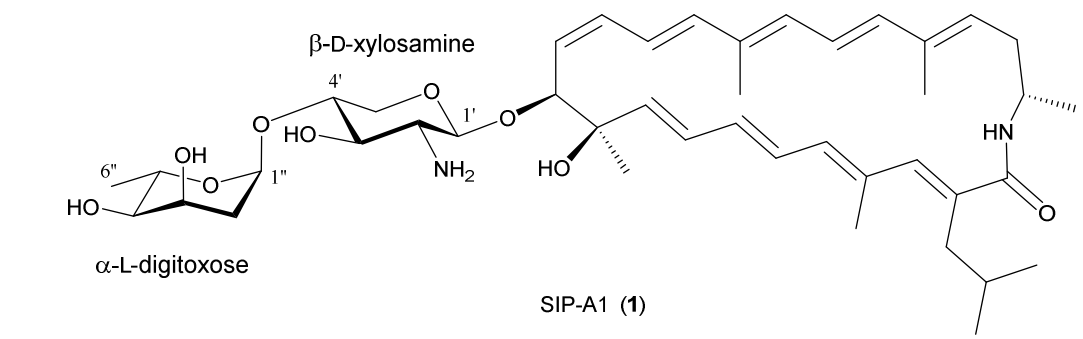

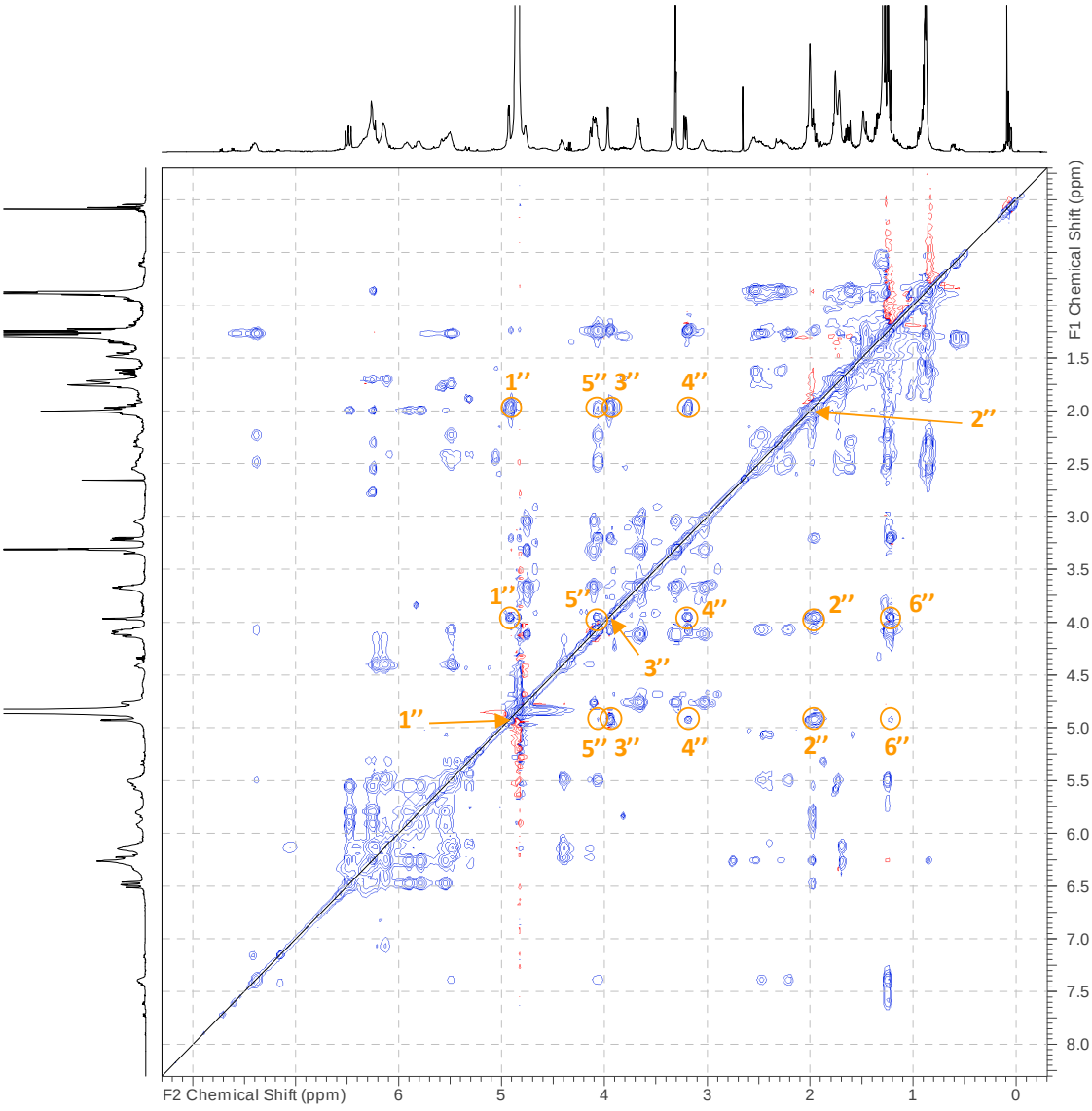

Fig. S8. TOCSY spectrum of SIP-A1 (**1**). Key correlations corresponding to the α-L-digitoxose spin system are highlighted. The corresponding proton signals at the diagonal are indicated by an arrow.

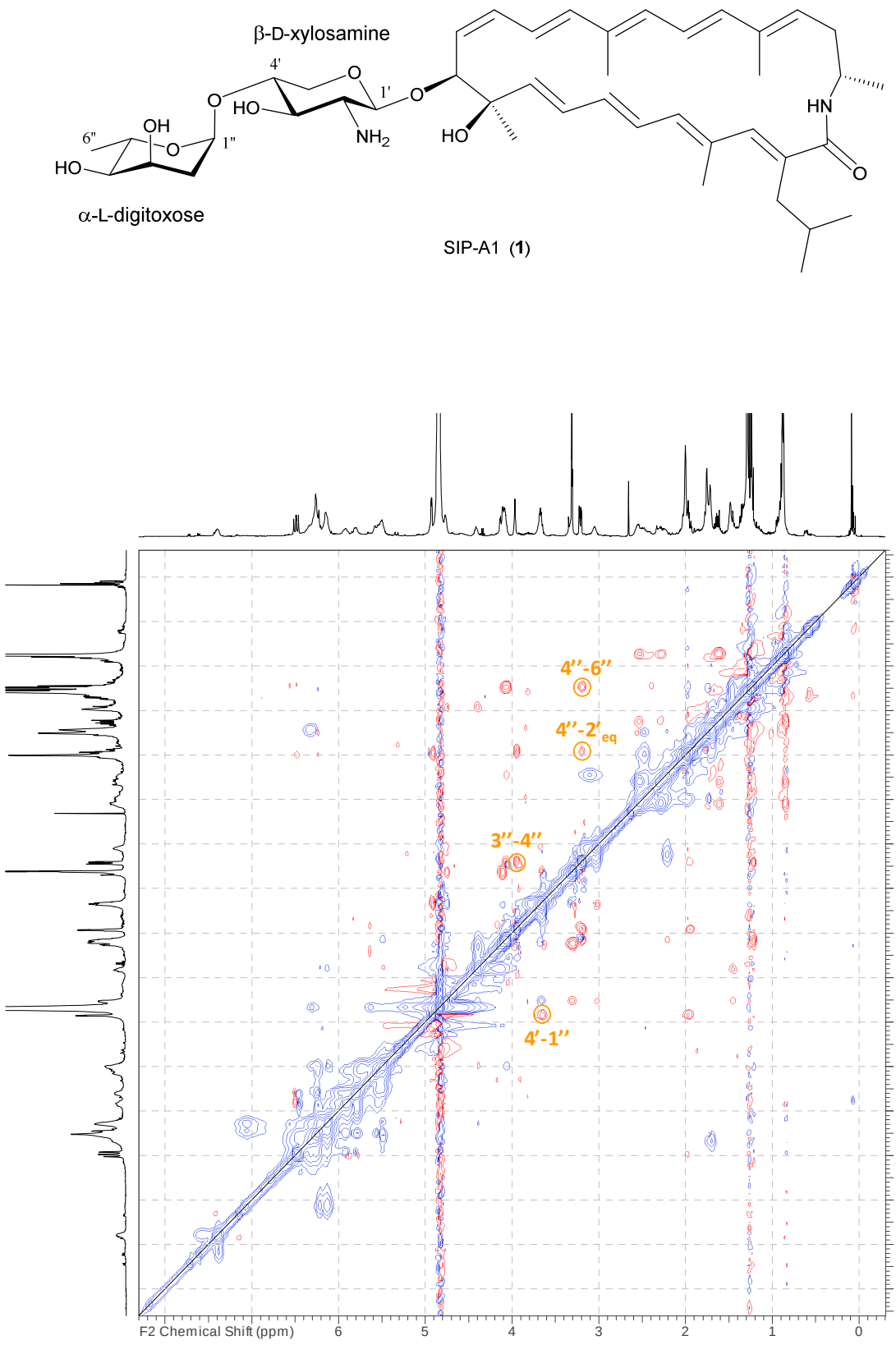

Fig. S9. NOESY spectrum of SIP-A1 (**1**). Key correlations rendering the relative and absolute configuration of the α-L-digitoxose residue are highlighted (first proton in each pair corresponds to F2 dimension and the second proton to the indirect F1 dimension).

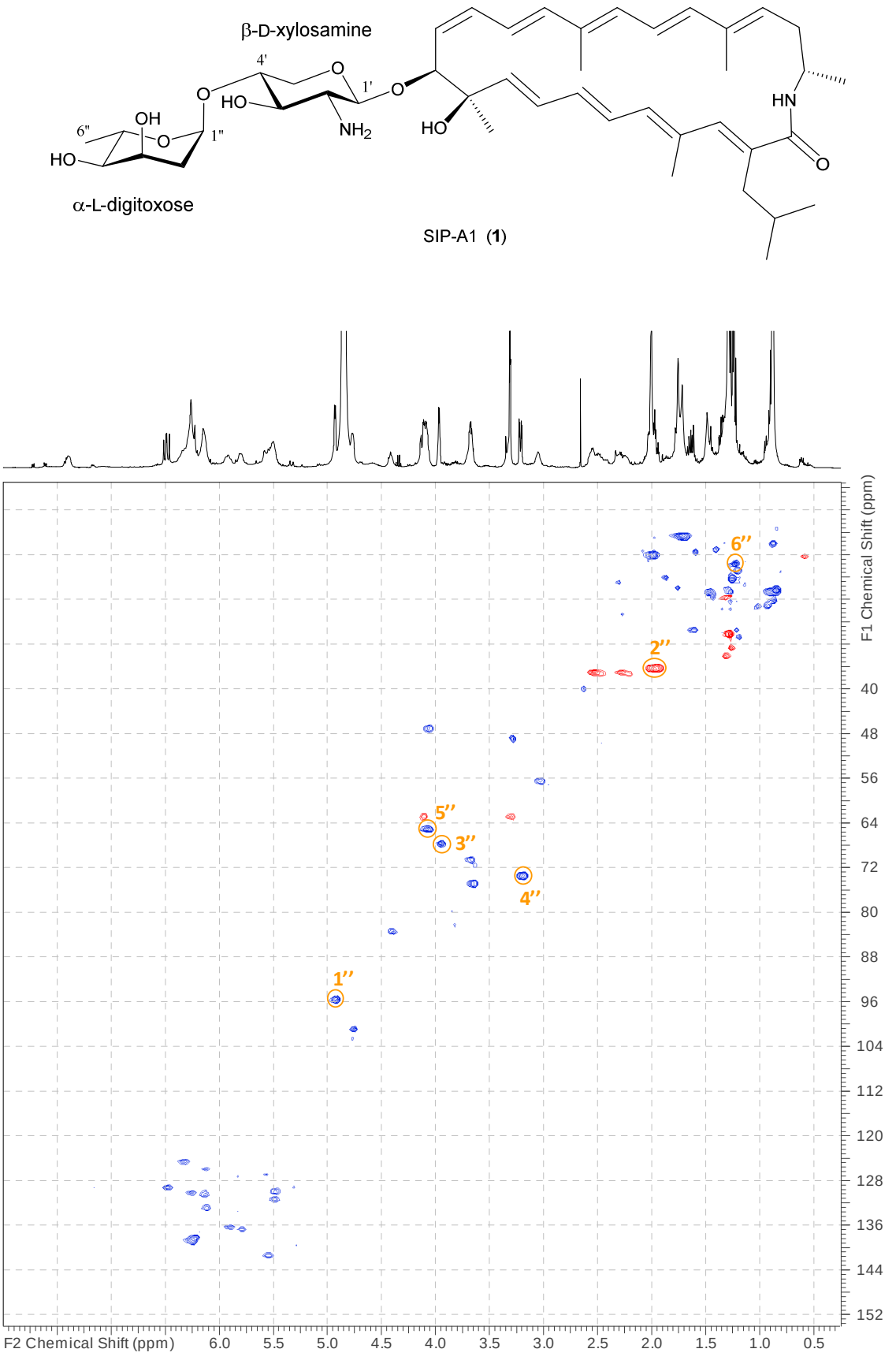

Fig. S10. Edited HSQC spectrum of SIP-A1 (**1**). Key correlations corresponding to the α-L-digitoxose moiety are highlighted.

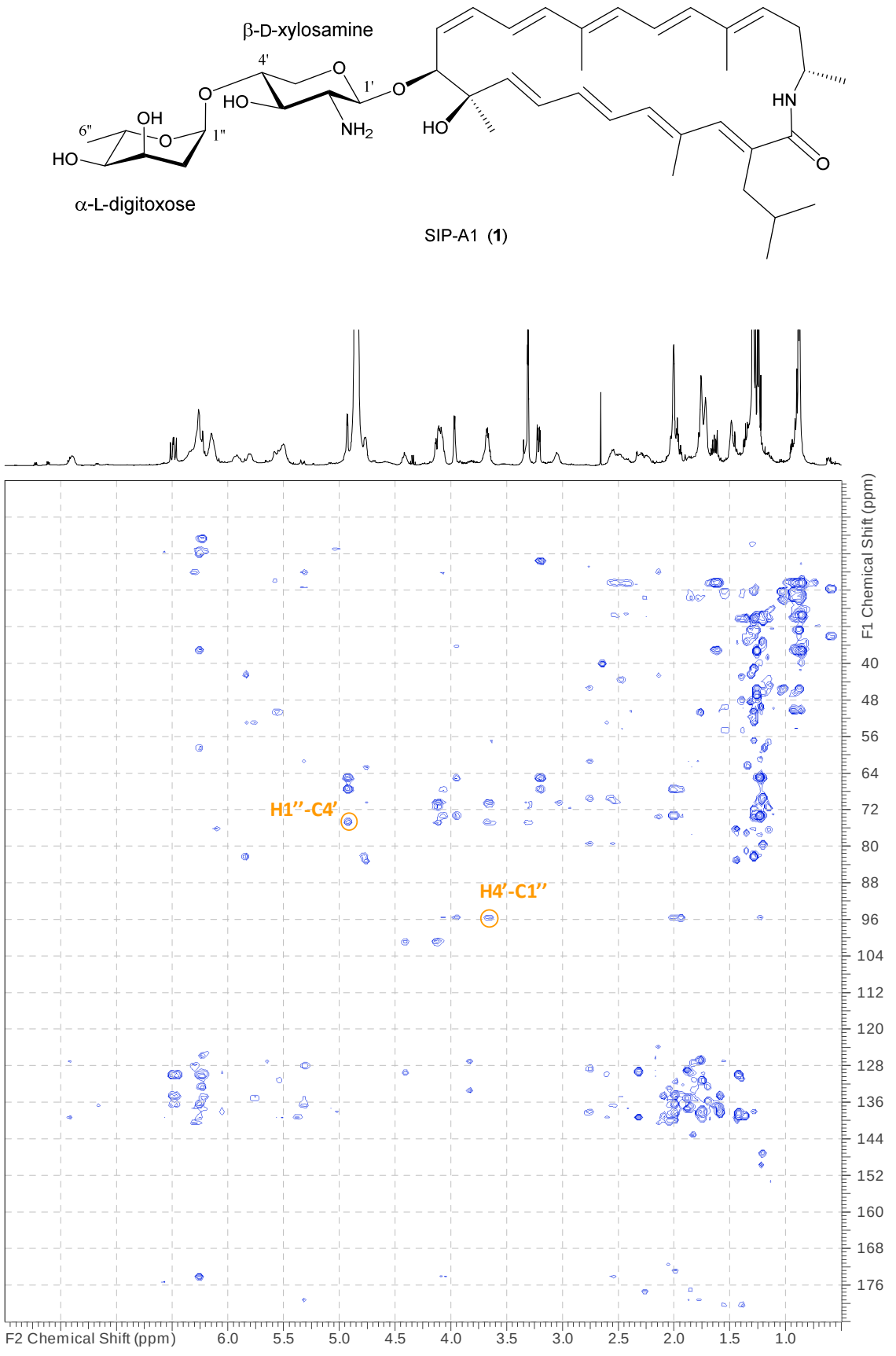

Fig. S11. HMBC spectrum of SIP-A1 (**1**). Key correlations connecting the α-L-digitoxose and β-D-xylosamine moieties are highlighted.

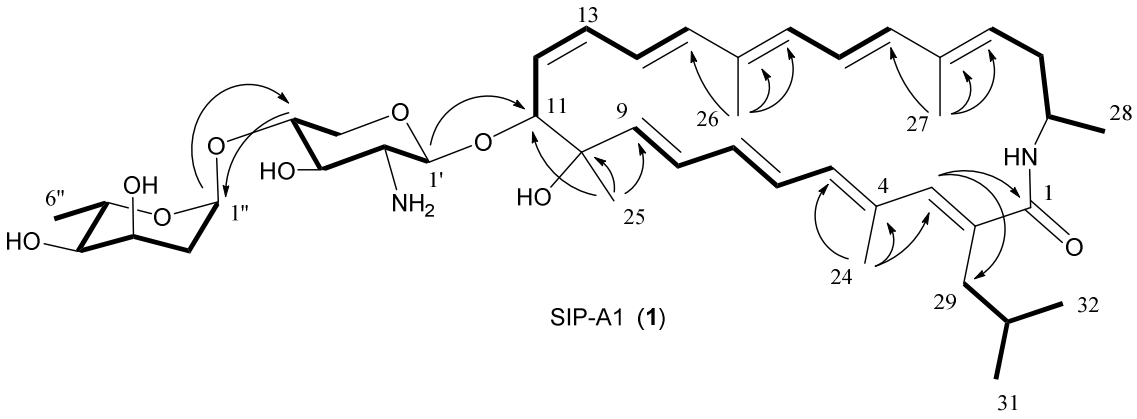

Fig. S12. Gross structure of SIP-A1 (**1**) determined by 2D NMR and comparisons with the NMR data of SIP-A. COSY correlations (further corroborated by the spin systems observed in the TOCSY spectrum) are indicated as bold bonds. Key HMBC correlations connecting independent spin systems are indicated by arrows.

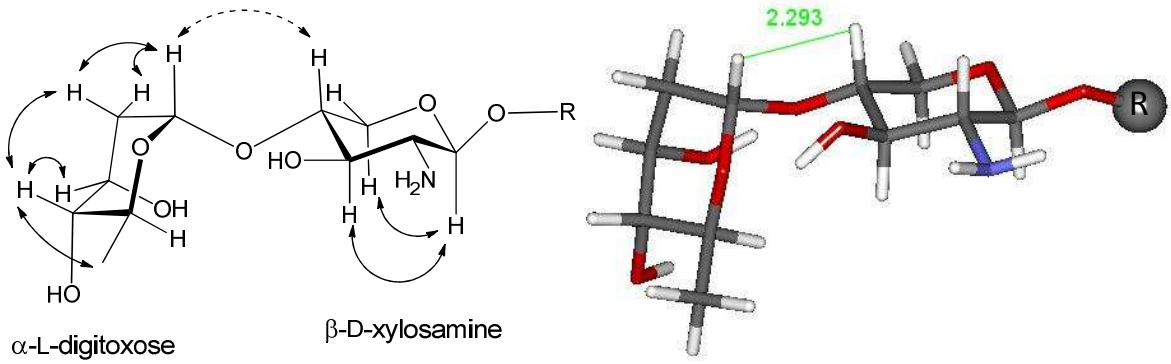

Fig. S13. Key intra-ring NOESY correlations (solid arrows) which, together with the observed coupling constants, allow stablishing the relative configuration of each monosaccharide. There is only one observable inter-ring NOESY correlation (dashed arrow) connecting both monosaccharides in agreement with the L- absolute configuration of the digitoxose residue as reflected by the minimized molecular model and the corresponding interproton distance.

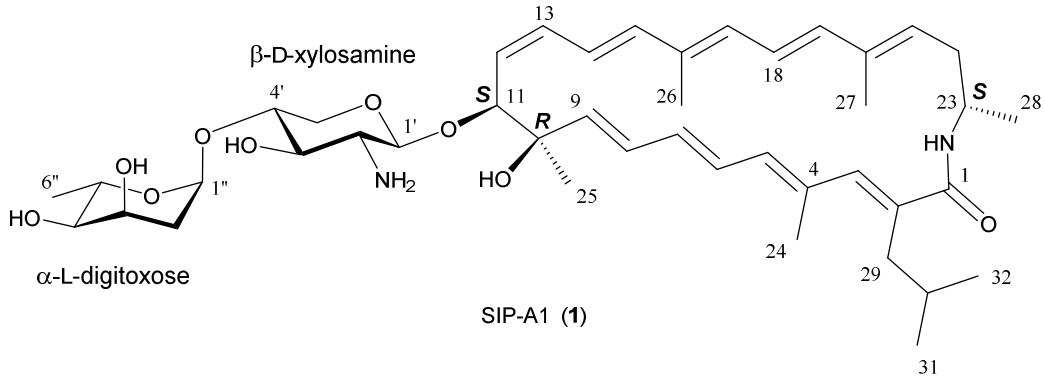

Fig. S14. Structure of SIP-A1 (**1**).

Table S1. ^{1}H and ^{13}C NMR data for SIP-A1 (**1**) in CD_3OD at 24 °C.

Position	δ_C, type	δ_H (*J* in Hz)	Position	δ_C, type	δ_H (*J* in Hz)
1	174.2, C	-	1'	101.0, CH	4.77, br d (ca. 5.7)
2	136.7, C	-	2'	56.6, CH	3.06, br t (ca. 5.7)
3	138.6, CH	6.26, m	3'	70.6, CH	3.65, m
4	134.8, C	-	4'	75.0, CH	3.67, m
5	136.6, CH	5.80, m	5'	62.9, CH_2	4.12, dd (12.2, 3.6) 3.32, m
6	129.2, CH	6.49, dd (15.4, 11.4)	1"	95.8, CH	4.93, br d (3.8)
7	136.2, CH	5.91, br t (11.2)	2"	36.5, CH_2	2.00, m 1.95, dt (14.9, 3.9)
8	130.1, CH	6.27, m	3"	67.7, CH	3.97, ddd (3.1, 3.1, 3.1)
9	141.2, CH	5.56, br d (15.8)	4"	73.5, CH	3.21, dd (9.5, 3.1)
10	76.3, C	-	5"	65.2, CH	4.09, dq (9.4, 6.2)
11	83.5, CH	4.41, m	6"	17.9, CH_3	1.25, d (6.3)
12	129.9, CH	5.49, m			
13	130.3, CH	6.14, m			
14	125.9, CH	6.13, m			
15	138.1, CH	6.24, m			
16	135.8, C	-			
17	132.8, CH	6.14, m			
18	124.5, CH	6.34, m			
19	138.6, CH	6.27, m			
20	137.5, C	-			
21	131.3, CH	5.51, m			
22	37.4, CH_2	2.50, m 2.26, m			
23	47.2, CH	4.08, m			
24	16.2, CH_3	2.00, br s			
25	22.9, CH_3	1.49, br s			
26	12.8, CH_3	1.72, br s			
27	12.8, CH_3	1.76, br s			
28	20.6, CH_3	1.28, d (6.9)			
29	37.2, CH_2	2.56, m 2.31, m			
30	29.5, CH	1.64, m			
31	22.5, CH_3	0.88, d (6.4)			
32	22.5, CH_3	0.88, d (6.4)			
1-NH	-	7.40 br s*			

^{13}C chemical shifts obtained from HSQC and HMBC spectra.

* The amide proton exchanges very slowly and can be observed in the spectra.

Structure elucidation of sipanmycin B1 (2).

The molecular formula of **2** was established as $C_{44}H_{66}N_2O_9$ based on the observed ion [M+H]+ at *m/z* 767.4832 (calcd. for $C_{44}H_{67}N_2O_9$+ = 767.4841, Δm = 1.2 ppm). As found for the molecular formula difference between sipanmycins A and B, compound **2** also contains one carbon atom and two hydrogen atoms more than SIP-A1 (**1**), suggesting it should correspond to the expected congener of SIP-A1 having a 2-methyl-1-butyl group rather than an isobutyl group as aliphatic substituent at C-2. As expected, its UV (DAD) spectrum is also identical to that of SIP-A1. The key in-source fragment ion at *m/z* = 131.0701, found also in SIP-A1, supports that **2** contains the same terminal digitoxose monosaccharide residue. Comparison of the NMR data of **2** with those of SIP-A1 and sipanmycin B (SIP-B) reveals that **2** and SIP-A1 share the same disaccharide moiety while the macrolactam aglycon of **2** and SIP-B are, as expected, identical. For obvious biosynthetic reasons, the absolute configuration the carbohydrate units in **2** is the same as found in SIP-A1, while the chiral centers of the aglycon share the same absolute configuration reported for SIP-B [1, 3].

Compound **2** was trivially designated as sipanmycin B1 (SIP-B1).

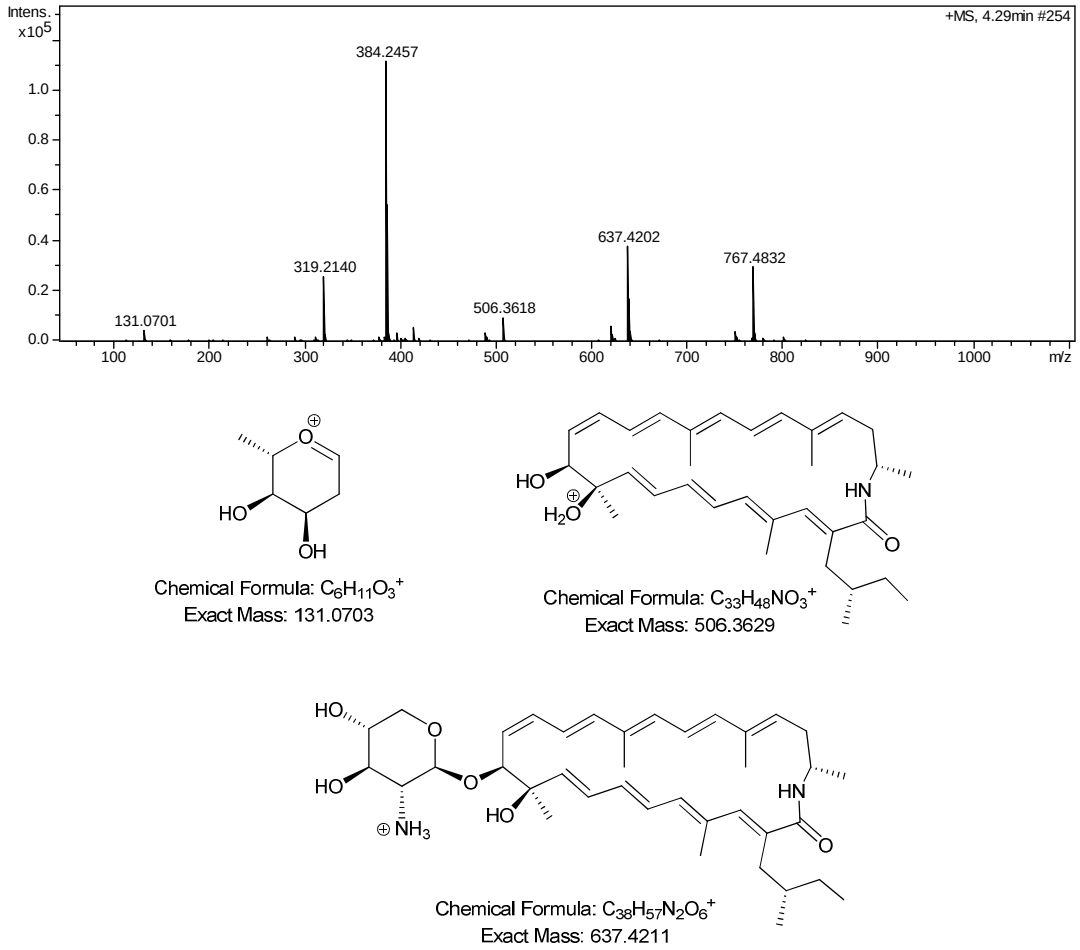

Fig. S15. HRMS spectrum of SIP-B1 (**2**) and identification of the key in-source fragment ions.

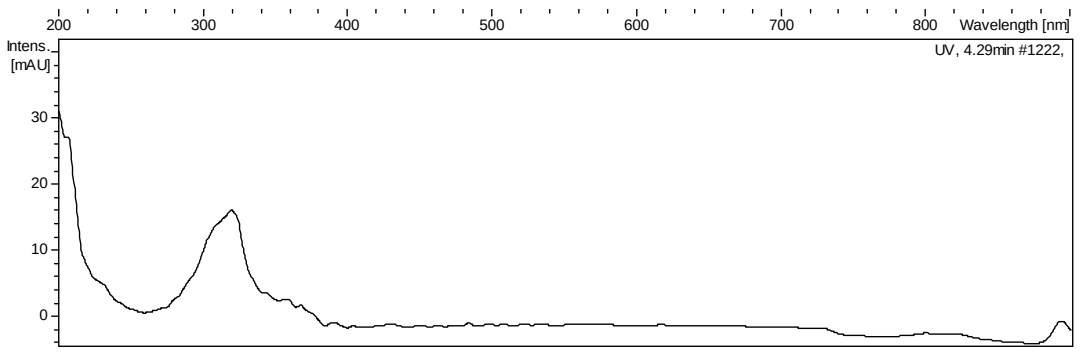

Fig. S16. UV-vis (DAD) spectrum of SIP-B1 (**2**).

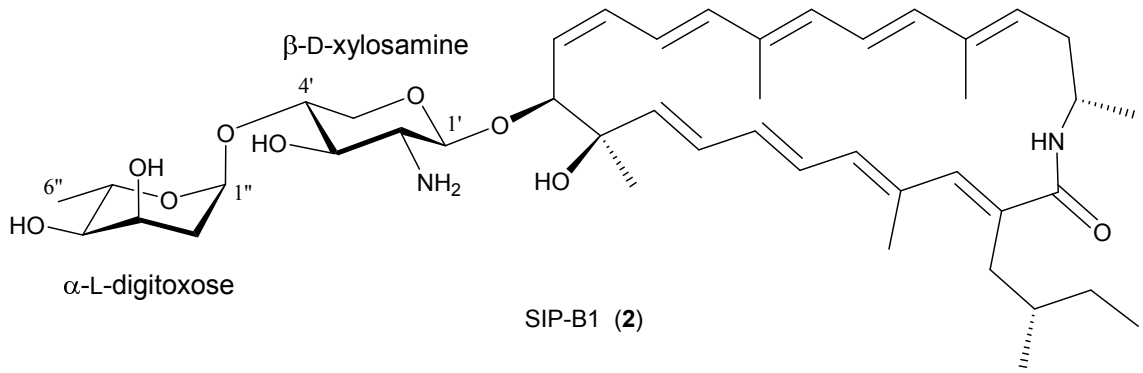

SIP-B1 (**2**)

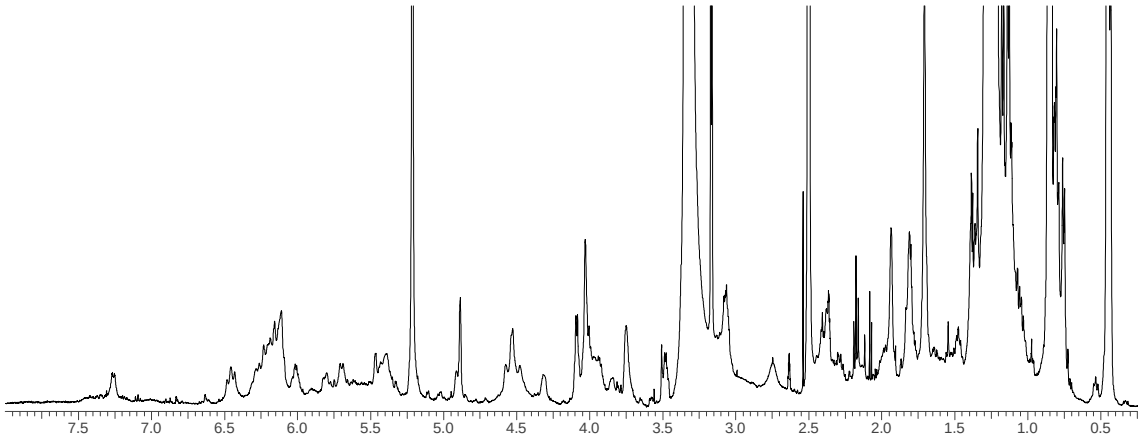

Fig. S17. ^{1}H NMR spectrum (DMSO-d_6, 500 MHz) of SIP-B1 (**2**).

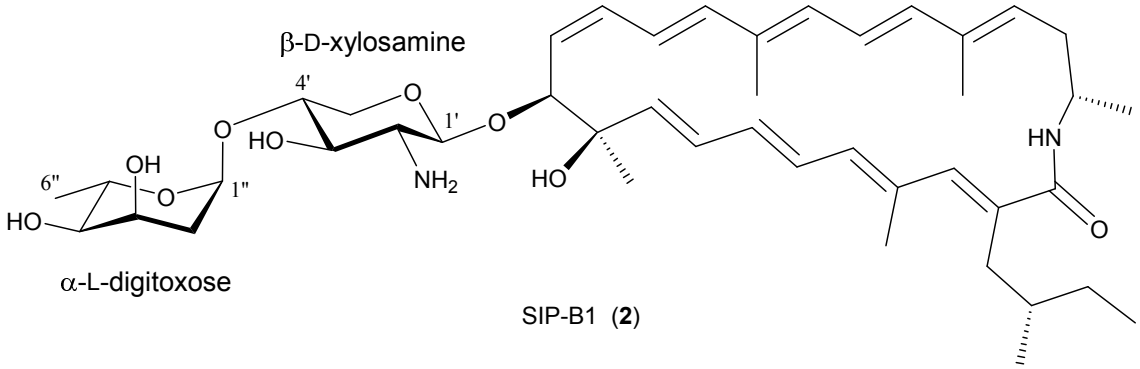

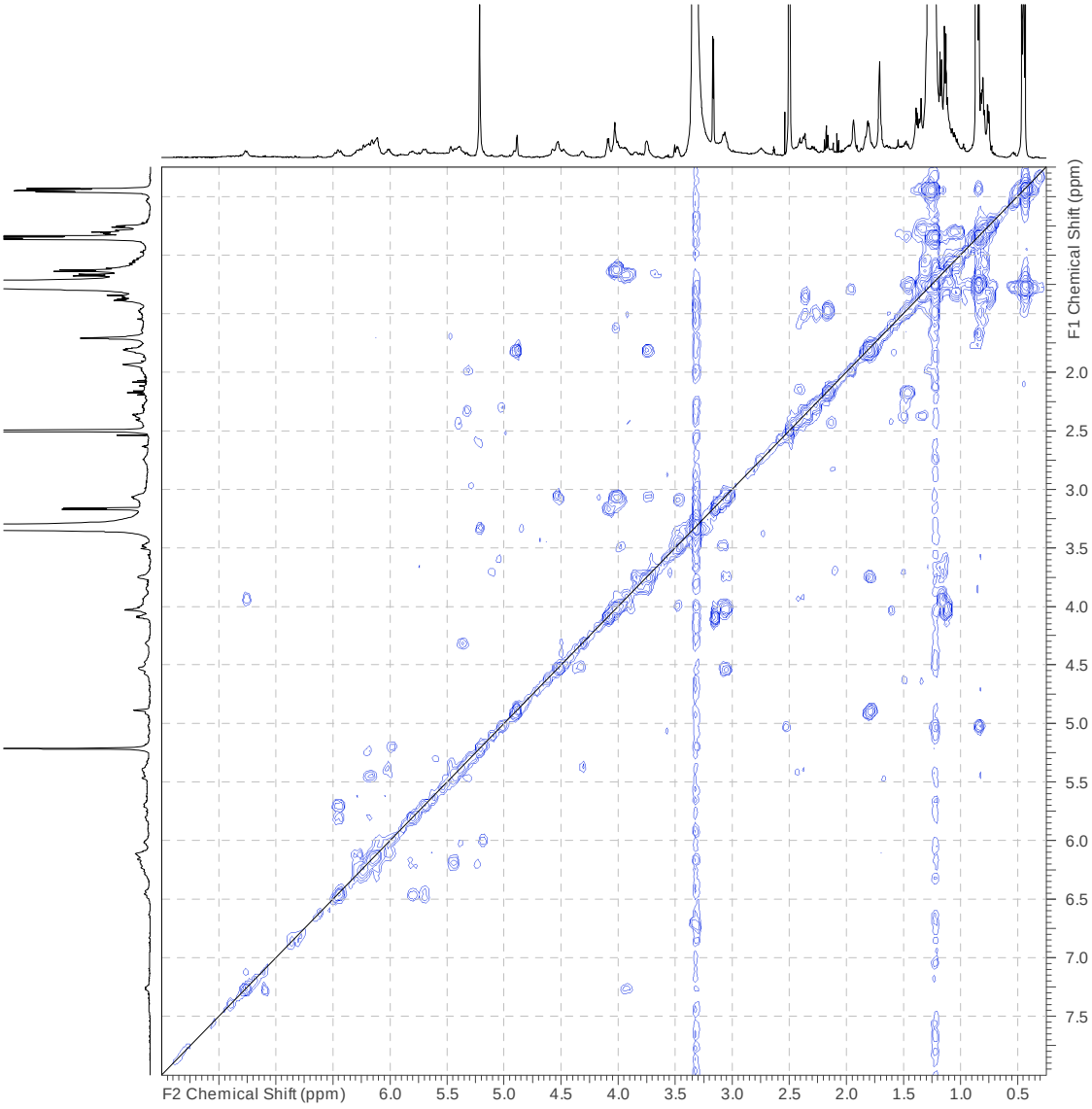

Fig. S18. COSY spectrum of SIP-B1 (**2**).

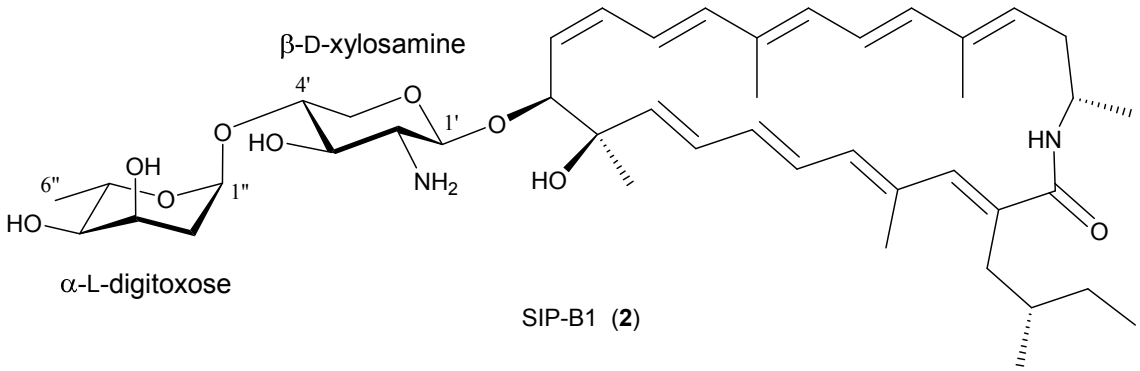

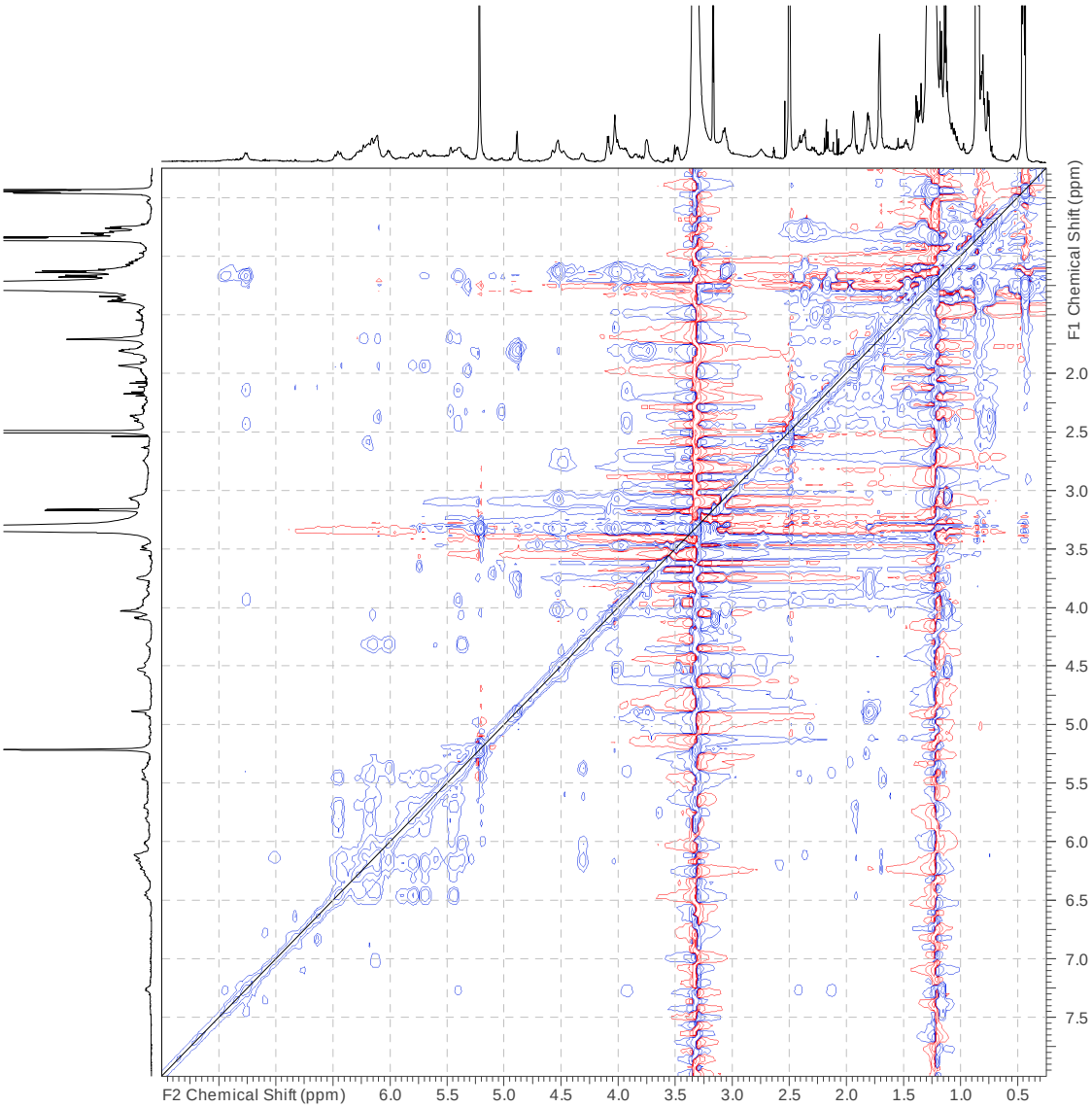

Fig. S19. TOCSY spectrum of SIP-B1 (**2**).

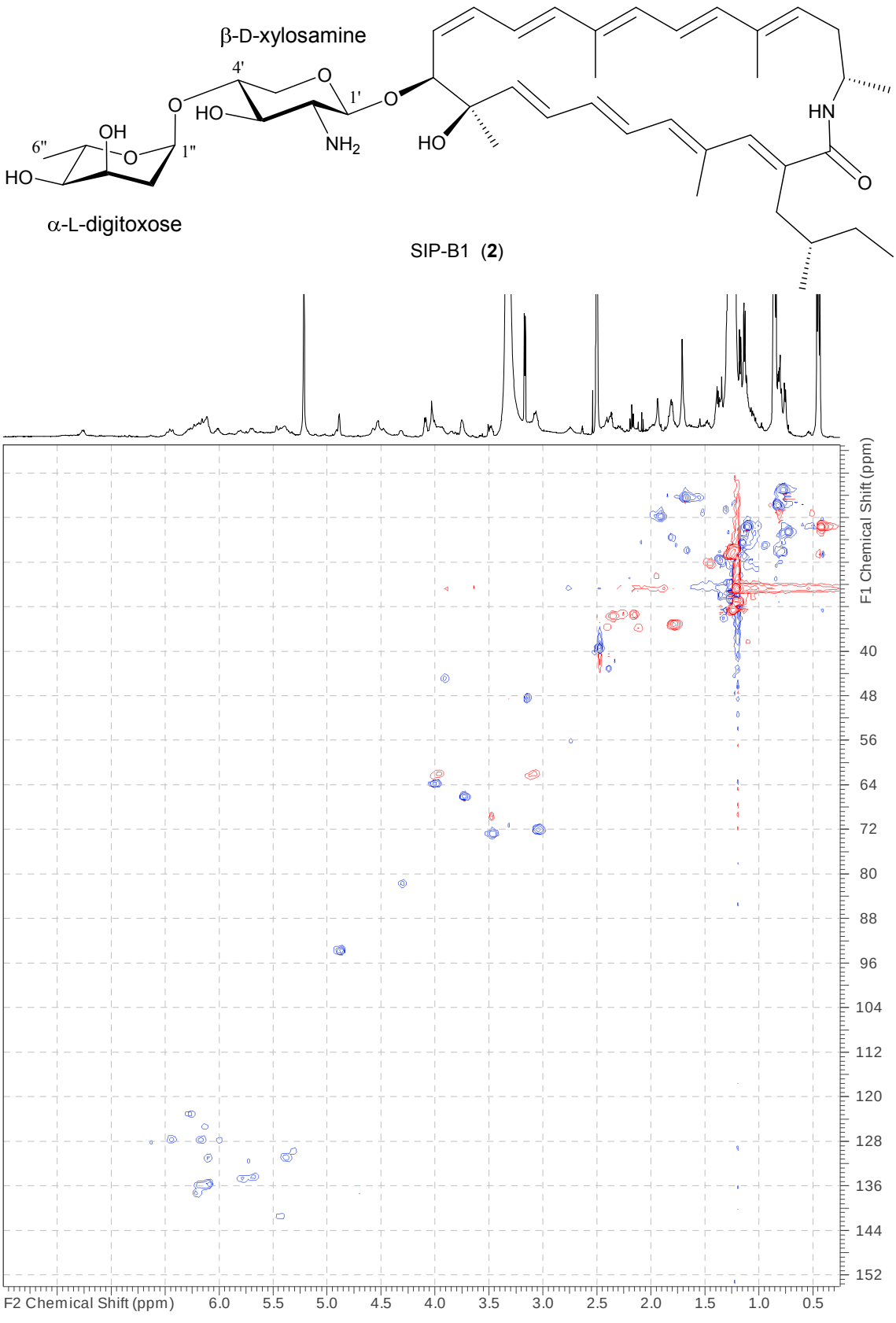

Fig. S20. Edited HSQC spectrum of SIP-B1 (**2**).

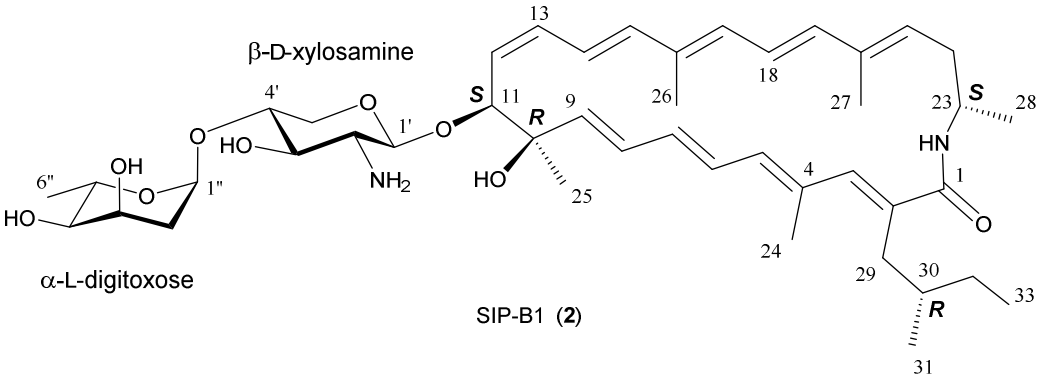

Fig. S21. Structure of SIP-B1 (**2**).

Table S2. ^{1}H and ^{13}C NMR data for SIP-B1 (**2**) in DMSO-d_6 at 24 °C.

Position	δ_C, type	δ_H (*J* in Hz)	Position	δ_C, type	δ_H (*J* in Hz)
1	n.d., C	-	1'	n. d., CH	n. d., m
2	n.d., C	-	2'	56.6, CH	2.76, m
3	137.8, CH	6.22, m	3'	n. d., CH	n. d.
4	n. d., C	-	4'	73.6, CH	3.50, m
5	134.9, CH	5.70, m	5'	62.9, CH_2	4.00, m 3.12, m
6	128.2, CH	6.46, br t (13.0)	1"	94.4, CH	4.89, m
7	135.3, CH	5.80, m	2"	36.1, CH_2	1.82, m
8	128.2, CH	6.19, m	3"	66.8, CH	3.75, m
9	142.0, CH	5.45, m	4"	72.8, CH	3.06, m
10	n. d., C	-	5"	64.6, CH	4.02, m
11	82.3, CH	4.32, m	6"	18.5, CH_3	1.13, d (6.4)
12	130.2, CH	5.33, m			
13	128.3, CH	6.02, m			
14	125.8, CH	6.15, m			
15	136.1, CH	6.13, m			
16	n. d., C	-			
17	131.5, CH	6.12, m			
18	123.5, CH	6.29, m			
19	136.3, CH	6.17, m			
20	n. d., C	-			
21	131.3, CH	5.40, m			
22	34.4, CH_2	2.37, m 2.17, m			
23	45.5, CH	3.92, m			
24	16.4, CH_3	1.94, br s			
25	24.2, CH_3	1.39, br s			
26	13.1, CH_3	1.71, br s			
27	13.1, CH_3	1.71, br s			
28	21.2, CH_3	1.17, d (6.6)			
29	34.4, CH_2	2.37, m 2.17, m			
30	34.8, CH	1.35, m			
31	19.3, CH_3	0.76, d (6.5)			
32	31.8, CH_2	1.22, m			
33	11.7, CH_3	0.80, m			
1-NH	-	7.26 br s			

^{13}C chemical shifts obtained from HSQC spectra.

Structure elucidation of sipanmycin A2 (3).

The molecular formula of **3** was established as $C_{43}H_{64}N_2O_9$ based on the observed ion $[M+H]^+$ at *m/z* 753.4692 (calcd. for $C_{43}H_{65}N_2O_9^+$ = 753.4685, Δm = 0.9 ppm). Such formula confirmed its structural relationship with sipanmycin A (SIP-A) [3]. Likewise, its UV (DAD) spectrum is the expected one for a sipanmycin analogue. The in-source fragment ions at *m/z* = 623.4060 and *m/z* = 492.3474 indicate that the macrolactam aglycon and its directly attached aminosugar are identical for **3** and SIP-A and automatically manifest that **3** and SIP-A just differ in the terminal monosaccharide moiety which in the case of **3**, according to the molecular formula, does not contain any nitrogen atom. Substitution of the native terminal sipanose residue in SIP-A by olivose (the monosaccharide encoded by the introduced plasmid pLNRT) perfectly accounts for the molecular formula of **3.** Comparison of the NMR data of **3** and SIP-A show that the signals of the aglycon and its directly attached xylosamine are essentially identical for both compounds. As expected, the characteristic NMR signals of the D-sipanose residue of SIP-A do not appear in the spectra of **1**. Instead, a new set of signals is found which was revealed to correspond to the new terminal desoxysugar. Analysis of the TOCSY spectrum provided the connectivity and the relative configuration (based on the magnetization transfer from H-1'' to H6'' as described by Martins and co-workers [5]) of this monosaccharide residue which corresponds to the expected olivose with a β anomeric configuration (equatorial glycosidic linkage). Comparison with the NMR data of the β-D-olivose residue of kerriamycin B [6] further confirmed this assignment**.** Once again, according to Klyne's rule [2] the olivose residue has an β-D absolute configuration. Compound **3** thus corresponds to β-D-olivosyl-(1→4')-3'-*O*-demethylsilvalactam and was trivially designated as sipanmycin A2 (SIP-A2).

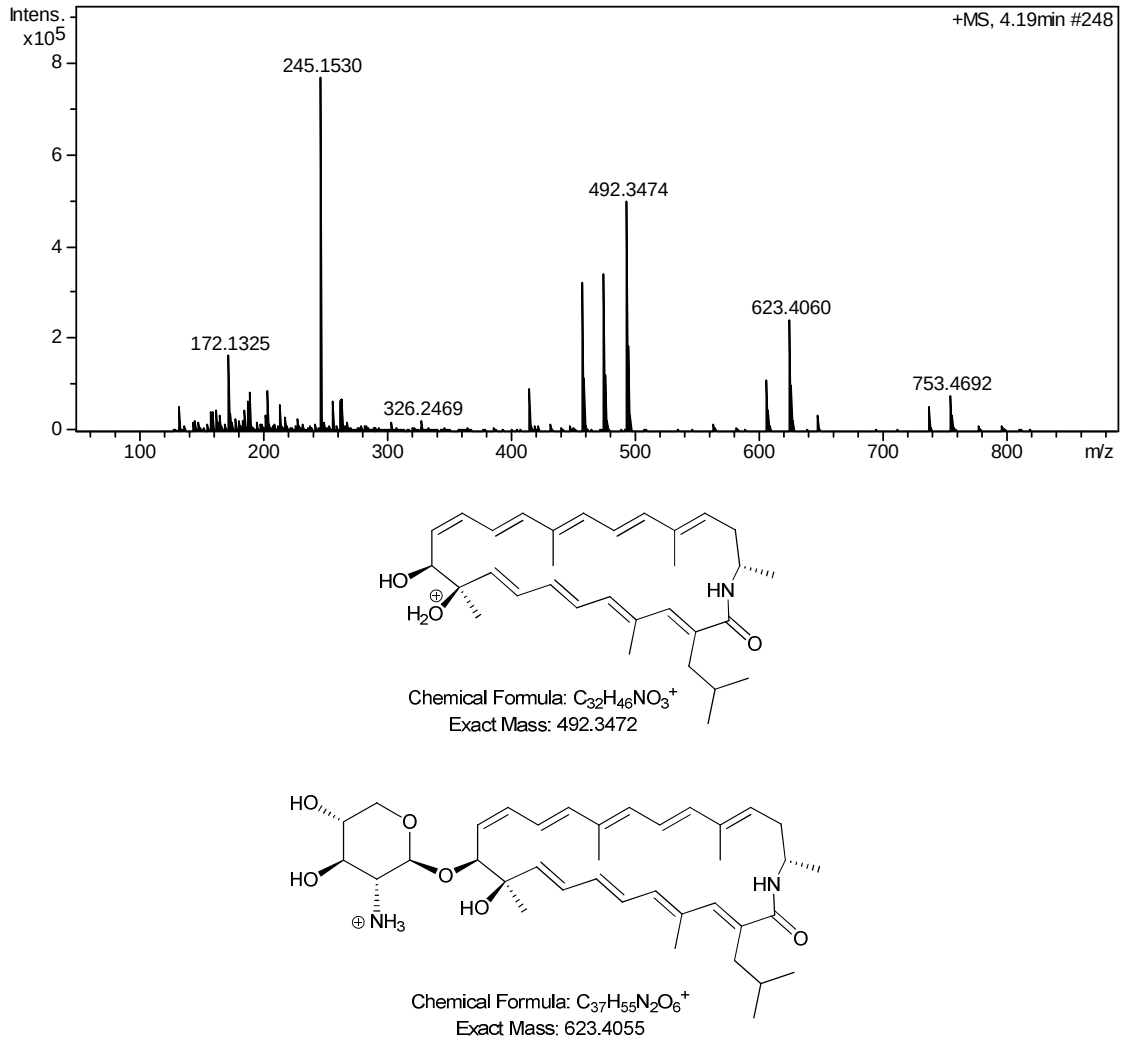

Fig. S22. HRMS spectrum of SIP-A2 (**3**) and identification of the key in-source fragment ions.

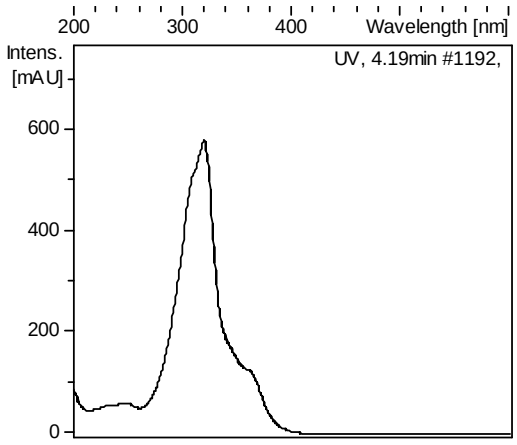

Fig. S23. UV-vis (DAD) spectrum of SIP-A2 (**3**).

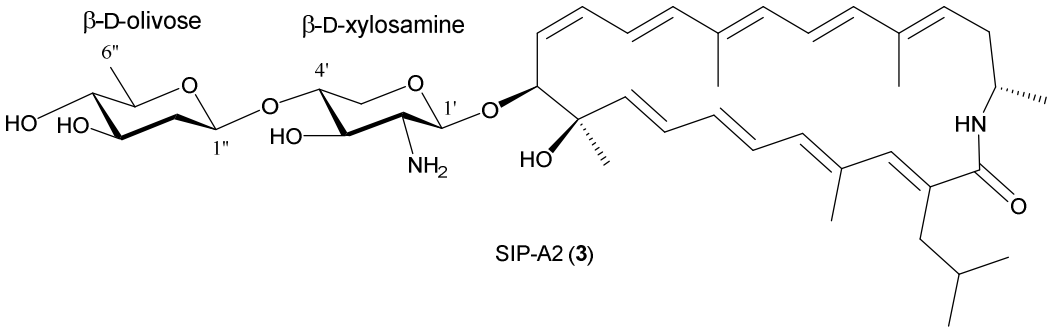

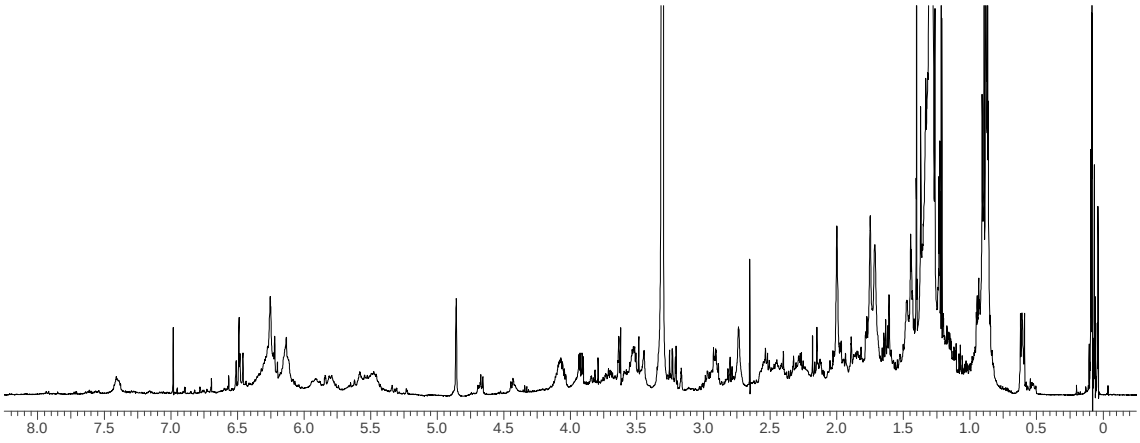

Fig. S24. ^{1}H NMR spectrum (CD_3OD, 500 MHz, water suppression) of SIP-A2 (**3**).

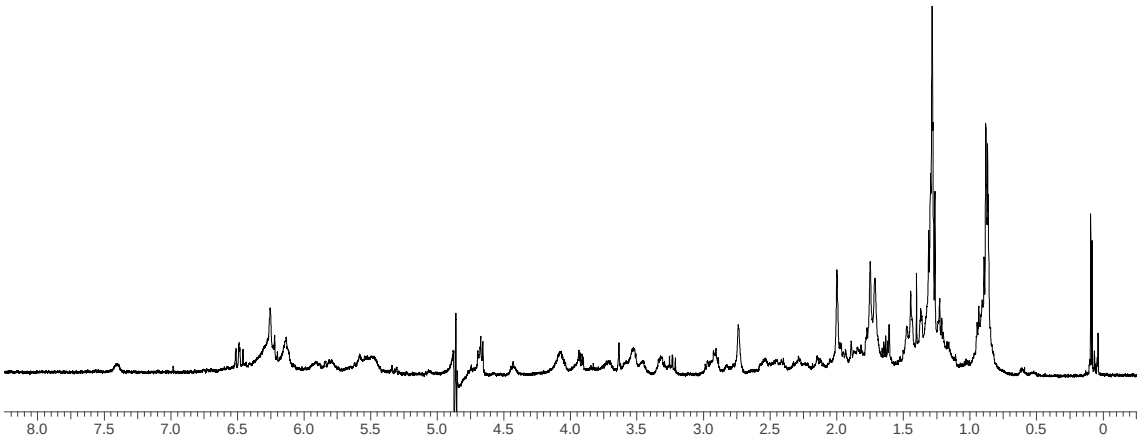

Fig. S25. Diffusion-filtered ^{1}H NMR spectrum of SIP-A2 (**3**).

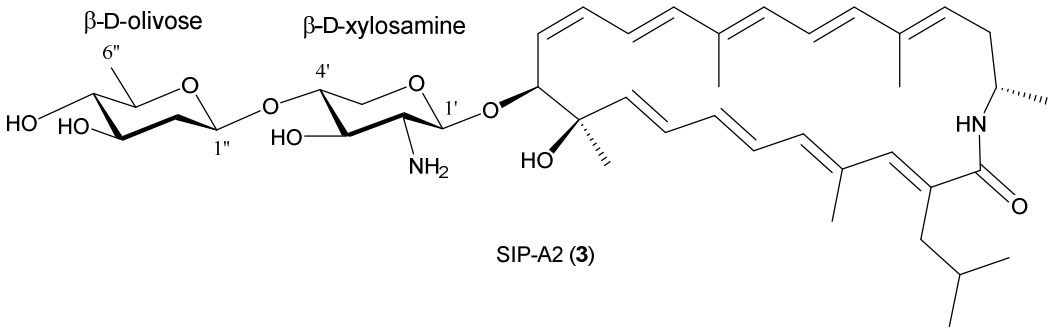

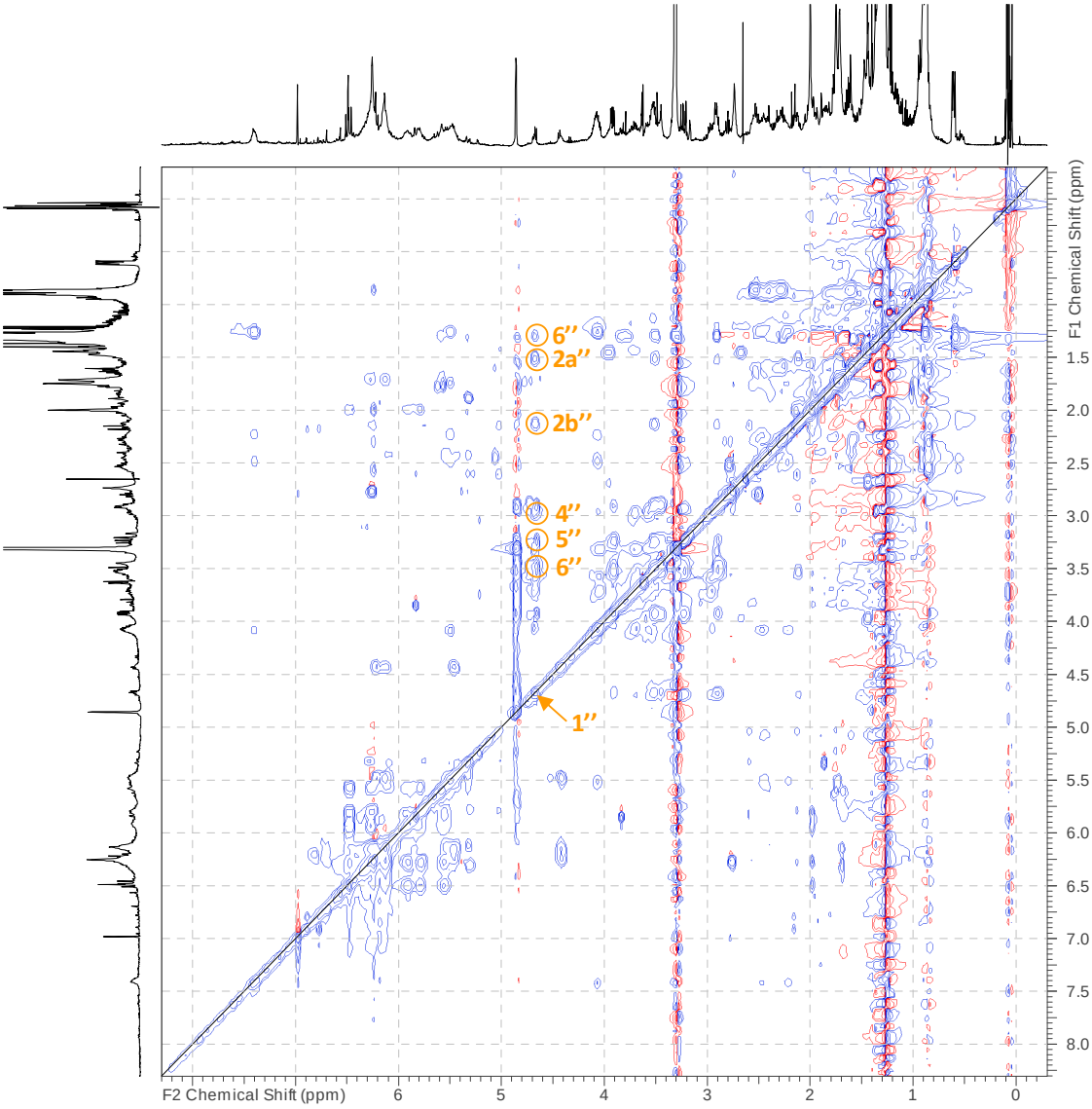

Fig. S26. TOCSY spectrum of SIP-A2 (**3**). Key correlations corresponding to the β-D-olivose spin system are highlighted. The corresponding anomeric proton (1'') signal at the diagonal is indicated by an arrow.

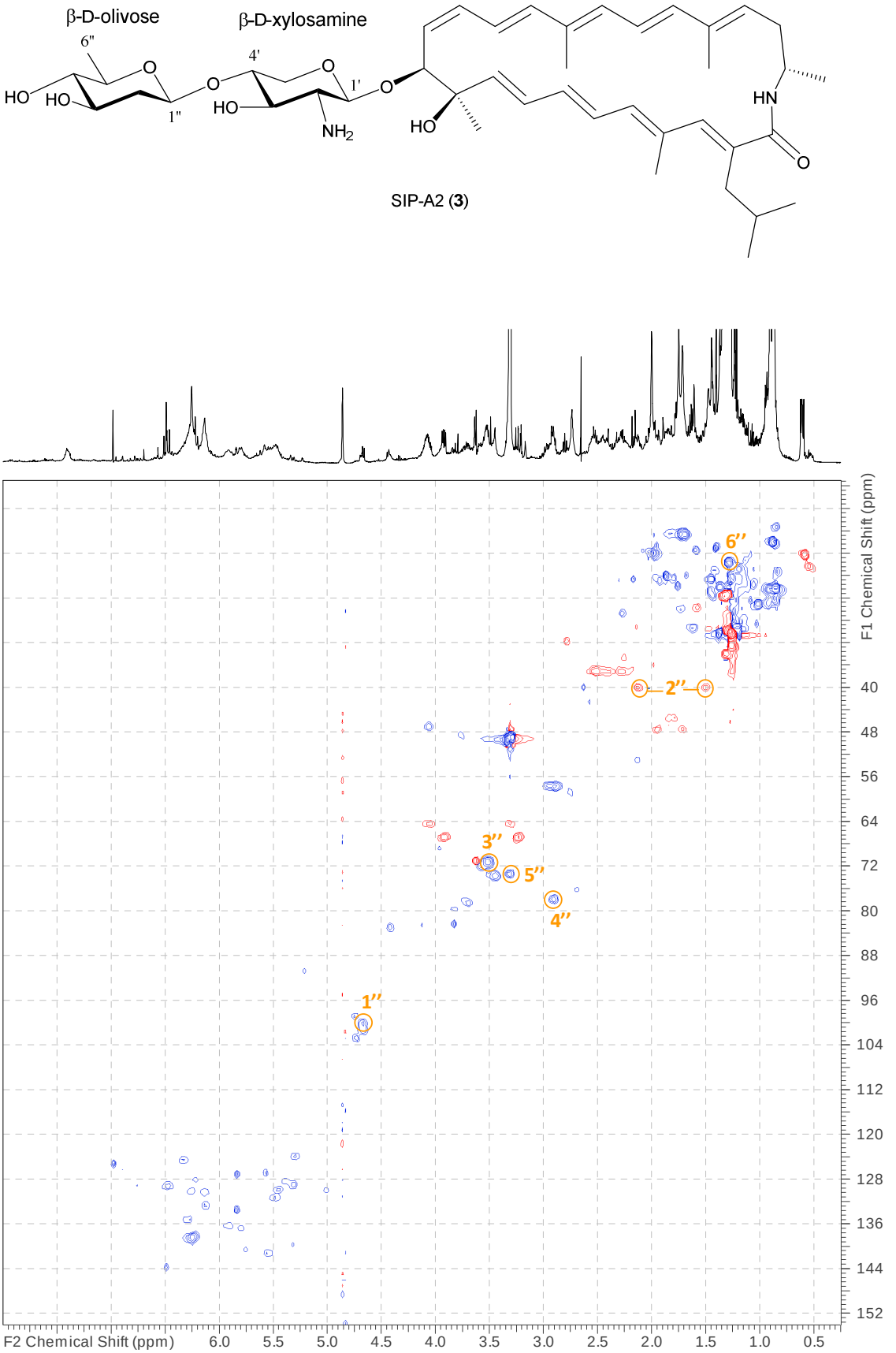

Fig. S27. Edited HSQC spectrum of SIP-A2 (**3**). Key correlations corresponding to the β-D-olivose moiety are highlighted.

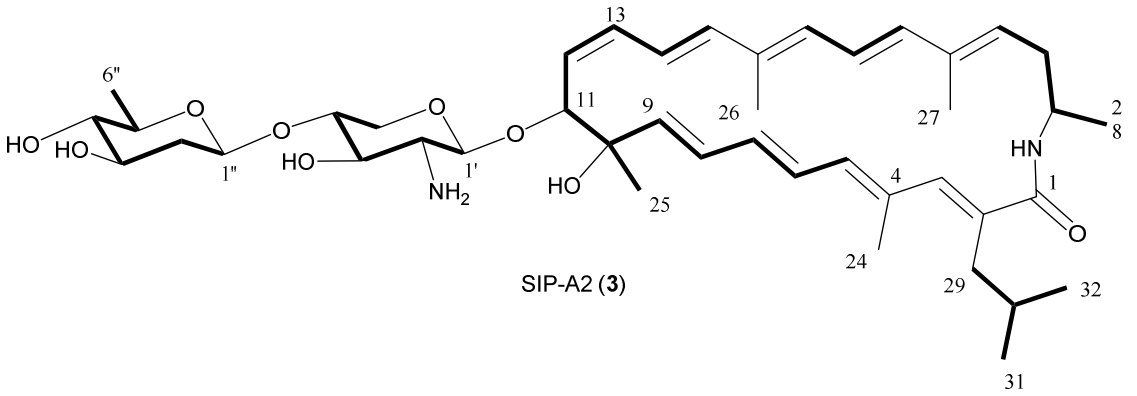

Fig. S28. Gross structure of SIP-A2 (**3**) determined by 2D-NMR and comparisons with the NMR data of SIP-A and kerriamycin B. Spin systems observed in the TOCSY spectrum are indicated as bold bonds.

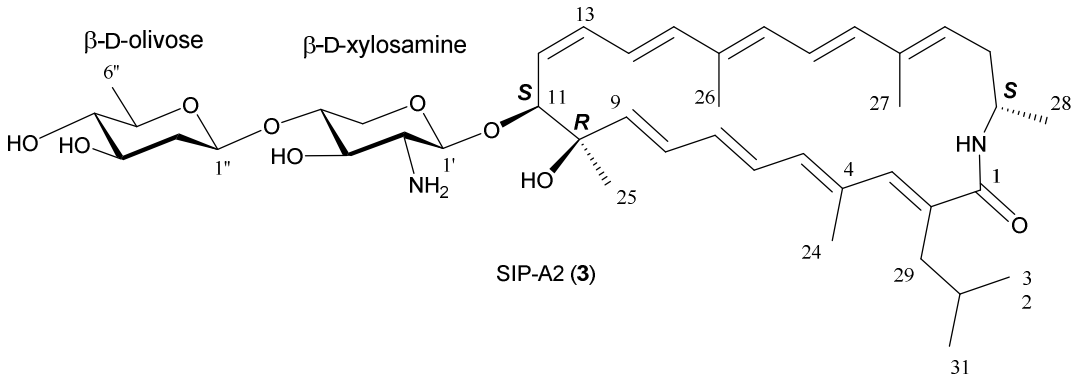

Fig. S29. Structure of SIP-A2 (**3**).

Table S3. ^{1}H and ^{13}C NMR data for SIP-A2 (**3**) in CD_3OD at 24 °C.

Position	δ_C, type	δ_H (*J* in Hz)	Position	δ_C, type	δ_H (*J* in Hz)
1	n. d., C	-	1'	101.3, CH	4.68, d (ca. 7.8)
2	n. d., C	-	2'	57.6, CH	2.96, m
3	138.6, CH	6.26, m	3'	72.0, CH	3.59, m
4	n. d., C	-	4'	78.3,CH	3.72, m
5	136.6, CH	5.80, m	5'	64.5, CH_2	4.08, m 3.32, m
6	129.2, CH	6.49, dd (14.5, 11.5)	1"	100.3, CH	4.70,br d (ca. 9.7)
7	136.2, CH	5.92, m	2"	40.1, CH_2	2.14, m 1.52, m
8	130.1, CH	6.27, m	3"	71.4, CH	3.54, m
9	141.2, CH	5.56, m	4"	78.0, CH	2.93, m
10	n. d., C	-	5"	73.4, CH	3.33, m
11	83.2, CH	4.43, m	6"	18.0, CH_3	1.31, m
12	130.0, CH	5.47, m			
13	130.3, CH	6.15, m			
14	125.9, CH	6.13, m			
15	138.1, CH	6.24, m			
16	n. d., C	-			
17	132.8, CH	6.14, m			
18	124.5, CH	6.34, m			
19	138.6, CH	6.27, m			
20	n. d., C	-			
21	131.3, CH	5.51, m			
22	37.4, CH_2	2.50, m 2.26, m			
23	47.2, CH	4.08, m			
24	16.2, CH_3	2.00, br s			
25	22.9, CH_3	1.49, br s			
26	12.8, CH_3	1.72, br s			
27	12.8, CH_3	1.76, br s			
28	20.6, CH_3	1.28, m			
29	37.2, CH_2	2.56, m 2.31, m			
30	29.5, CH	1.65, m			
31	22.5, CH_3	0.88, m			
32	22.5, CH_3	0.88, m			
1-NH	-	7.40 br s*			

^{13}C chemical shifts obtained from HSQC spectrum.

* The amide proton exchanges very slowly and can be observed in the spectra.

Structure elucidation of sipanmycin A2b (4).

The UV (DAD) spectrum of **4** shows the typical absorbance of the sipanmycin aglycon chromophore, indicating **4** is another analogue of this family of compounds. Its molecular formula was established as $C_{44}H_{66}N_2O_9$ based on the observed ion $[M+H]^+$ at *m/z* 767.4843 (calcd. for $C_{44}H_{67}N_2O_9^+$ = 767.4841, Δm = 0.3 ppm). This formula differs from that of SIP-A2 (**3**) in one extra carbon atom and two extra hydrogen atoms. Such "CH_2" difference is expected for a hypothetical "B" congener of SIP-A2 carrying an extra carbon in the aliphatic chain substituent at C-2. However, the in-source fragment ions at *m/z* = 623.4060 and *m/z* = 492.3474 indicate that the macrolactam aglycon and its directly attached aminosugar are identical for **4** and SIP-A2 manifesting that the "CH_2" difference is localized in the terminal monosaccharide moiety. Methylation of a hydroxyl or one of the carbons of the olivose moiety of SIP-A2 would account for such difference.

Comparison of the NMR data of **4** and SIP-A2 shows that the signals of the aglycon and its directly attached xylosamine are essentially identical for both compounds. The signals of the new terminal deoxysugar could be identified after comparison of the HSQC spectra of both compounds and analysis of the COSY, TOCSY and HMBC spectra of **4**. Based on the key correlations found in these spectra the identity of this sugar residue was established as olivomycose with a β anomeric configuration (equatorial glycosidic linkage). This sugar can be considered as a 3-methylolivose and perfectly explains the abovementioned "CH_2" difference in the molecular formulae of SIP-A2 and **4**. The axial orientation of this methyl group (H-7'') was unambiguously established on the basis of its key NOESY correlation with H-5''. The coupling constants observed for the anomeric H-1'' and H-4'' were also employed for establishing the β-olivomycose relative configuration of the terminal sugar residue.

Comparison with the NMR data of the β-olivomycose residues of ammocidins A and B [7, 8] further confirmed this assignment. As indicated for SIP-A2, according to Klyne's rule [4] the olivomycose residue has a β-D absolute configuration. Compound **4** thus corresponds to β-D-olivomycosyl-(1→4')-3'-*O*-demethylsilvalactam and was trivially designated as sipanmycin A2b (SIP-A2b).

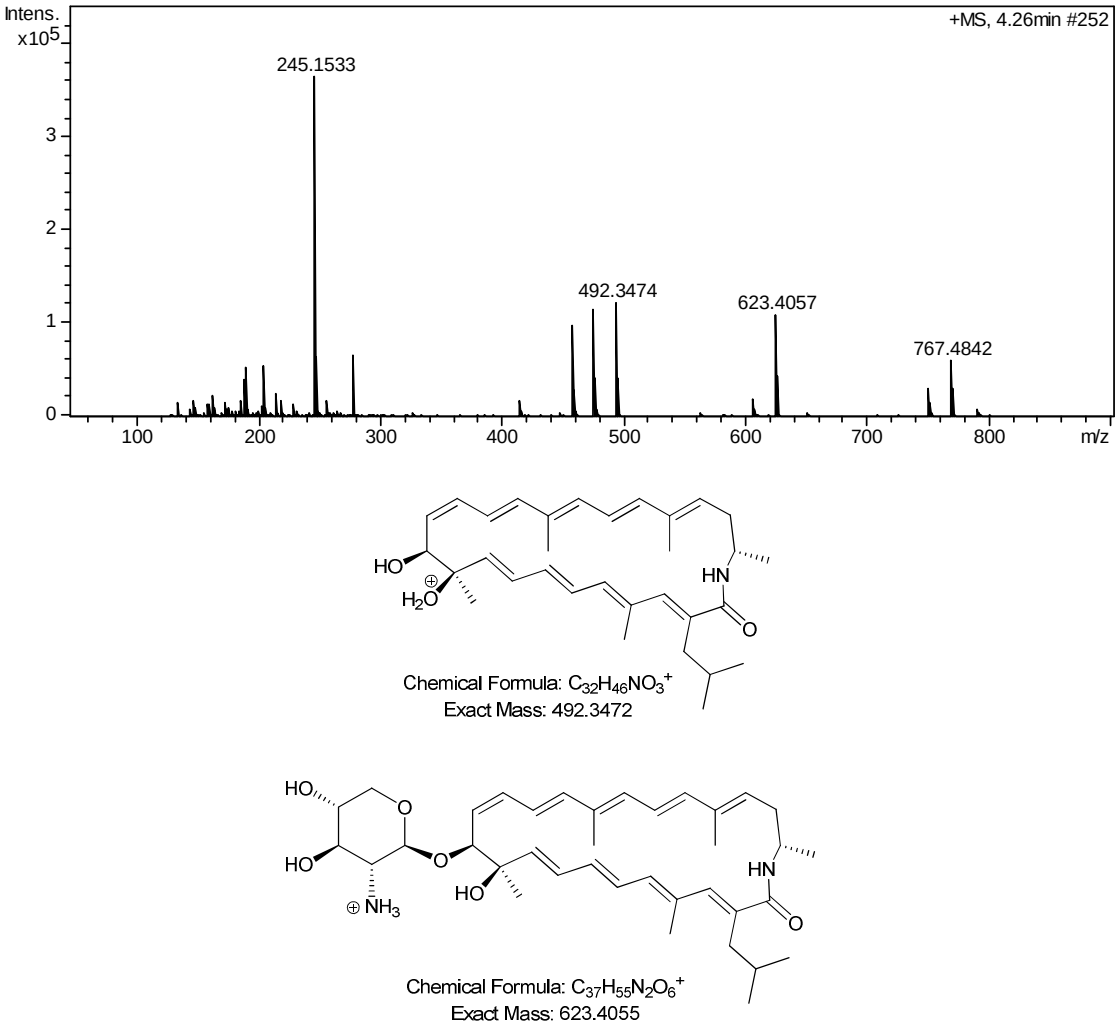

Fig. S30. HRMS spectrum of SIP-A2b (**4**) and identification of the key in-source fragment ions.

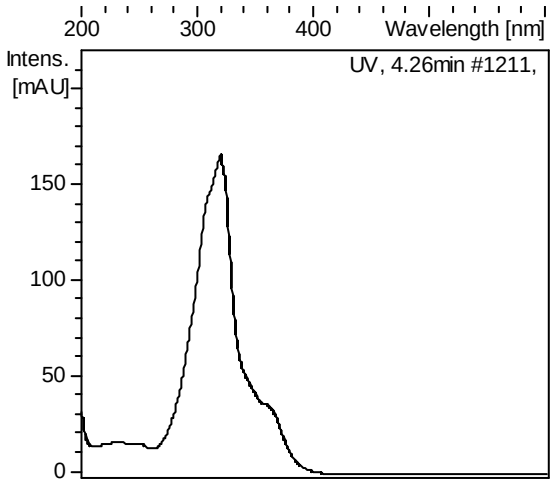

Fig. S31. UV-vis (DAD) spectrum of SIP-A2b (**4**).

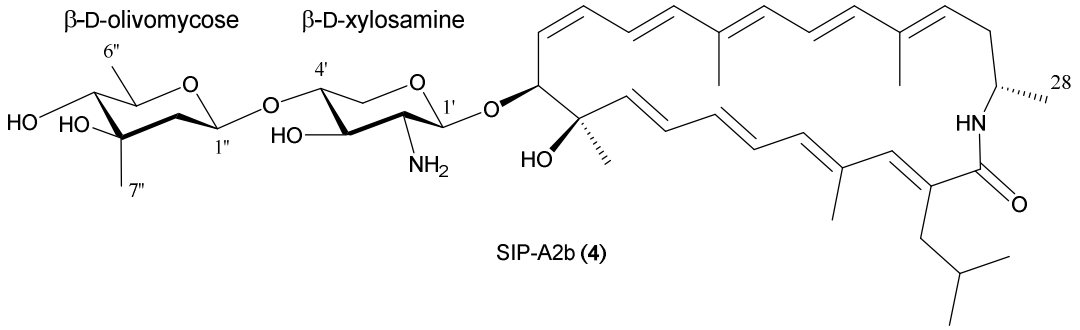

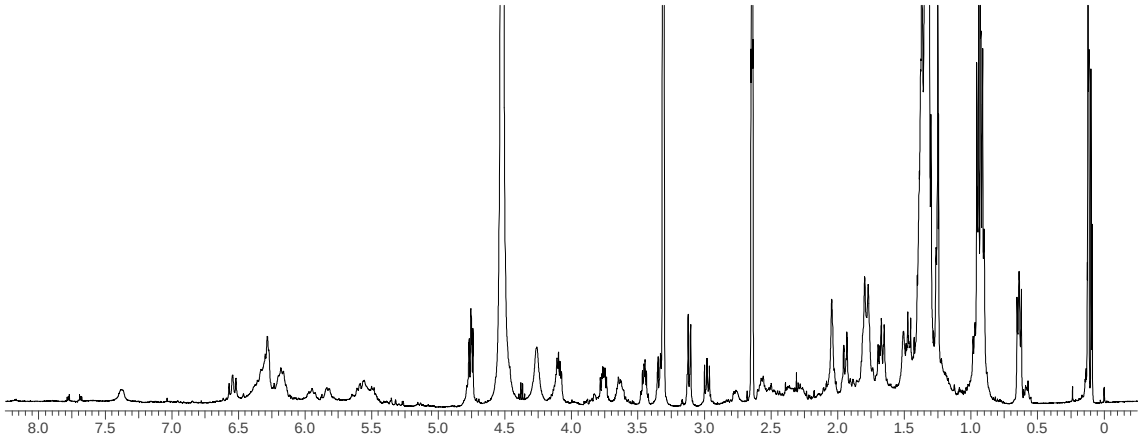

Fig. S32. ^{1}H NMR spectrum (CD_3OD, 500 MHz, water suppression) of SIP-A2b (**4**).

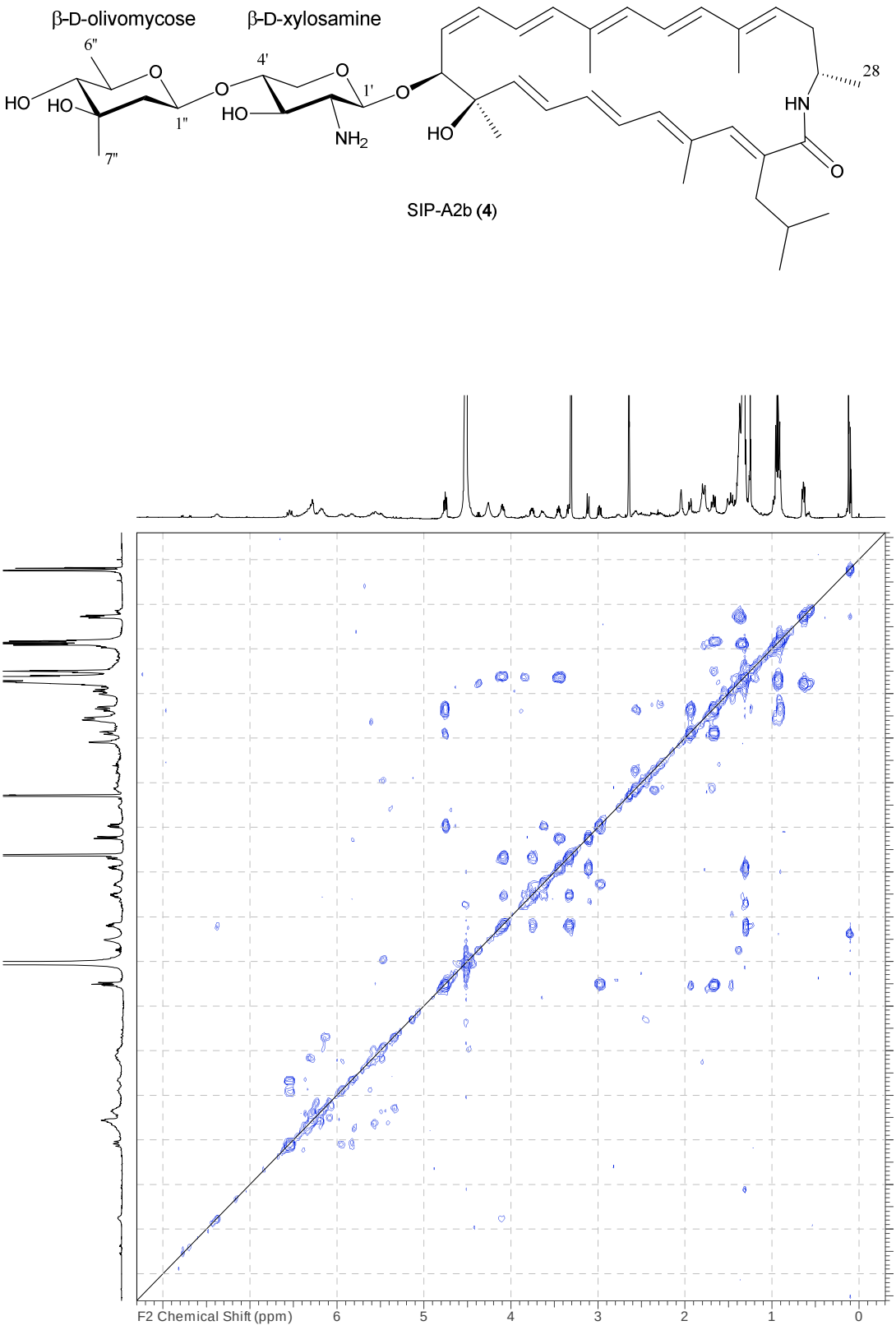

Fig. S33. COSY spectrum of SIP-A2b (**4**).

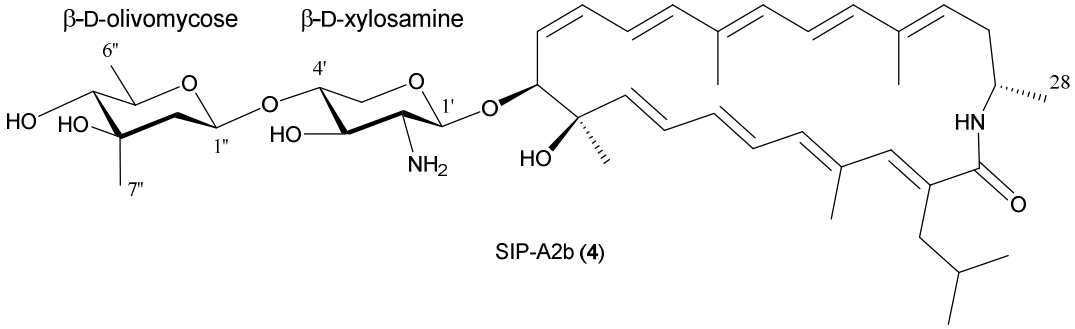

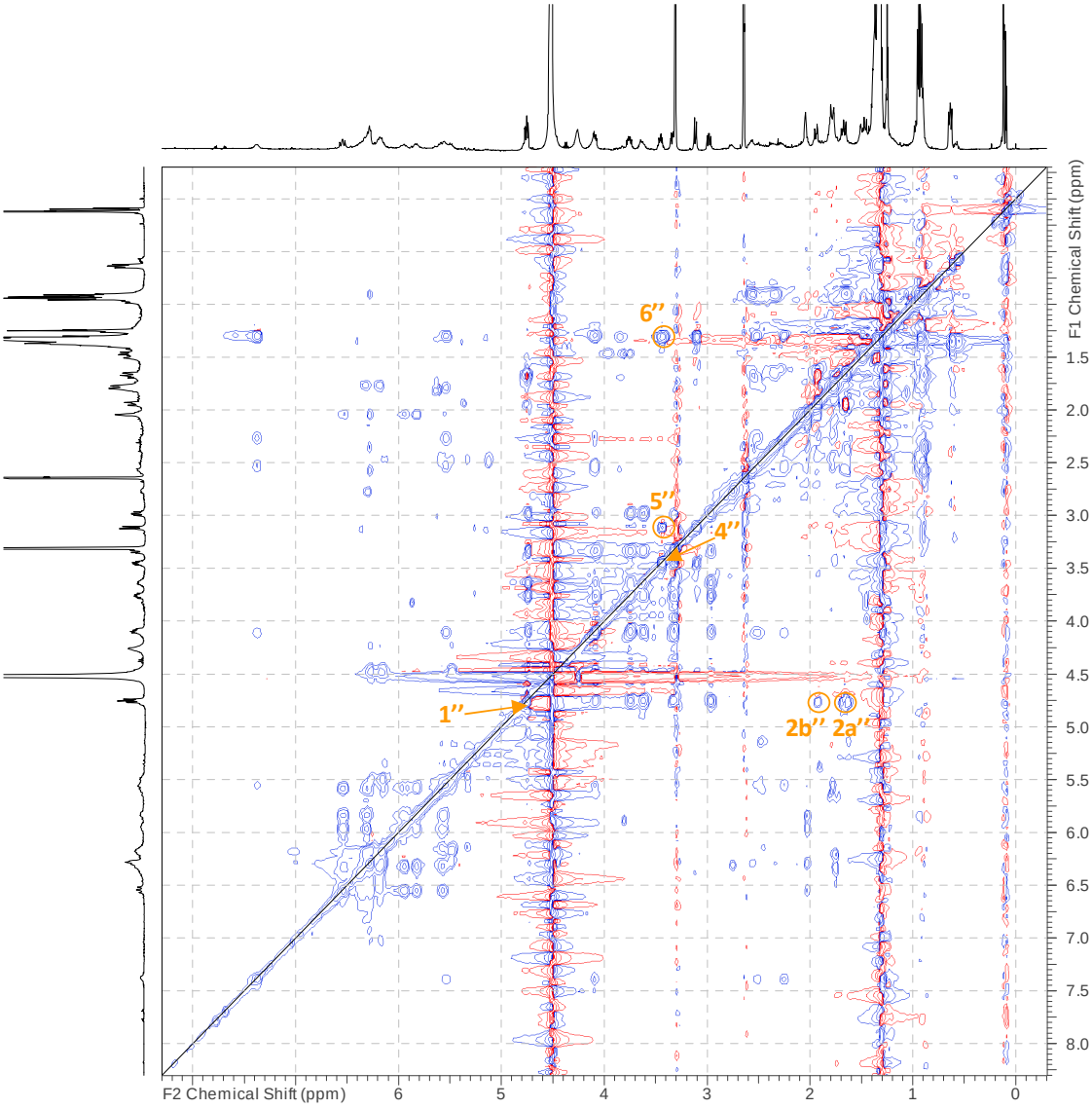

Fig. S34. TOCSY spectrum of SIP-A2b (**4**). Key correlations corresponding to the β-D-olivomycose spin systems are highlighted. The corresponding proton signals at the diagonal are indicated by an arrow.

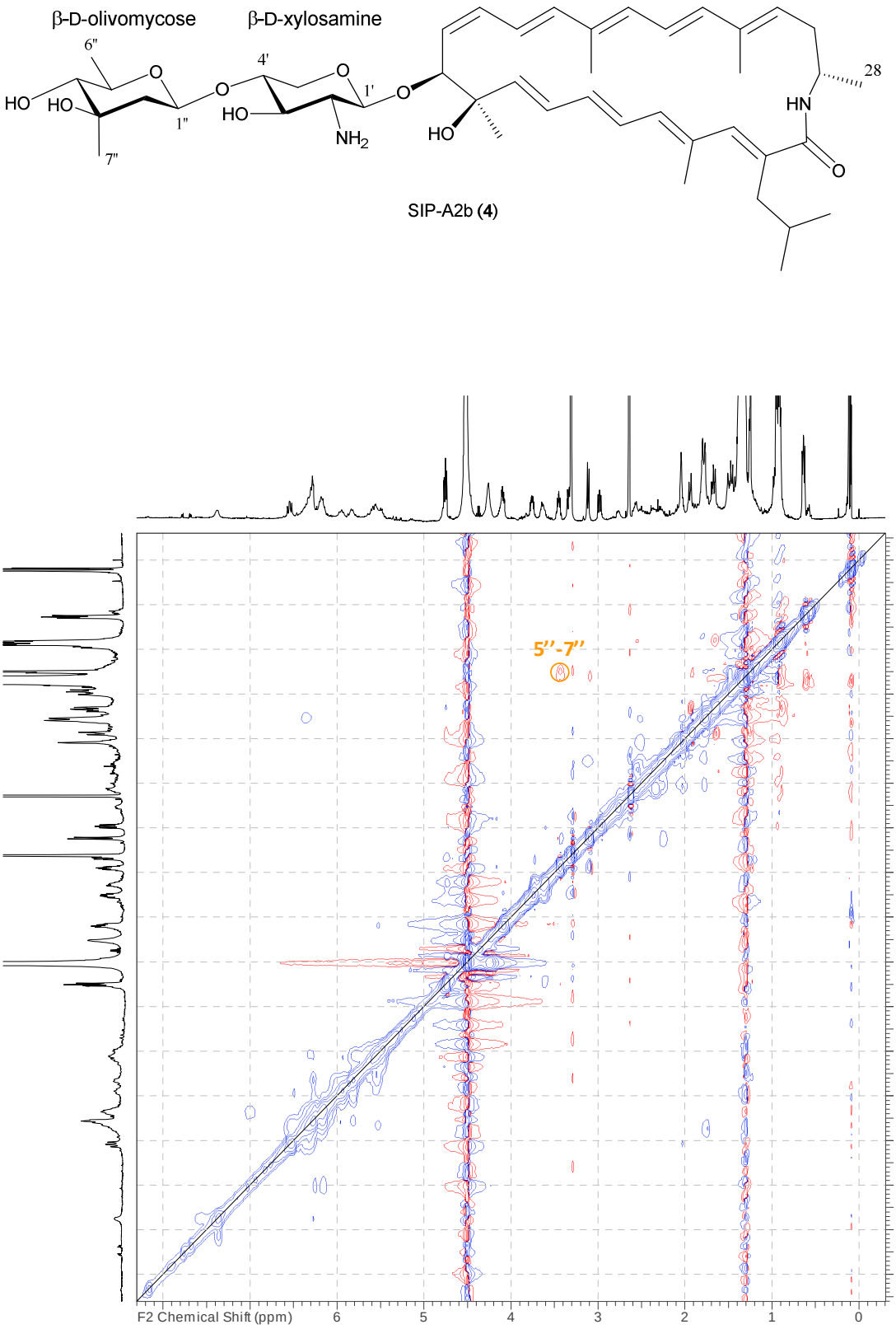

Fig. S35. NOESY spectrum of SIP-A2b (**4**). Key correlation for determining the relative configuration of the β-D-olivomycose residue is highlighted (first proton in the pair corresponds to F2 dimension and the second proton to the indirect F1 dimension).

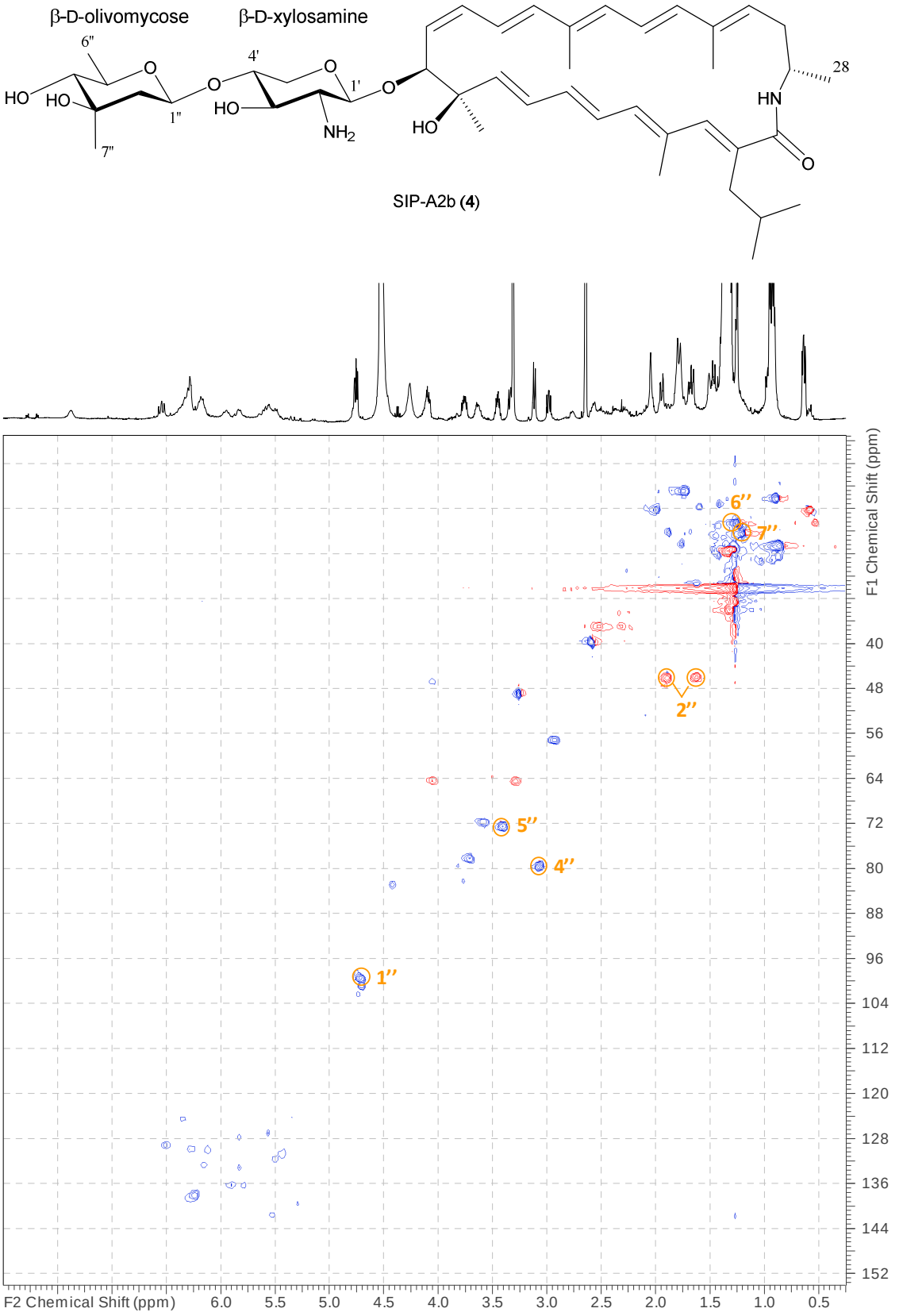

Fig. S36. Edited HSQC spectrum of SIP-A2b (**4**). Key correlations corresponding to the β-D-olivomycose moiety are highlighted.

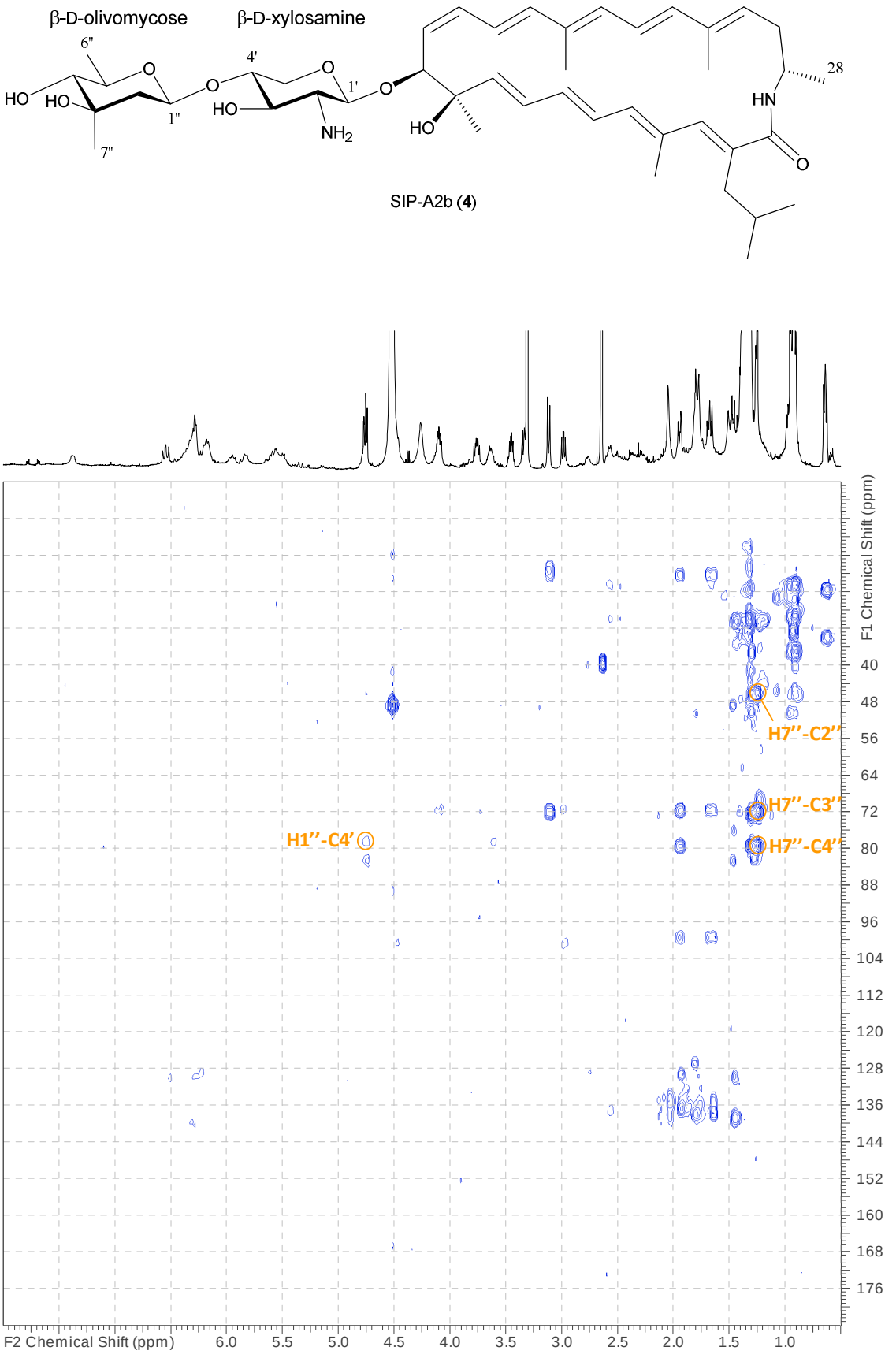

Fig. S37. HMBC spectrum of SIP-A2b (**4**). Key correlations involving the β-D-olivomycose residue and establishing its linkage to the β-D-xylosamine moiety are highlighted.

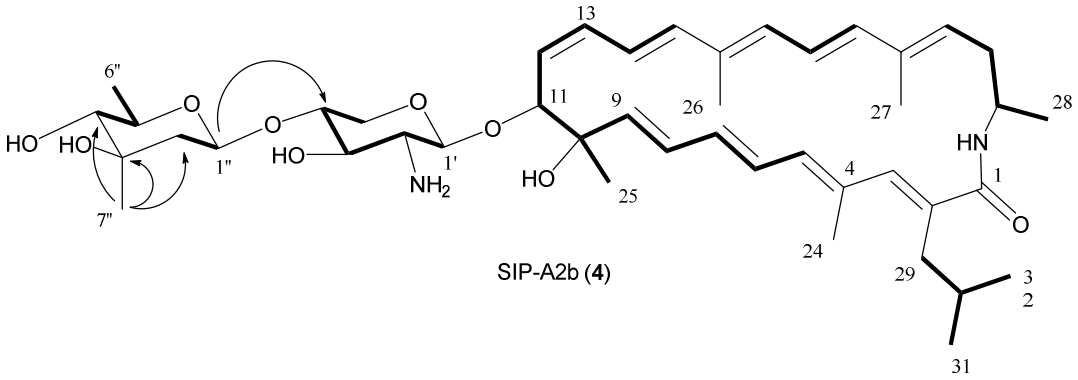

Fig. S38. Gross structure of SIP-A2b (**4**) determined by 2D-NMR and comparisons with the NMR data of SIP-A, SIP-A2 and ammomicins A and B. Spin systems observed in the COSY and TOCSY spectra are indicated as bold bonds. Key HMBC correlations involving the terminal olivomycose residue are indicated by arrows.

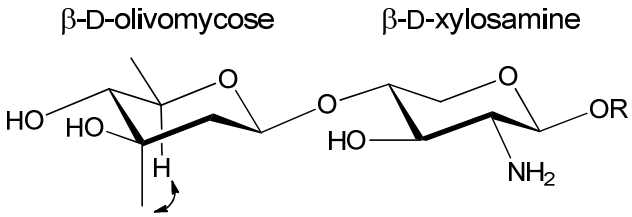

Fig. S39. Key NOESY correlation (solid arrow) between H-5'' and H-7'' (methyl) which, together with the observed coupling constants, allow stablishing the β-olivomycose relative configuration for the terminal monosaccharide.

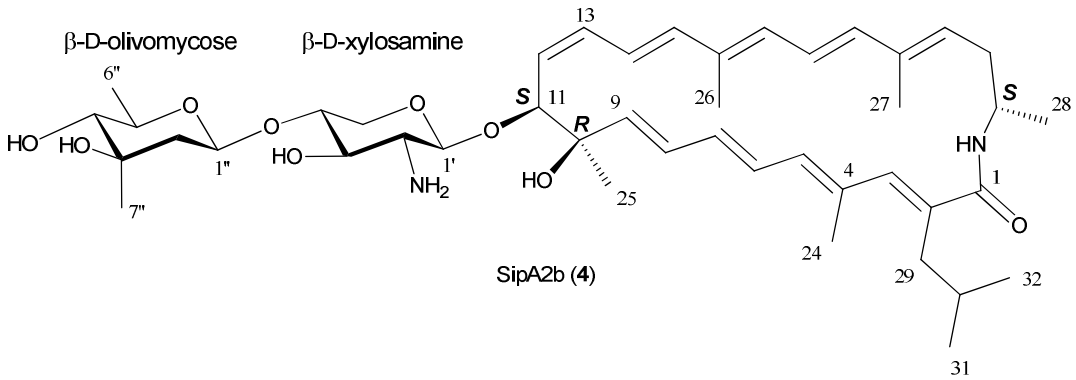

Fig. S40. Structure of SIP-A2b (**4**).

Table S4. ^{1}H and ^{13}C NMR data for SIP-A2b (**4**) in CD_3OD/DMSO-d_6 (4:1) at 24 °C.

Position	δ_C, type	δ_H (*J* in Hz)	Position	δ_C, type	δ_H (*J* in Hz)
1	n. d., C	-	1'	100.8, CH	4.75, d (ca. 7.6)
2	n. d., C	-	2'	57.2, CH	2.98, dd (9.8, 7.8)
3	138.4, CH	6.32, m	3'	71.3, CH	3.63, m
4	134.8, C	-	4'	78.3, CH	3.76, ddd (9.8, 8.6, 5.4)
5	136.3, CH	5.84, m	5'	64.5, CH_2	4.09, m 3.34, m
6	129.1, CH	6.51, dd (14.1, 11.8)	1"	99.5, CH	4.76, dd (9.8, 1.8)
7	136.2, CH	5.95, m	2"	46.2, CH_2	1.95, dd (12.7, 1.8) 1.67, dd (12.8, 9.8)
8	129.8, CH	6.32, m	3"	71.9, C	-
9	141.5, CH	5.57, m	4"	79.6, CH	3.12, d (9.6)
10	76.2, C	-	5"	72.6, CH	3.45, dq (9.6, 6.0)
11	82.9, CH	4.47, m	6"	18.8, CH_3	1.32, m
12	130.5, CH	5.49, m	7"	20.5, CH_3	1.25, m
13	130.0, CH	6.17, m			
14	126.1, CH	6.17, m			
15	137.9, CH	6.29, m			
16	136.0, C	-			
17	132.7, CH	6.20, m			
18	124.5, CH	6.38, m			
19	138.2, CH	6.31, m			
20	137.8, C	-			
21	131.6, CH	5.54, m			
22	37.1, CH_2	2.57, m 2.36, m			
23	46.9, CH	4.10, m			
24	16.4, CH_3	2.04, br s			
25	23.7, CH_3	1.51, br s			
26	13.0, CH_3	1.77, br s			
27	13.0, CH_3	1.80, br s			
28	20.4, CH_3	1.26, m			
29	37.3, CH_2	2.59, m 2.35, m			
30	29.5, CH	1.67, m			
31	22.7, CH_3	0.91, m			
32	22.7, CH_3	0.91, m			
1-NH	-	7.38 br s*			

^{13}C chemical shifts obtained from HSQC and HMBC spectra.

* The amide proton exchanges very slowly and can be observed in the spectra.

Structure elucidation of sipanmycin A3 (5).

The UV (DAD) spectrum of **5** shows the typical absorbance pattern of the sipanmycin aglycon chromophore, indicating **5** is another analogue of this family of compounds. Its molecular formula was established as $C_{45}H_{69}N_3O_7$ based on the observed ion $[M+H]^+$ at *m/z* 764.5221 (calcd. for $C_{45}H_{70}N_3O_7^+$ = 764.5208, Δ*m* = 0.9 ppm). Such formula contains one carbon atom, one oxygen atom and two hydrogen atoms less than the molecular formula of sipanmycin A (SIP-A) [3]. Comparison of the in-source fragment ion at *m/z* = 142.1230 with the corresponding one from SIP-A (*m/z* =172.1332) suggested that **5** and SIP-A just differ (by a formal "CH_2O") in the terminal monosaccharide moiety. Comparison of the NMR data of **5** and SIP-A show the expected small differences related to the substitution of sipanose by a different deoxyaminosugar in **5**. The connectivity (based on COSY, TOCSY and HMBC correlations) and the relative configuration (based on coupling constants and NOE analysis) of this monosaccharide residue was found to correspond to forosamine, with a β anomeric configuration (equatorial glycosidic linkage). Comparison with the NMR data reported for the forosamine residues in forazoline A [9] and spiramycin [10] further supported the monosaccharide identity. Forosamine is structurally related to sipanose (the wild type deoxyaminosugar of sipanmycins) and can be considered as a 3-demethyl,3-deoxysipanose. Once again, according to Klyne's rule [4] the forosamine residue of **5** has a β-D absolute configuration. Another evidence for this absolute configuration is found in the homologous compound incednine [11], biosynthesized by a homolog gene cluster [12], and which contains a β-D-*N*-demethylforosamine residue as terminal monosaccharide. Not surprisingly, the same key inter-sugar NOESY correlations (H-1'' with both H-4' and H-5_{eq}') already reported for SIP-A [3] are likewise found in **5**. As already indicated for the other analogs, the absolute

configuration of the D-xylose residue and the chiral centers in the macrolactam aglycon of **5** must be identical to that of SIP-A for obvious biosynthetic reasons. Compound **5** thus corresponds to β-D-forosaminyl-(1→4')-3'-*O*-demethylsilvalactam and was trivially designated as sipanmycin A3 (SIP-A3).

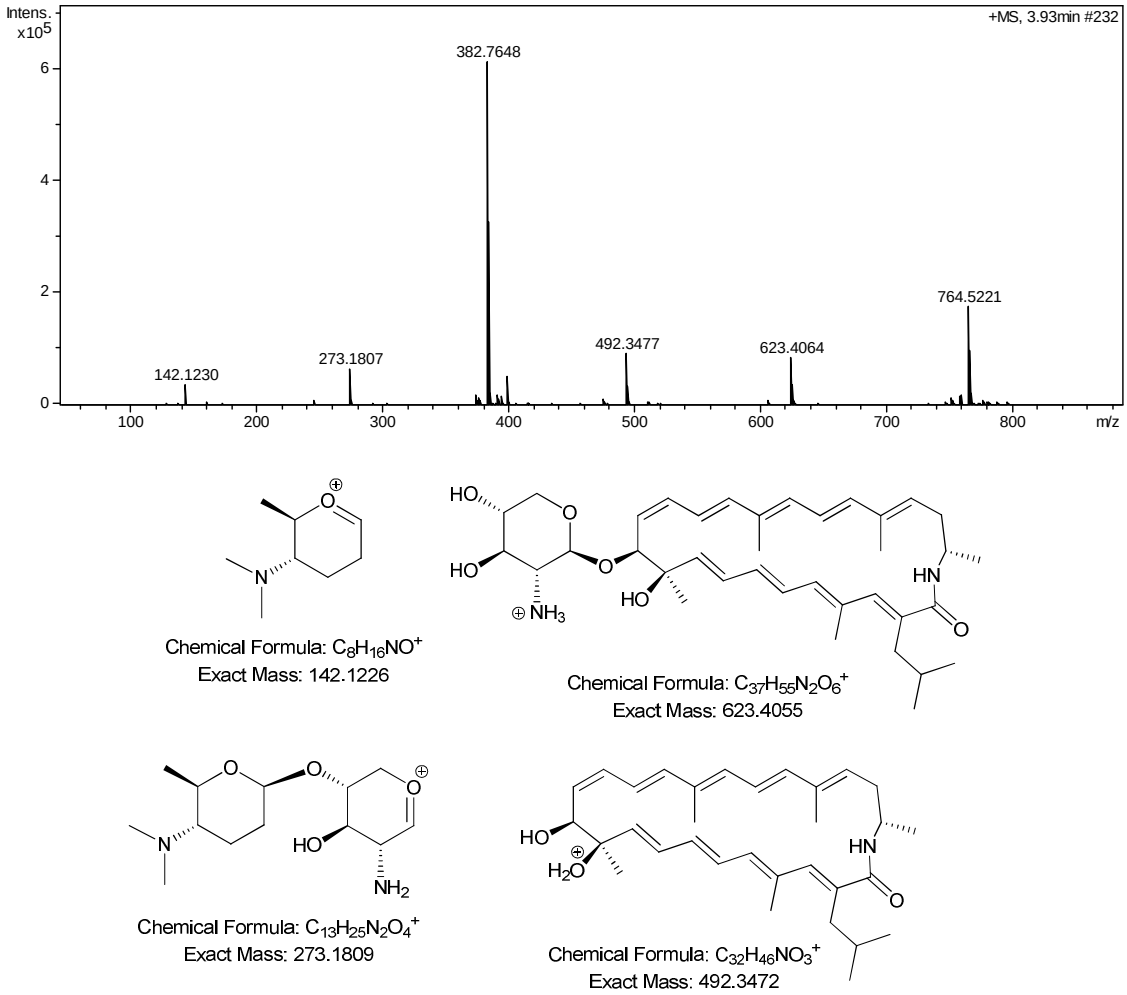

Fig. S41. HRMS spectrum of SIP-A3 (**5**) and identification of the key in-source fragment ions.

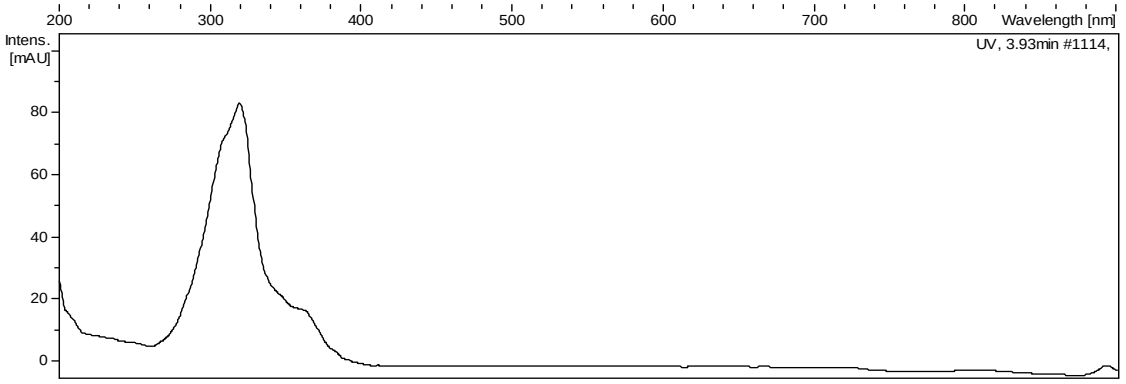

Fig. S42. UV-vis (DAD) spectrum of SIP-A3 (**5**).

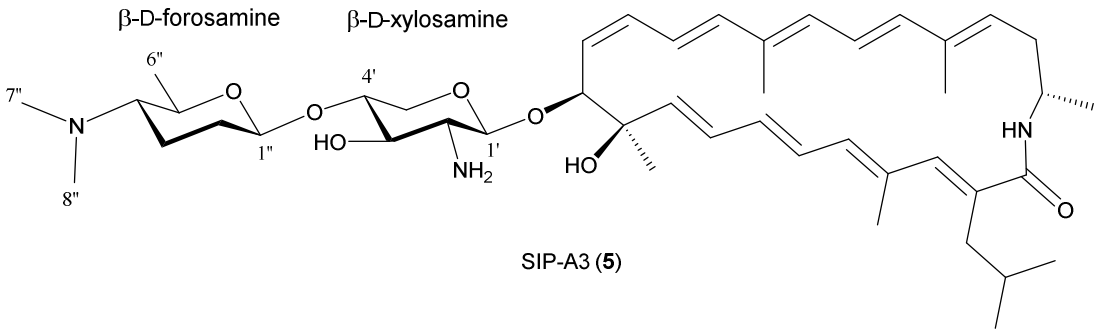

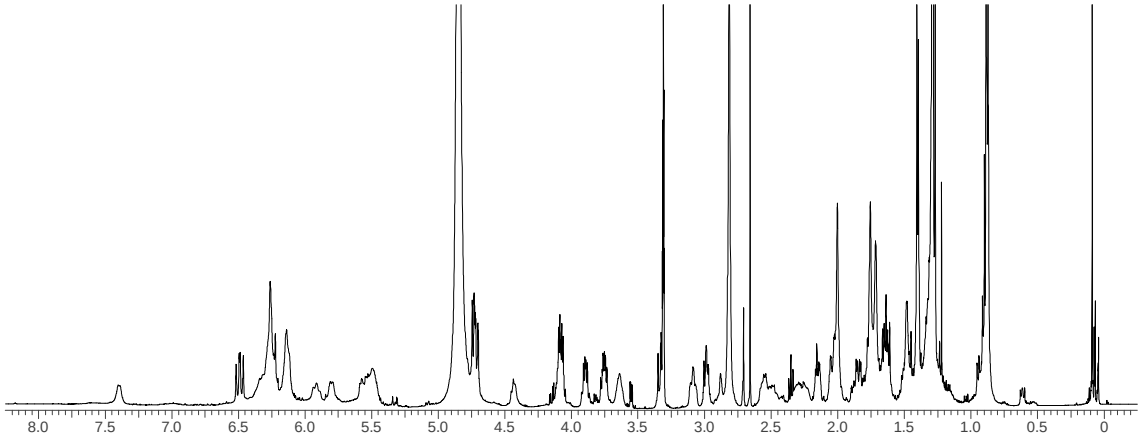

Fig. S43. ^{1}H NMR spectrum (CD_3OD, 500 MHz) of SIP-A3 (**5**).

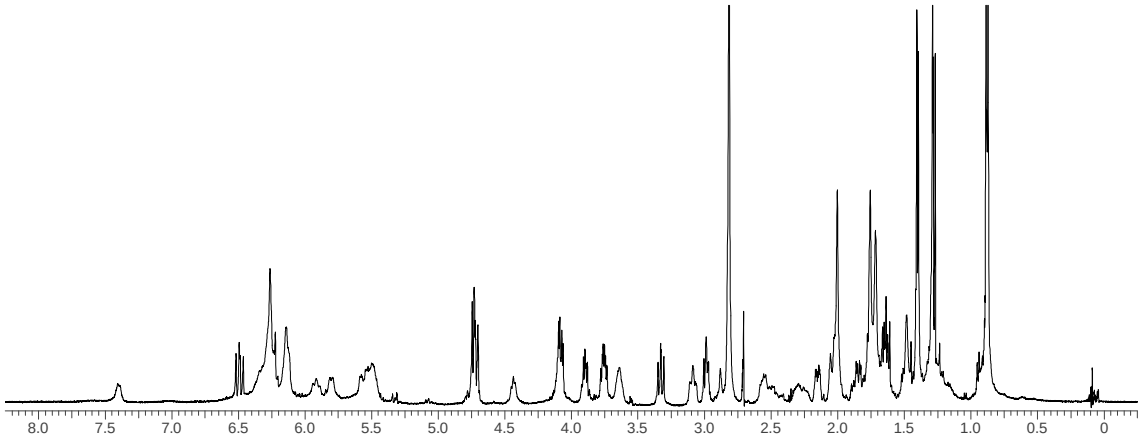

Fig. S44. Diffusion-filtered ^{1}H NMR spectrum of SIP-A3 (**5**).

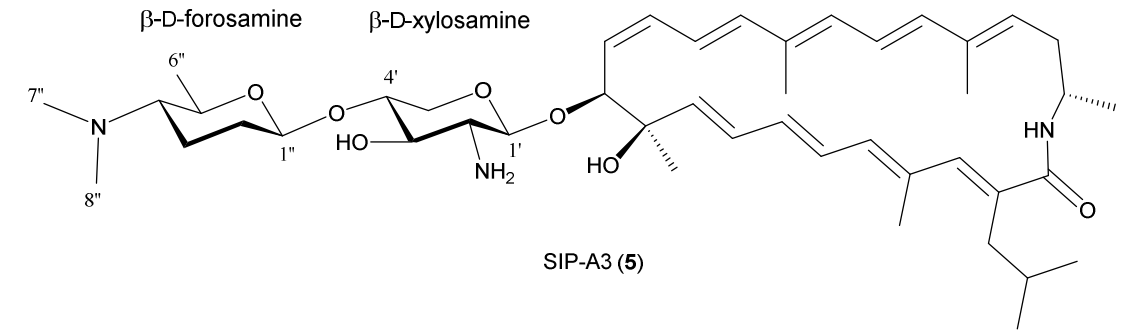

SIP-A3 (**5**)

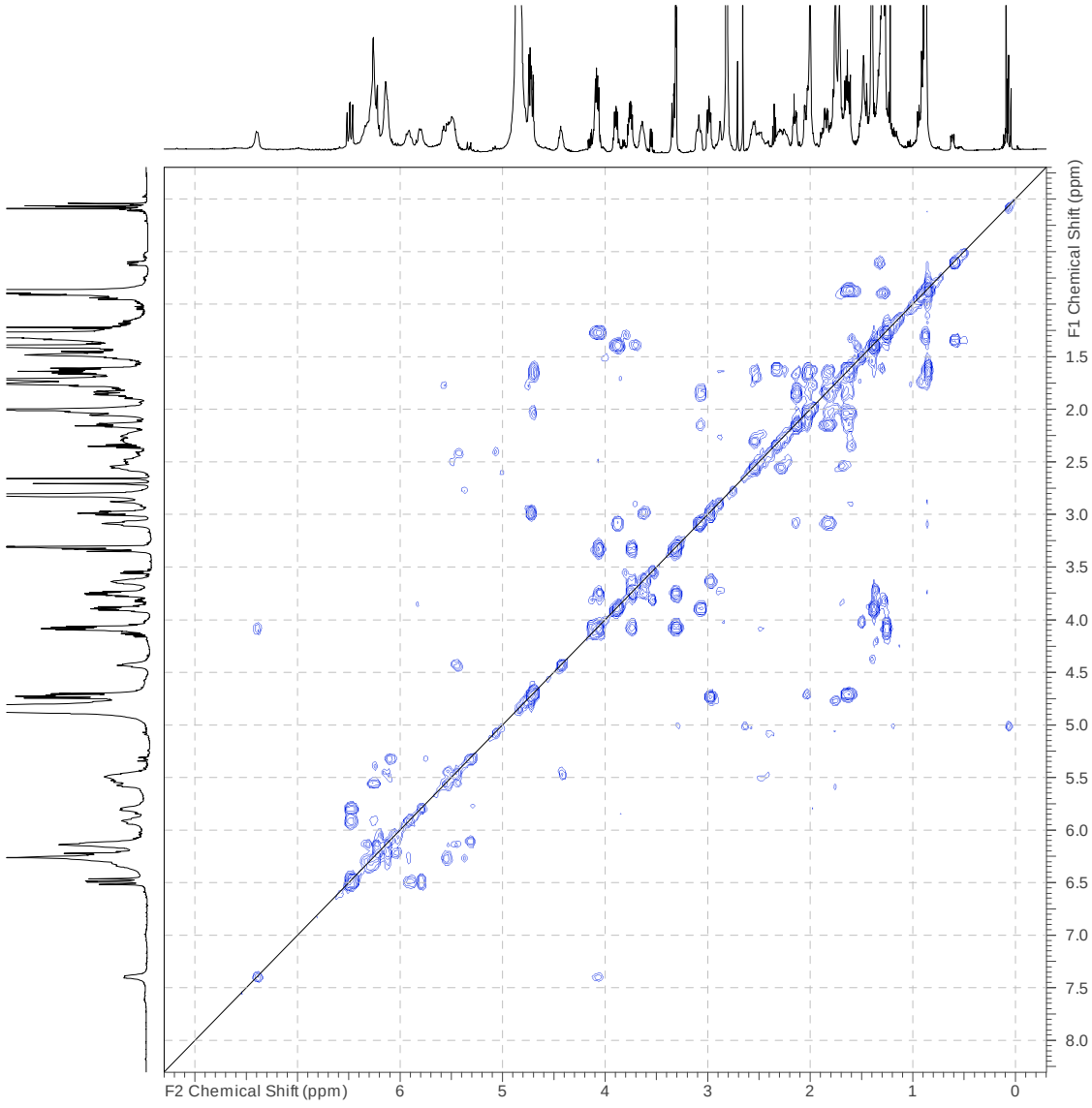

Fig. S45. COSY spectrum of SIP-A3 (**5**).

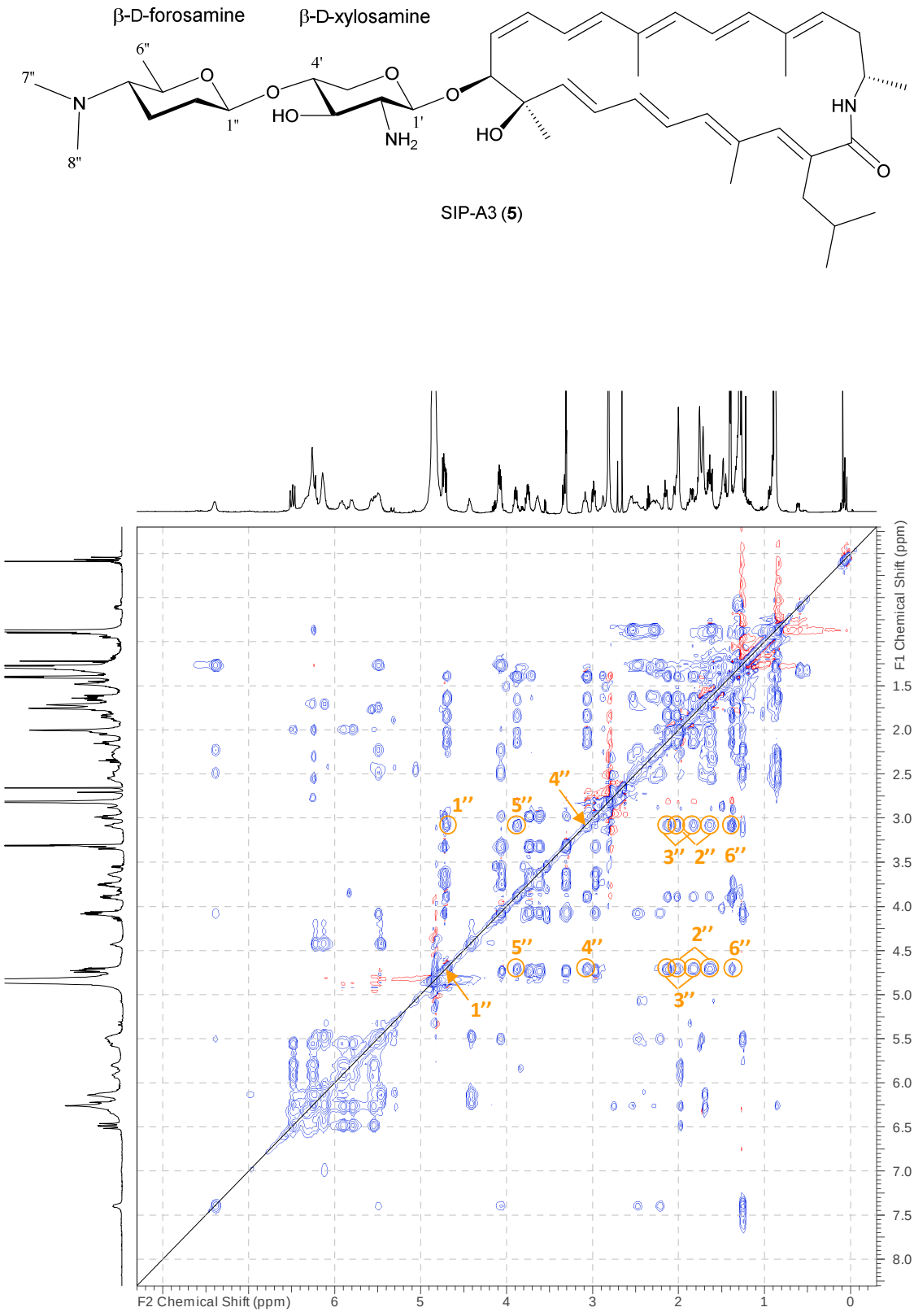

Fig. S46. TOCSY spectrum of SIP-A3 (**5**). Key correlations corresponding to the β-D-forosamine spin system are highlighted. The corresponding proton signals at the diagonal are indicated by an arrow.

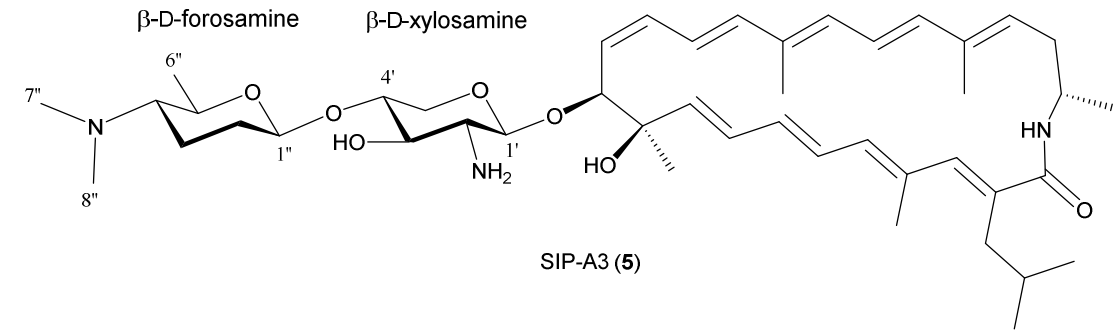

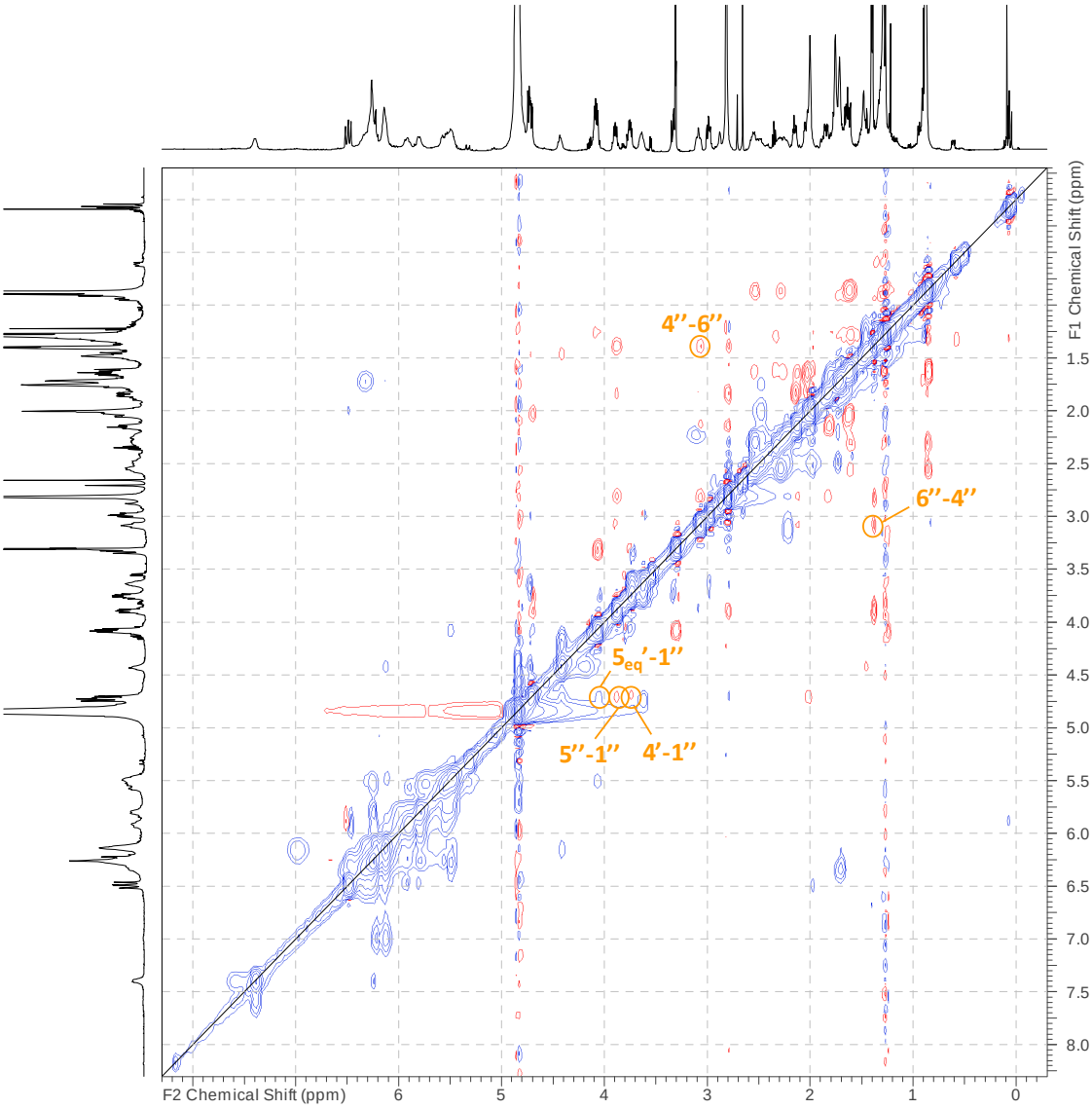

Fig. S47. NOESY spectrum of SIP-A3 (**5**). Key correlations rendering the relative and absolute configuration of the β-D-forosamine residue are highlighted (first proton in each pair corresponds to F2 dimension and the second proton to the indirect F1 dimension).

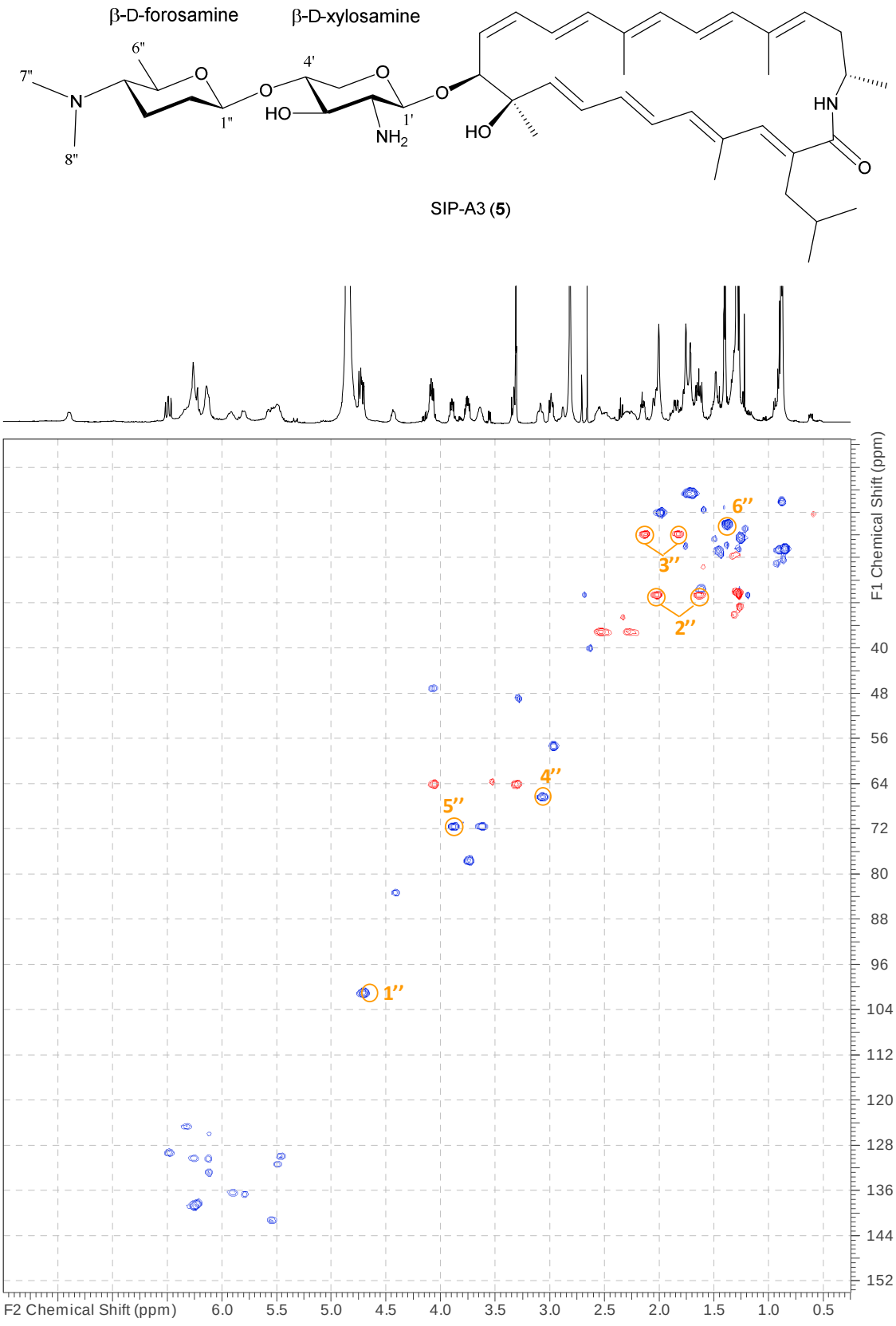

Fig. S48. Edited HSQC spectrum of SIP-A3 (**5**). Key correlations corresponding to the β-D-forosamine moiety are highlighted.

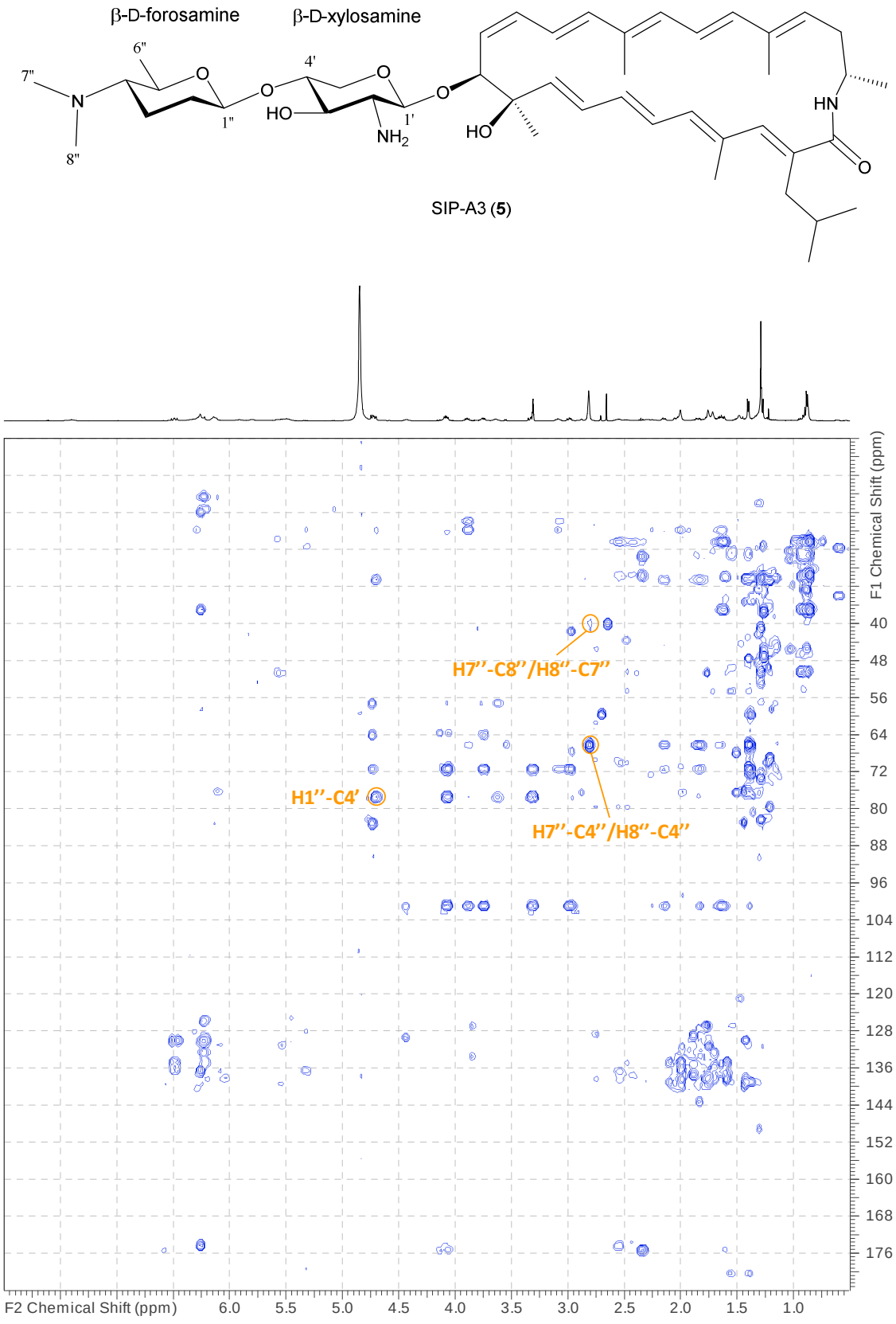

Fig. S49. HMBC spectrum of SIP-A3 (**5**). Key correlations involving the β-D-forosamine residue and establishing its linkage to the β-D-xylosamine moiety are highlighted.

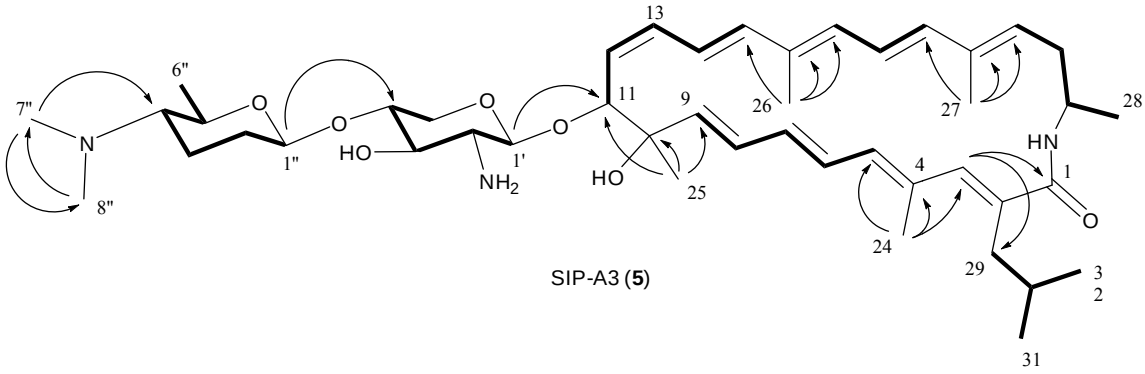

Fig. S50. Gross structuf SipA3 (**3**) determined by 2D NMR and comparisons with the NMR data of SIP-A. COSY correlations (further corroborated by the spin systems observed in the TOCSY spectrum) are indicated as bold bonds. Key HMBC correlations connecting independent spin systems are indicated by arrows.

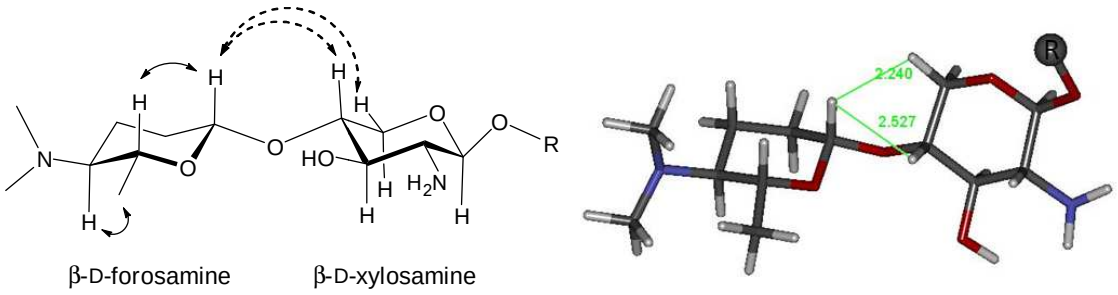

Fig. S51. Key intra-ring NOESY correlations (solid arrows) which, together with the observed coupling constants, allow stablishing the relative configuration of the forosamine residue. Key inter-ring NOESY correlations (dashed arrows) connecting both monosaccharides.The minimized molecular model for the disaccharide portion of **5** is in agreement with the key NOEs and further confirm the D- absolute configuration of the forosamine residue.

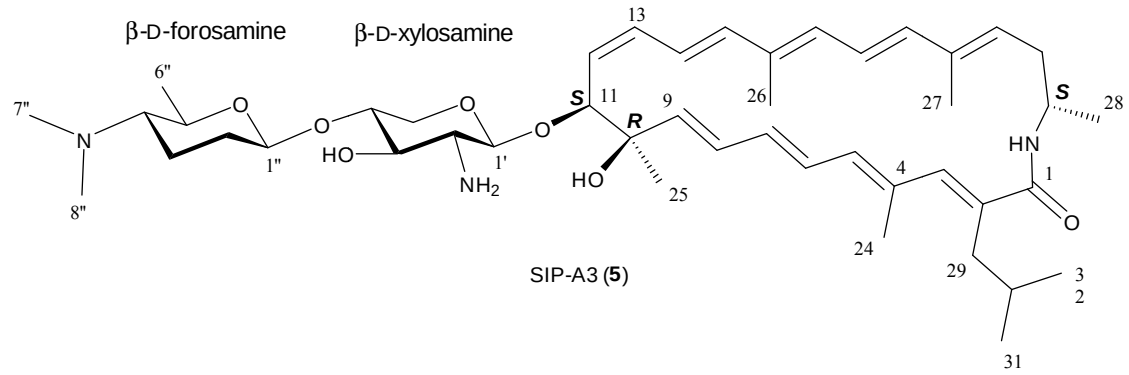

Fig. S52. Structure of SIP-A3 (**5**).

Table S5. ^{1}H and ^{13}C NMR data for SIP-A3 (**5**) in CD_3OD at °24 C.

Position	δ_C, type	δ_H (*J* in Hz)	Position	δ_C, type	δ_H (*J* in Hz)
1	174.2, C	-	1'	101.0, CH	4.73, d (7.8)
2	136.7, C	-	2'	57.4, CH	2.98, dd (9.3, 7.8)
3	138.6, CH	6.26, m	3'	71.7, CH	3.64, m
4	134.8, C	-	4'	77.7, CH	3.76, ddd (9.4, 8.3, 5.3)
5	136.6, CH	5.80, m	5'	64.2, CH_2	4.08, dd (12.4, 5.0) 3.33, dd (12.4, 9.6)
6	129.2, CH	6.49, dd (15.4, 11.5)	1"	101.0, CH	4.71, dd (9.4, 2.2)
7	136.2, CH	5.91, br t (11.2)	2"	30.7, CH_2	2.04, m 1.65, m
8	130.1, CH	6.27, m	3"	20.1, CH_2	2.15, m 1.85, br dd (12.6, 4.0)
9	141.2, CH	5.56, br d (15.8)	4"	66.4, CH	3.09, br td (9.7, 2.5)
10	76.5, C	-	5"	71.7, CH	3.90, dq (9.4, 6.2)
11	83.3, CH	4.42, m	6"	18.3, CH_3	1.40, d (6.2)
12	129.9, CH	5.47, m	7"	40.4, CH_3	2.82, br s
13	130.3, CH	6.14, m	8''	40.4, CH_3	2.82, br s
14	125.9, CH	6.13, m			
15	138.1, CH	6.24, m			
16	135.8, C	-			
17	132.8, CH	6.14, m			
18	124.5, CH	6.34, m			
19	138.6, CH	6.27, m			
20	137.5, C	-			
21	131.3, C	5.51, m			
22	37.4, CH_2	2.50, m 2.26, m			
23	47.2, CH	4.07, m			
24	16.2, CH_3	2.00, br s			
25	22.9, CH_3	1.49, br s			
26	12.8, CH_3	1.72, br s			
27	12.8, CH_3	1.76, br s			
28	20.6, CH_3	1.28, d (6.9)			
29	37.2, CH_2	2.56, m 2.31, m			
30	29.5, CH	1.65, m			
31	22.5, CH_3	0.88, d (6.4)			
32	22.5, CH_3	0.88, d (6.4)			
1-NH	-	7.40 br s*			

^{13}C chemical shifts obtained from HSQC and HMBC spectra.

* The amide proton exchanges very slowly and is clearly observed in the spectra.

Structure elucidation of sipanmycin B3 (6).

As expected, the UV (DAD) spectrum of **6** shows the typical absorbance pattern found for the sipanmycin family. Its molecular formula was established as $C_{46}H_{71}N_3O_7$ based on the observed ion $[M+H]^+$ at *m/z* 778.5363 (calcd. for $C_{46}H_{72}N_3O_7^+$ = 778.5365, Δm = 0.3 ppm). As the molecular formula difference found between sipanmycins A and B, compound **6** also contains one carbon atom and two hydrogen atoms more than SIP-A3 (**5**), suggesting it should correspond to the expected congener of SIP-A3 having a 2-methyl-1-butyl group rather than an isobutyl group as aliphatic substituent at C-2. The key in-source fragment ion at *m/z* = 142.1223, found also in SIP-A3, supports that **6** contains the same terminal forosamine monosaccharide residue. Comparison of the NMR data of **6** with those of SIP-A3 and sipanmycin B (SIP-B) reveals that **6** and SIP-A3 share the same disaccharide moiety while the macrolactam aglycon of **6** and SIP-B are, as expected, identical. The correlations observed in the set of 2D NMR spectra (COSY, NOESY, HSQC and HMBC) confirmed this structural determination. For obvious biosynthetic reasons, the absolute configuration of all chiral centers in **6** is the same as previously described for SIP-A3.

Compound **6** was trivially designated as sipanmycin B3 (SIP-B3).

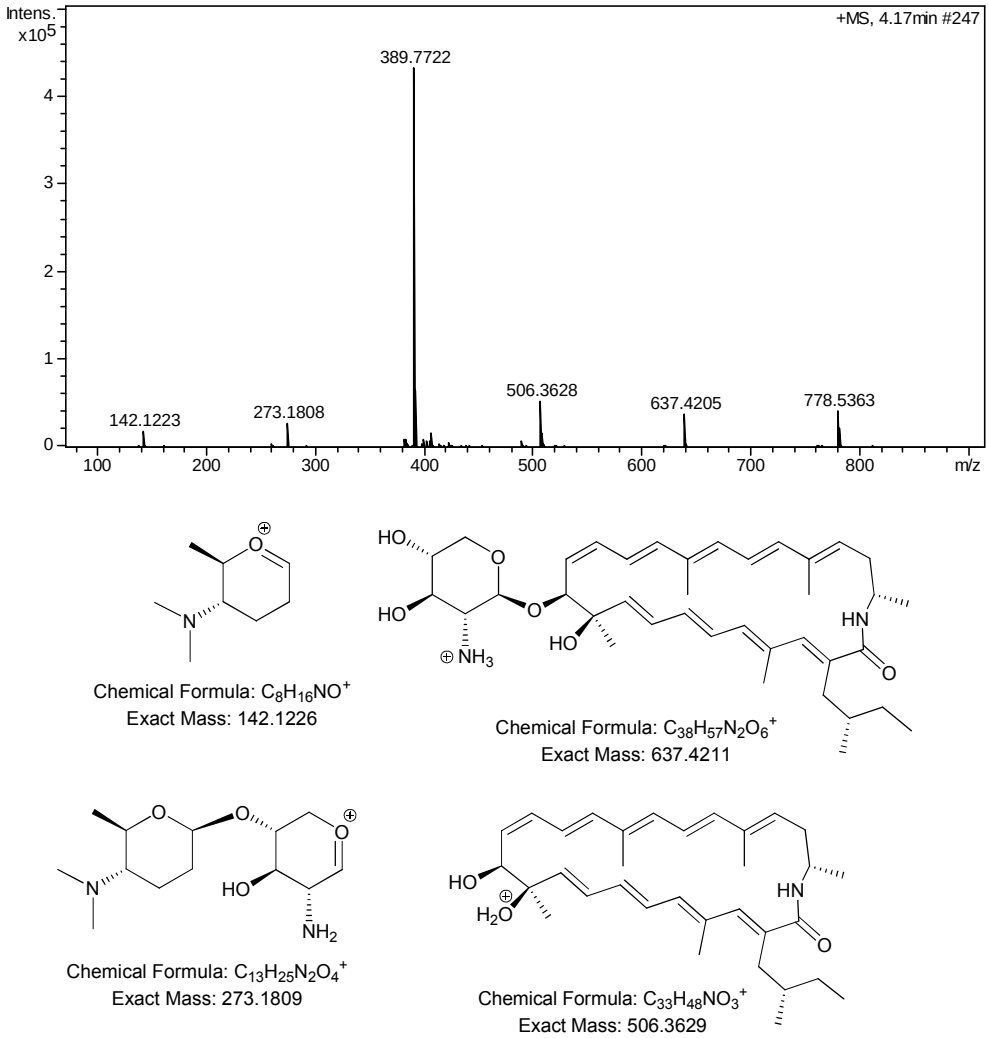

Fig. S53. HRMS spectrum of SIP-B3 (**6**) and identification of the key in-source fragment ions.

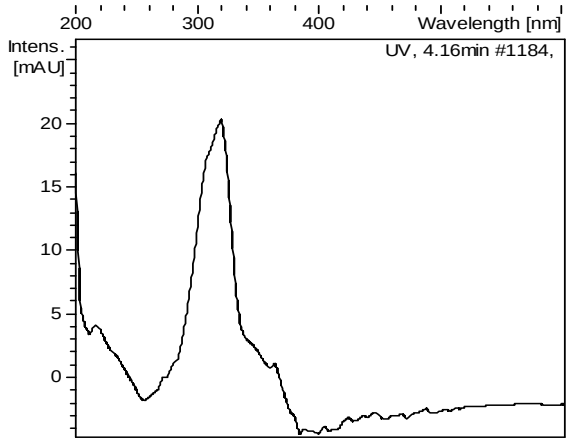

Fig. S54. UV-vis (DAD) spectrum of SIP-B3 (**6**)

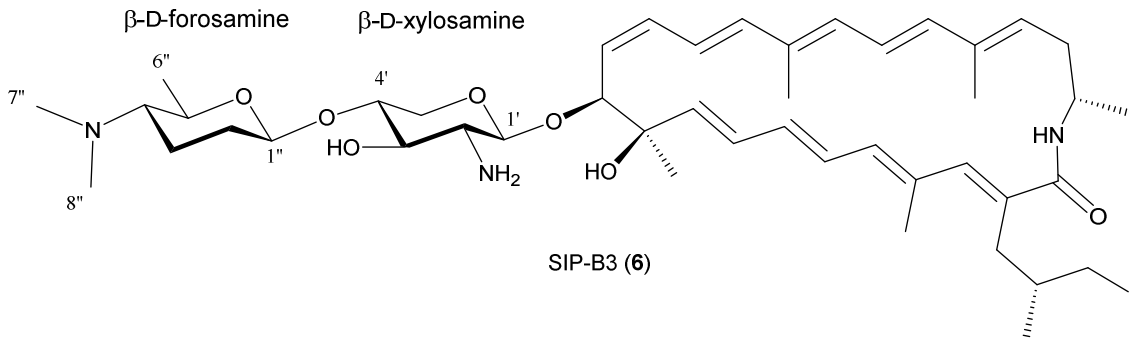

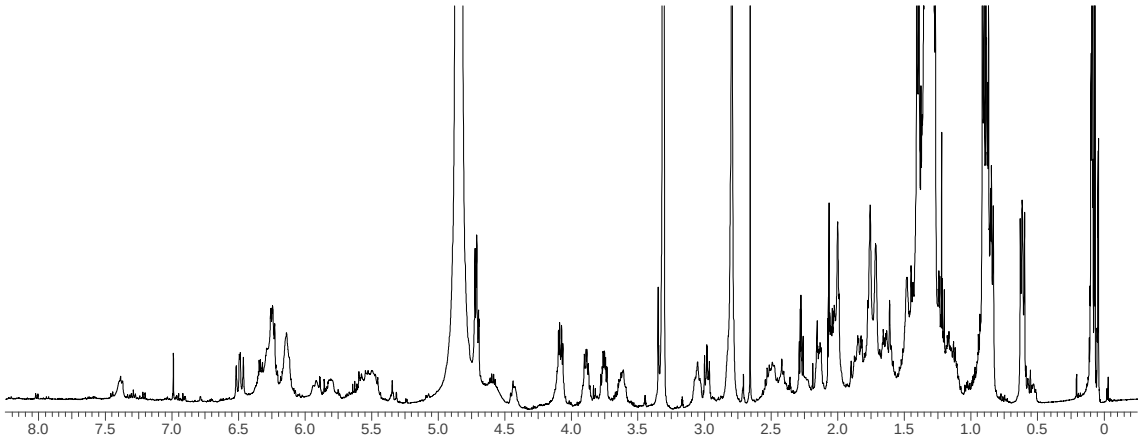

Fig. S55. ^{1}H NMR spectrum (CD_3OD, 500 MHz) of SIP-B3 (**6**).

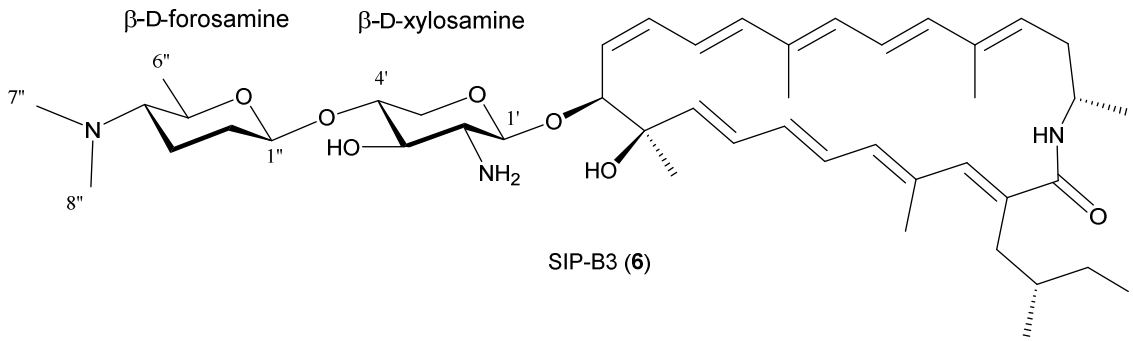

SIP-B3 (**6**)

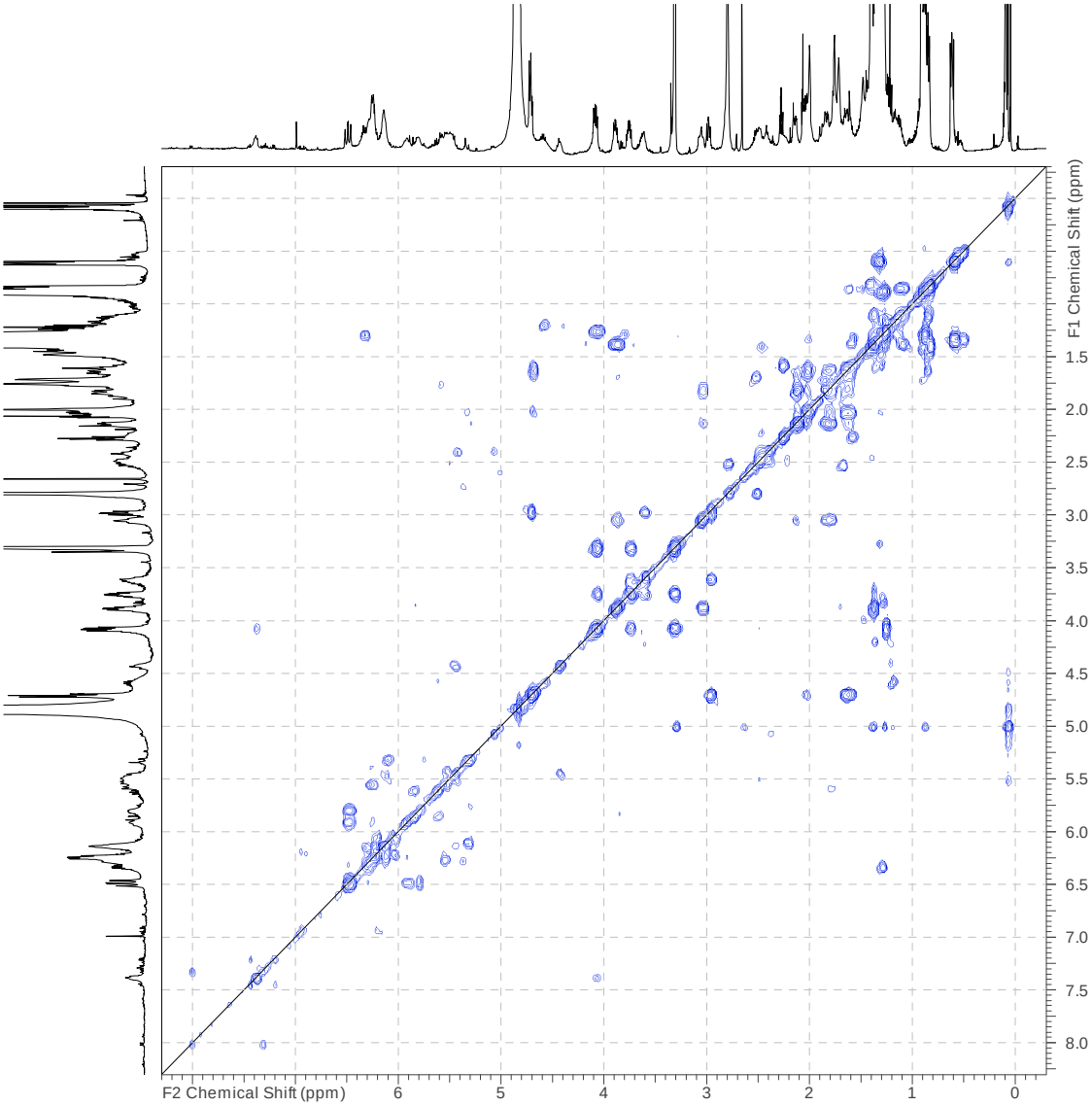

Fig. S56. COSY spectrum of SIP-B3 (**6**).

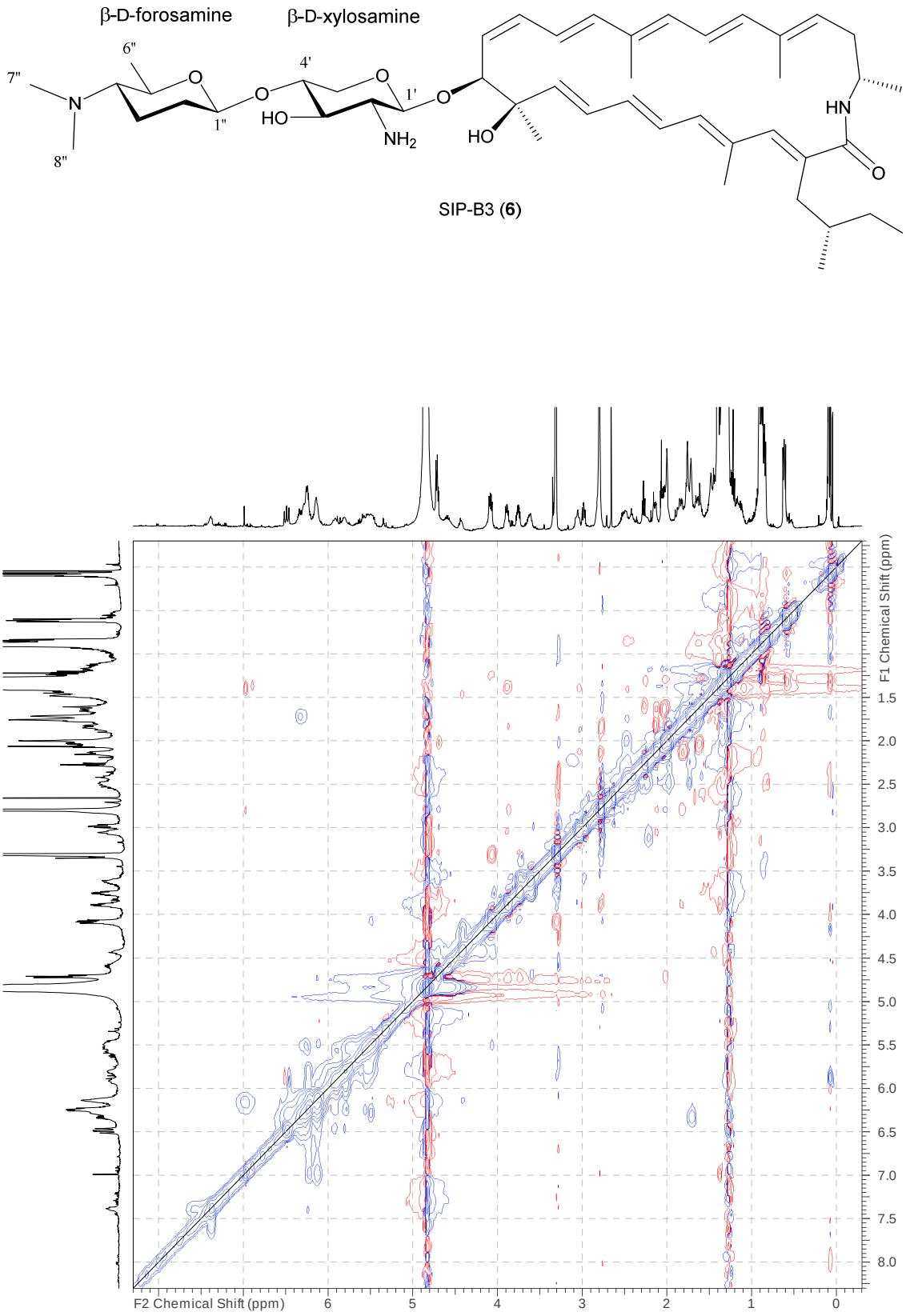

Fig. S57. NOESY spectrum of SIP-B3 (**6**).

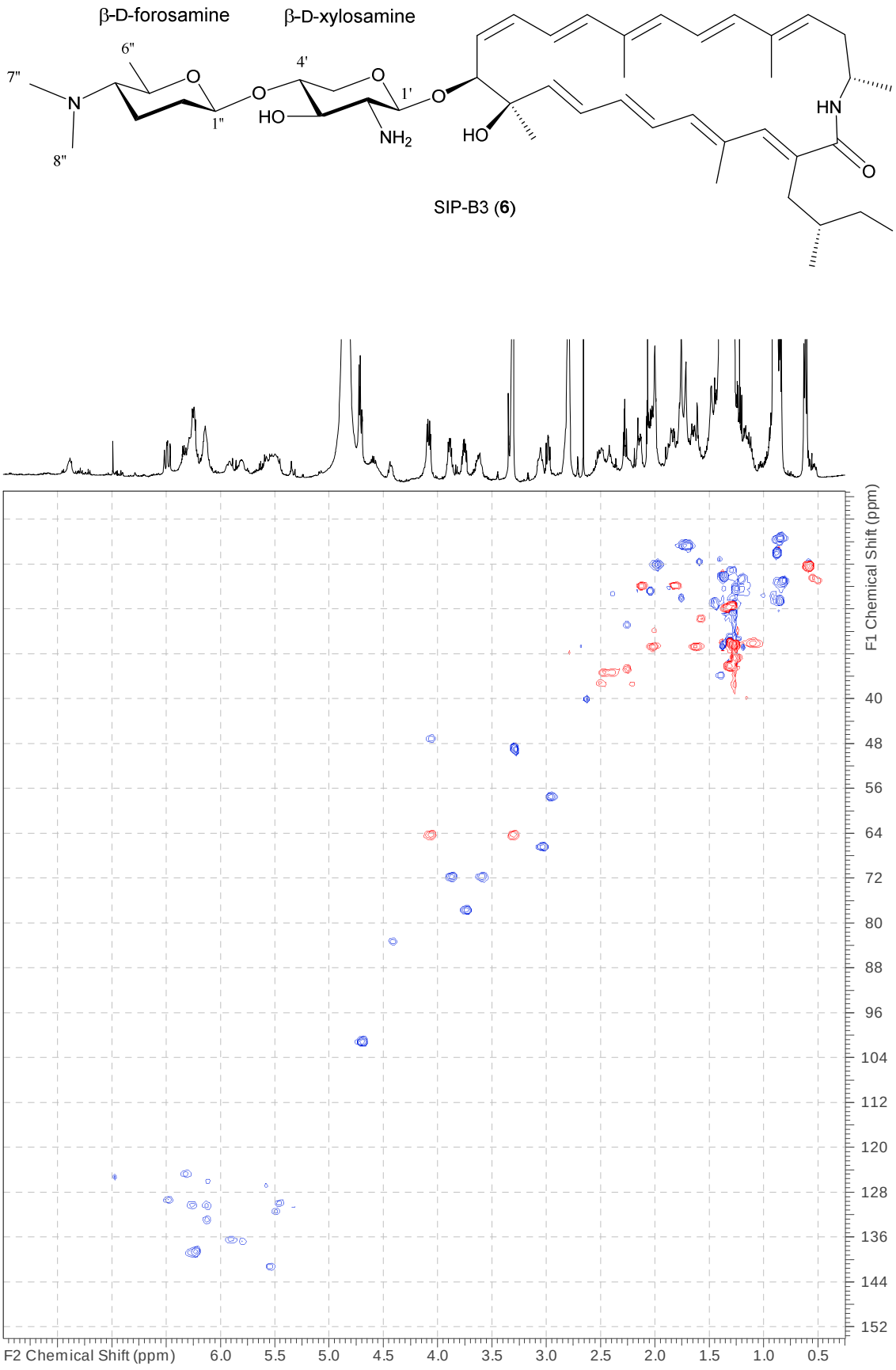

Fig. S58. Edited HSQC spectrum of SIP-B3 (**6**).

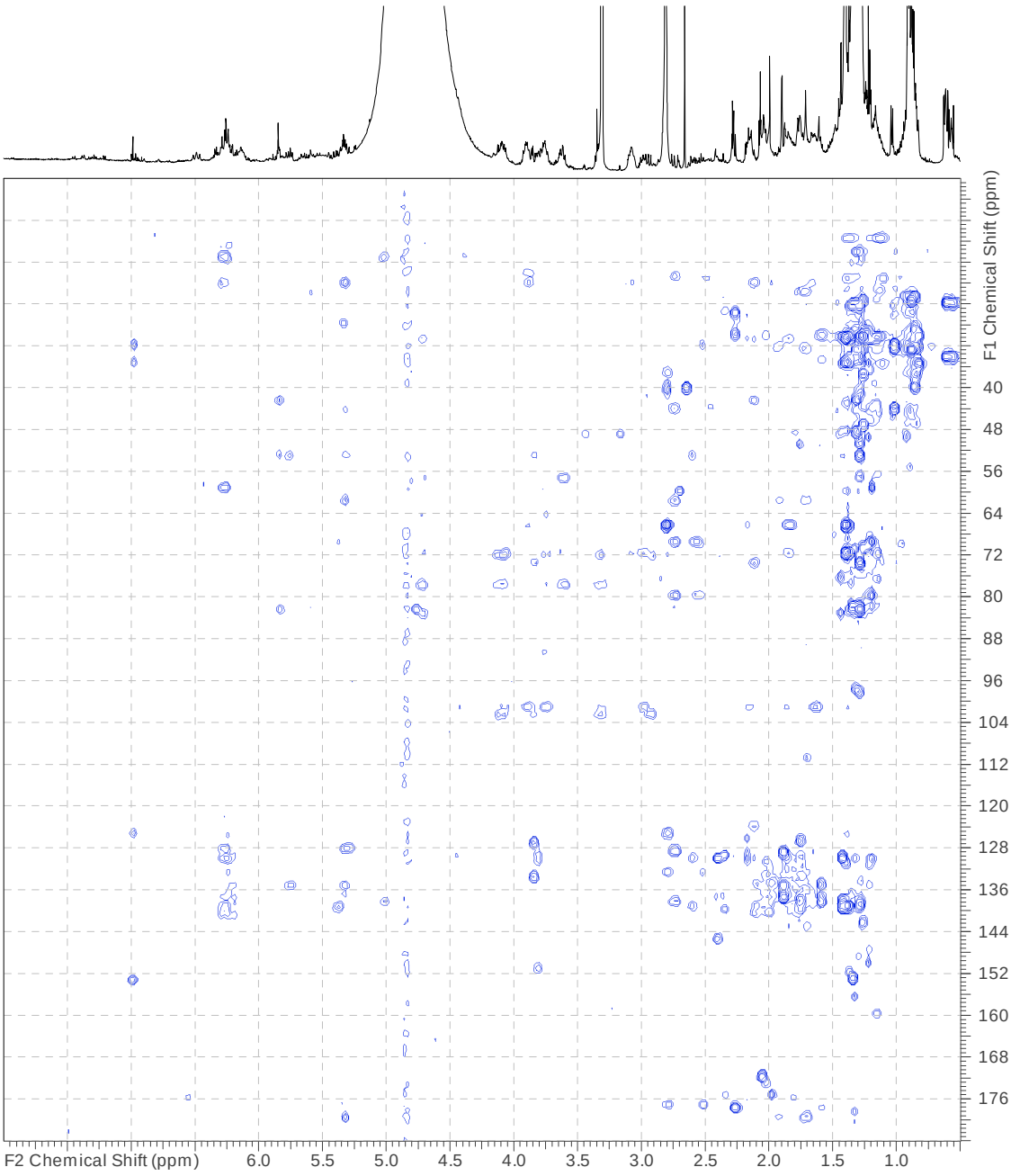

Fig. S59. HMBC spectrum of SIP-A3 (**5**).

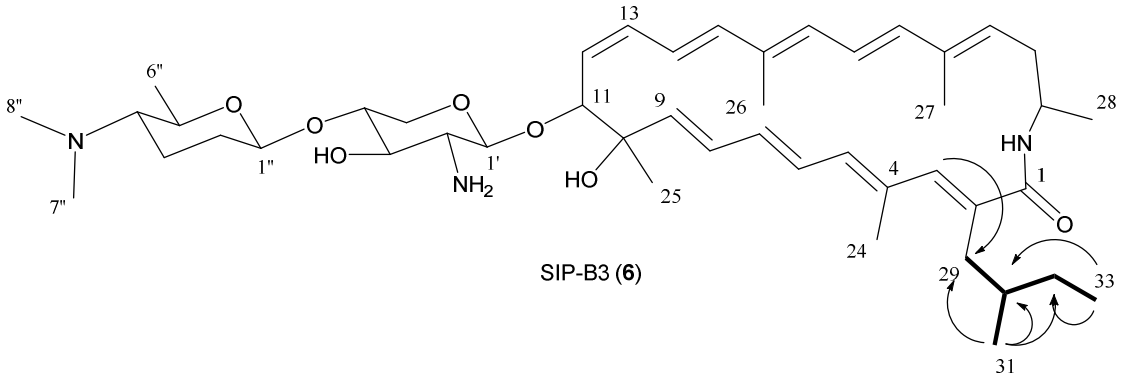

Fig. S60. Gross structure of SIP-B3 (**6**) determined by 2D-NMR and comparisons with SIP-A3 and SIP-B. Only the COSY correlations of the side chain at C-2 are shown as bold bonds. Key HMBC correlations of this side chain are indicated by arrows. The COSY and key HMBC correlations of the rest of the structure are identical to those of SIP-A3 (**5**) and are not shown.

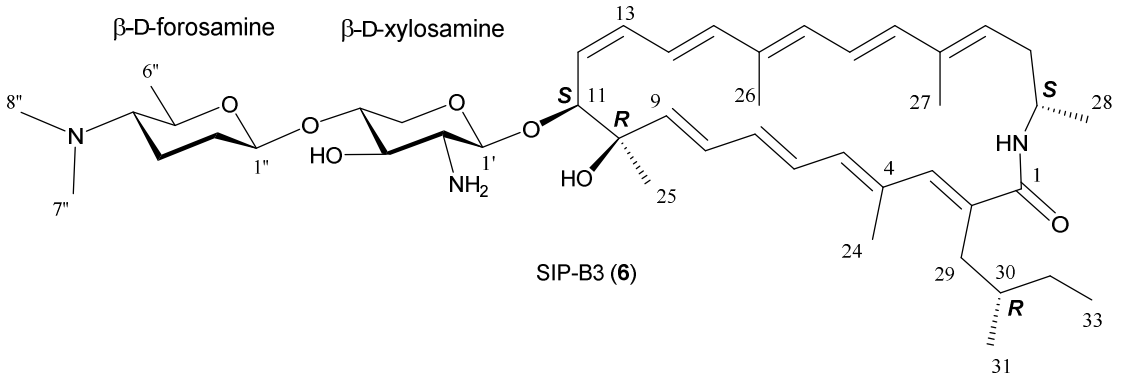

Fig. S61. Structure of SIP-B3 (**6**).

Table S6. ^{1}H and ^{13}C NMR data for SIP-B3 (**6**) in CD_3OD at 24 °C.

Position	δ_C, type	δ_H (*J* in Hz)	Position	δ_C, type	δ_H (*J* in Hz)
1	174.2, C	-	1'	101.0, CH	4.72, d (7.5)
2	136.7, C	-	2'	57.4, CH	2.98, dd (9.3, 7.8)
3	138.6, CH	6.26, m	3'	71.7, CH	3.64, m
4	134.8, CH	-	4'	77.7, CH	3.76, ddd (9.4, 8.3, 5.3)
5	136.6, CH	5.80, m	5'	64.2, CH_2	4.08, dd (12.4, 5.0) 3.32, m
6	129.2, CH	6.49, dd (15.4, 11.5)	1"	101.0, CH	4.71, dd (9.4, 2.2)
7	136.2, CH	5.91, br t (11.2)	2"	30.7, CH_2	2.04, m 1.65, m
8	130.1, CH	6.27, m	3"	20.1, CH_2	2.15, m 1.85, br dd (12.6, 4.0)
9	141.2, CH	5.56, m	4"	66.4, CH	3.09, br td (9.7, 2.5)
10	76.5, C	-	5"	71.7, CH	3.89, dq (9.4, 6.2)
11	83.3, CH	4.42, m	6"	18.3, CH_3	1.40, d (6.2)
12	129.9, CH	5.47, m	7"	40.4, CH_3	2.79, br s
13	130.3, CH	6.14, m	8''	40.4, CH_3	2.79, br s
14	125.9, CH	6.13, m			
15	138.1, CH	6.24, m			
16	135.8, C	-			
17	132.8, CH	6.14, m			
18	124.5, CH	6.34, m			
19	138.6, CH	6.27, m			
20	137.5, C	-			
21	131.3, CH	5.51, m			
22	37.4, CH_2	2.50, m 2.26, m			
23	47.2, CH	4.07, m			
24	16.2, CH_3	2.00, br s			
25	22.9, CH_3	1.49, br s			
26	12.8, CH_3	1.72, br s			
27	12.8, CH_3	1.76, br s			
28	20.6, CH_3	1.28, d (6.9)			
29	34.3, CH_2	2.48, m 2.41, m			
30	34.8, CH	1.41, m			
31	17.9, CH_3	0.84, d (6.4)			
32	29.0, CH_2	1.12, m			
33	10.4, CH_3	0.86, m			
1-NH	-	7.39, br s*			

^{13}C chemical shifts obtained from HSQC and HMBC spectra.

* The amide proton exchanges very slowly and is clearly observed in the spectra.

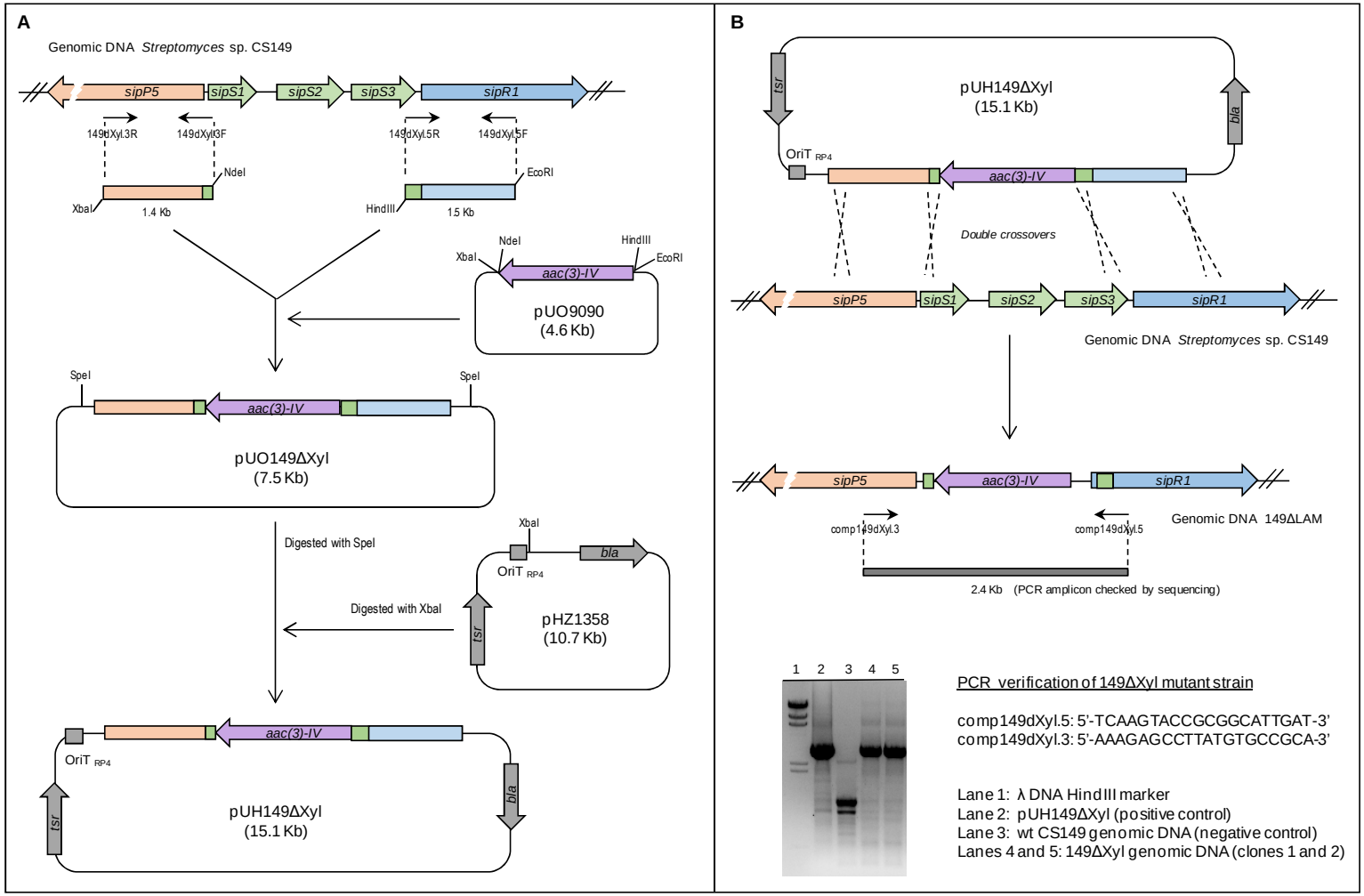

Fig. S62. Generation of 149ΔXyl mutant strain. A: construction of the conjugative plasmid pUH149ΔXyl. *aac(3)IV*, apramycin resistance marker; *bla*, β-lactamase resistance marker; *tsr*, thiostrepton resistance marker; oriT$_{RP4}$, origin of transfer of plasmid RP4. B: Schematic representation of double crossover events in 149ΔXyl mutant strain. Data for verification of the mutant strain by PCR are also shown.

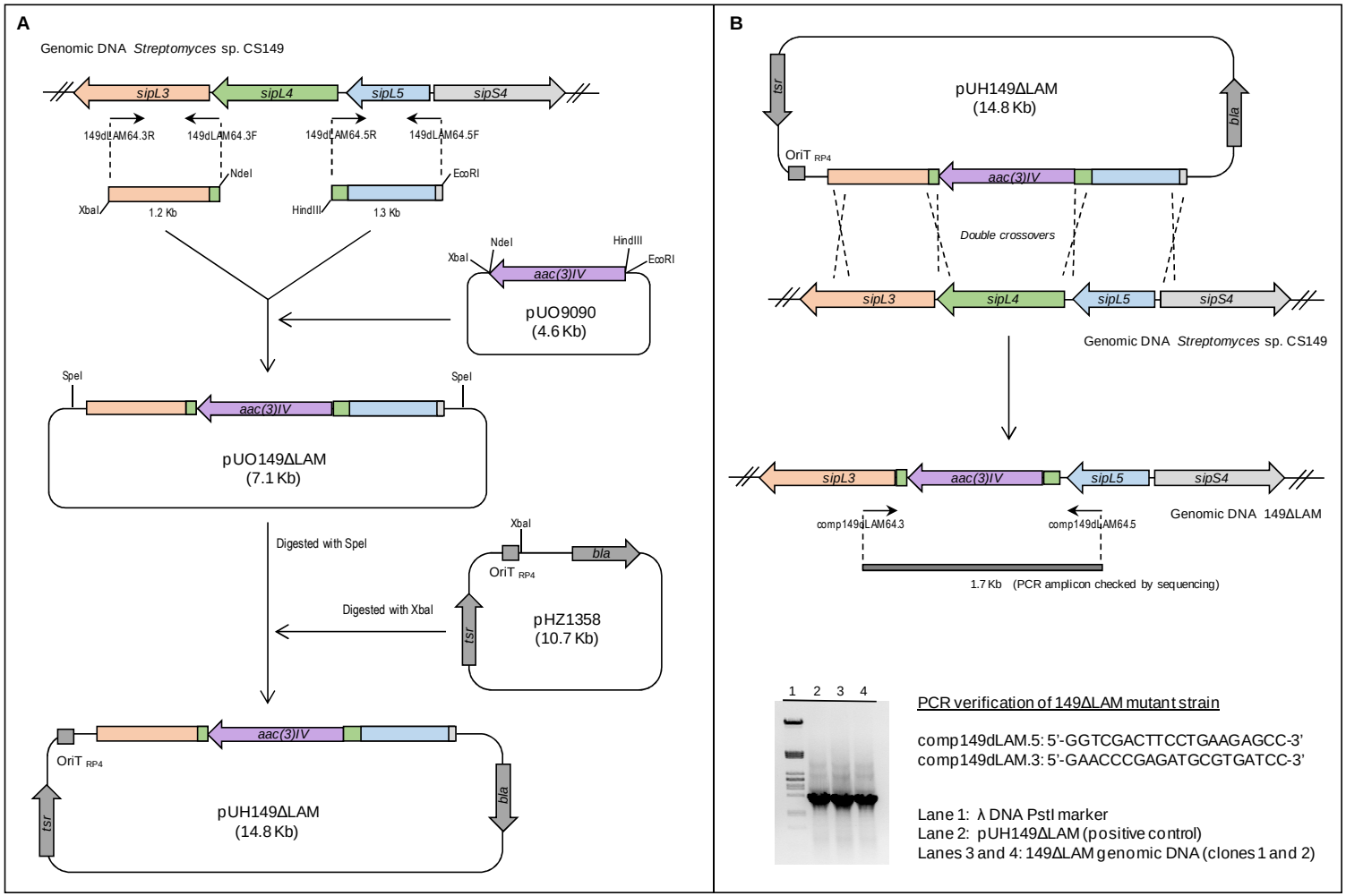

Fig. S63. Generation of 149ΔLAM mutant strain. A: construction of the conjugative plasmid pUH149ΔLAM. *aac(3)IV*, apramycin resistance marker; *bla*, β-lactamase resistance marker; *tsr*, thiostrepton resistance marker; oriT$_{RP4}$, origin of transfer of plasmid RP4. B: Schematic representation of double crossover events in 149ΔLAM mutant strain. Data for verification of the mutant strain by PCR are also shown.

Structure elucidation of sipanmycin C (7).

The UV (DAD) spectrum of **7** shows the characteristic absorbance pattern of sipanmycins. Its molecular formula was established as $C_{47}H_{73}N_3O_8$ based on the observed ion $[M+H]^+$ at *m/z* 808.5475 (calcd. for $C_{47}H_{74}N_3O_8^+$ = 808.5470, Δm = 0.6 ppm). This formula is identical to that of sipanmycin B (SIP-B) [3] and the observed in-source fragment ions at *m/z* = 172.1331, *m/z* = 303.1914 and *m/z* = 506.3637 also match those observed for SIP-B suggesting identical disaccharide moiety and macrolactam aglycon. However, comparison of the NMR data of **7** and SIP-B revealed that although the signals of the disaccharide portion are essentially identical for both compounds there are few but important differences for the aglycon. Interestingly, comparison with the NMR data of SIP-A also reveals essentially identical signals for the sugars and the aglycon with the exception that the C-28 methyl of SIP-A is not observed in **7** but signals for a new methylene and a new methyl group appear suggesting that the aliphatic substituent at C-23 (a methyl group in SIP-A) is different in **7**. An ethyl group substituent at C-23 rather than a methyl group (as found in native SIP-A and SIP-B) perfectly accounts for the molecular formula of **7** and the mentioned differential NMR features. The key correlations observed in the 2D NMR spectra (COSY, TOCSY and HMBC) unambiguously established that the substituent at C-2 corresponds to an ethyl group. This new ethyl substituent at C-23 is the consequence of replacing the native starter unit, (*S*)-3-aminobutanoic acid (derived from β-glutamic acid) [1], by 3-aminopentanoic acid in the 149ΔLAM mutant (see main text). Although the culture was fed with racemic 3-aminopentanoic acid only the *S* enantiomer is recognized by SipL1 (the first enzyme involved in the processing of the β-amino acid employed for the biosynthesis of the polyketide starter unit [1]) as demonstrated for its homolog (in the

incednine biosynthesis cluster) IdnL1 [13]. Thus, the absolute configuration at C-23 of **7** must be the same found for SIP-A and SIP-B [3].

Compound **7** corresponds to 28-methylsipanmycin A and was trivially designated as sipanmycin C (SIP-C).

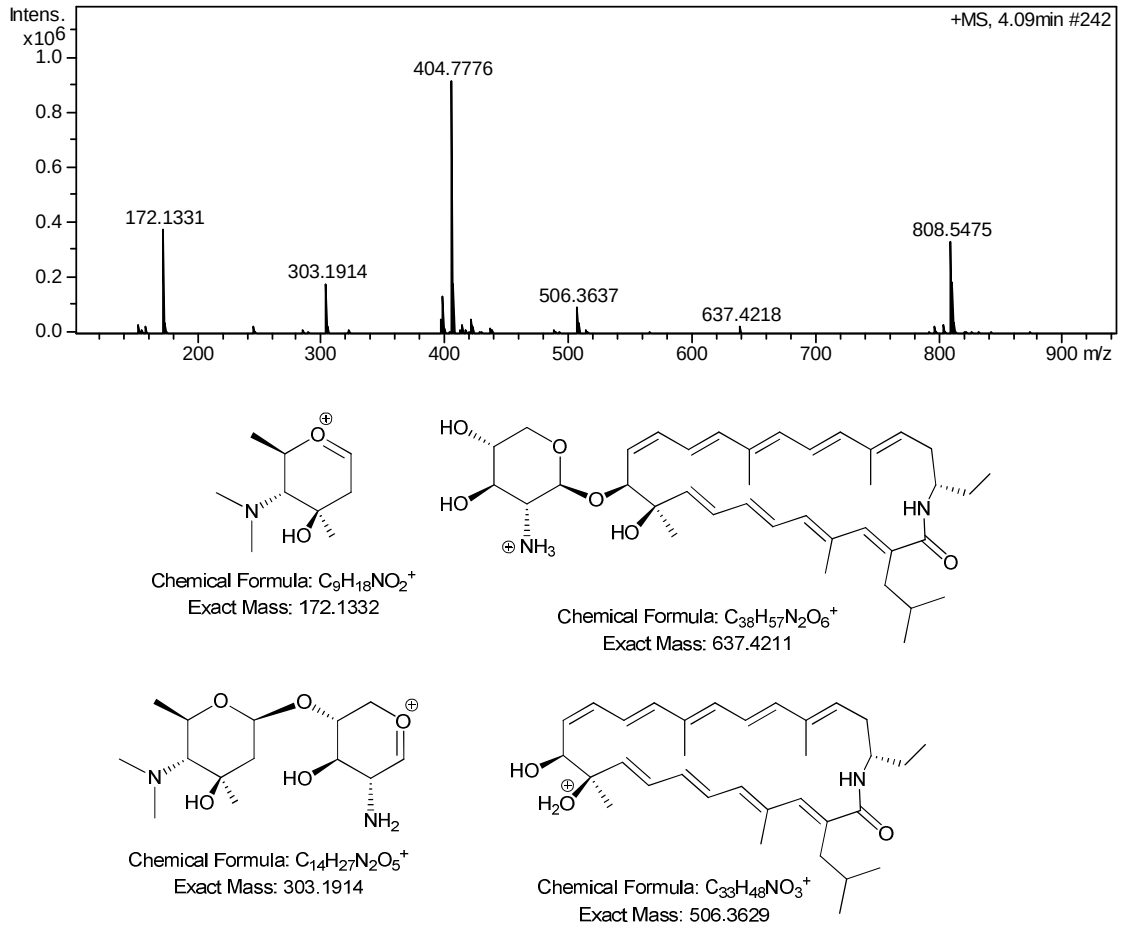

Fig. S64. HRMS spectrum of SIP-C (**7**) and identification of the key in-source fragment ions.

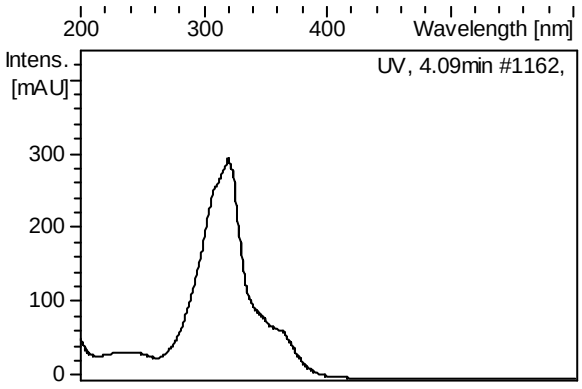

Fig. S65. UV-vis (DAD) spectrum of SIP-C (**7**).

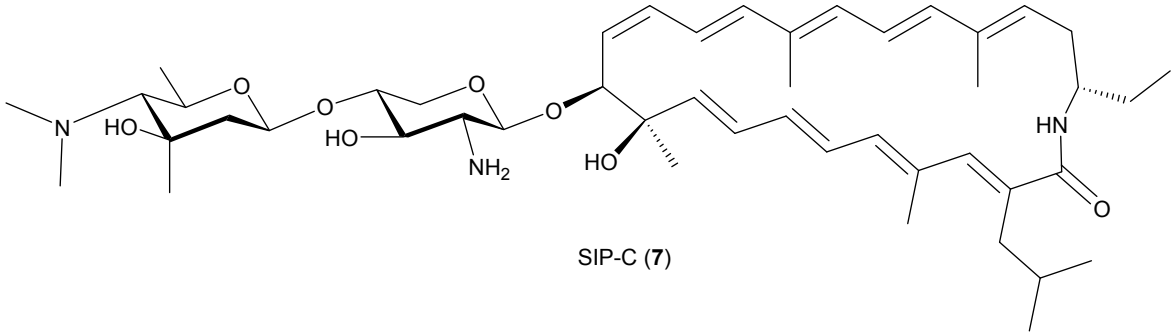

SIP-C (**7**)

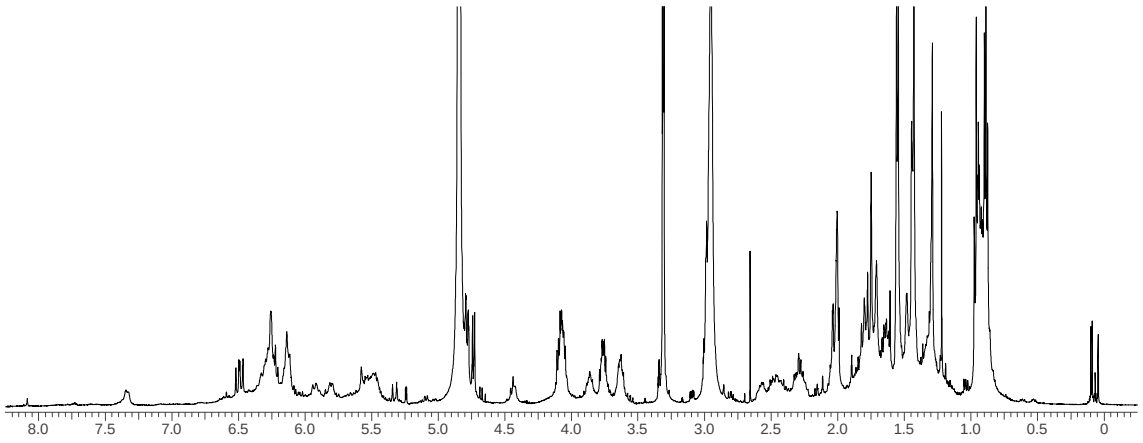

Fig. S66. ^{1}H NMR spectrum (CD_3OD, 500 MHz) of SIP-C (**7**).

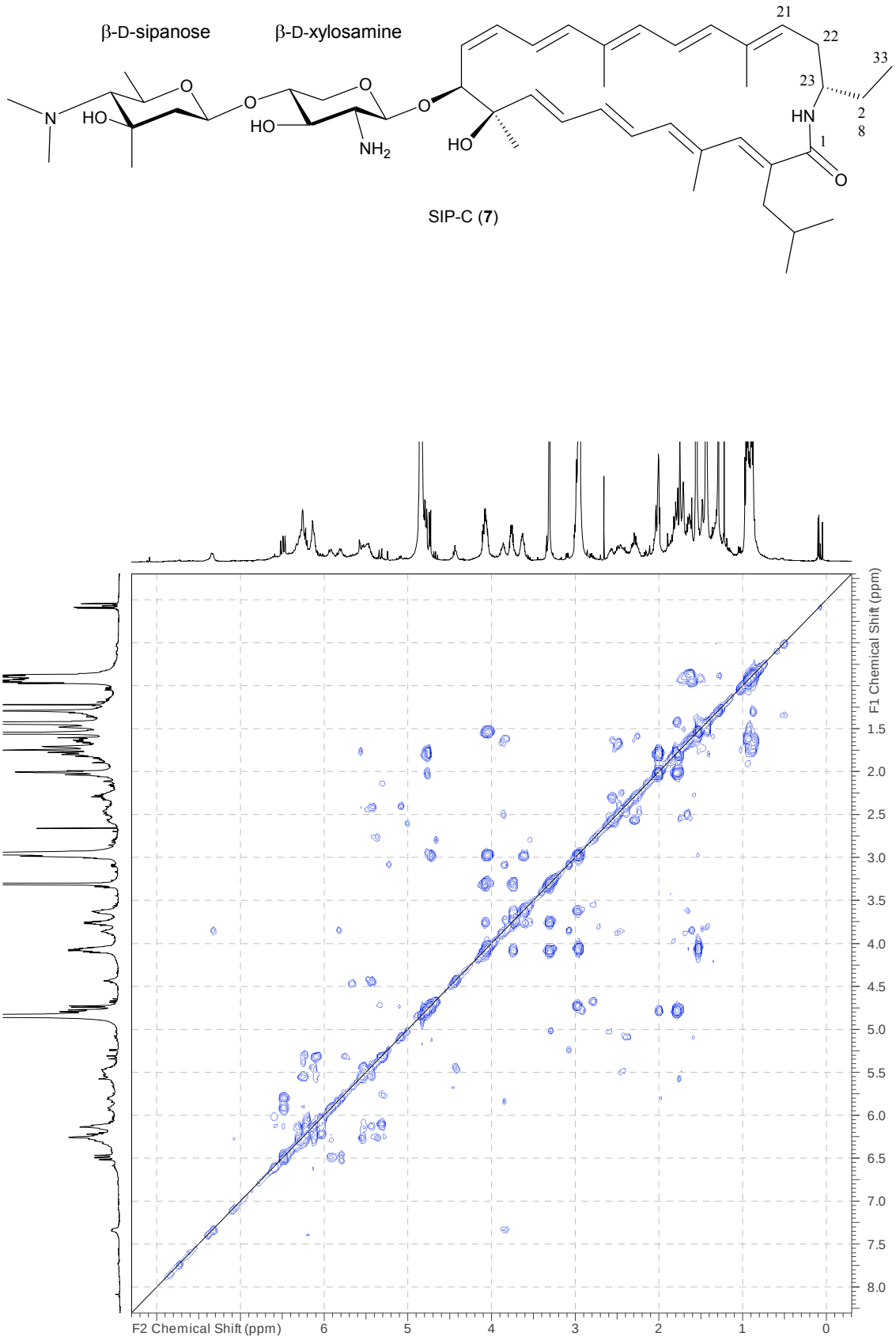

Fig. S67. COSY spectrum of SIP-C (**7**).

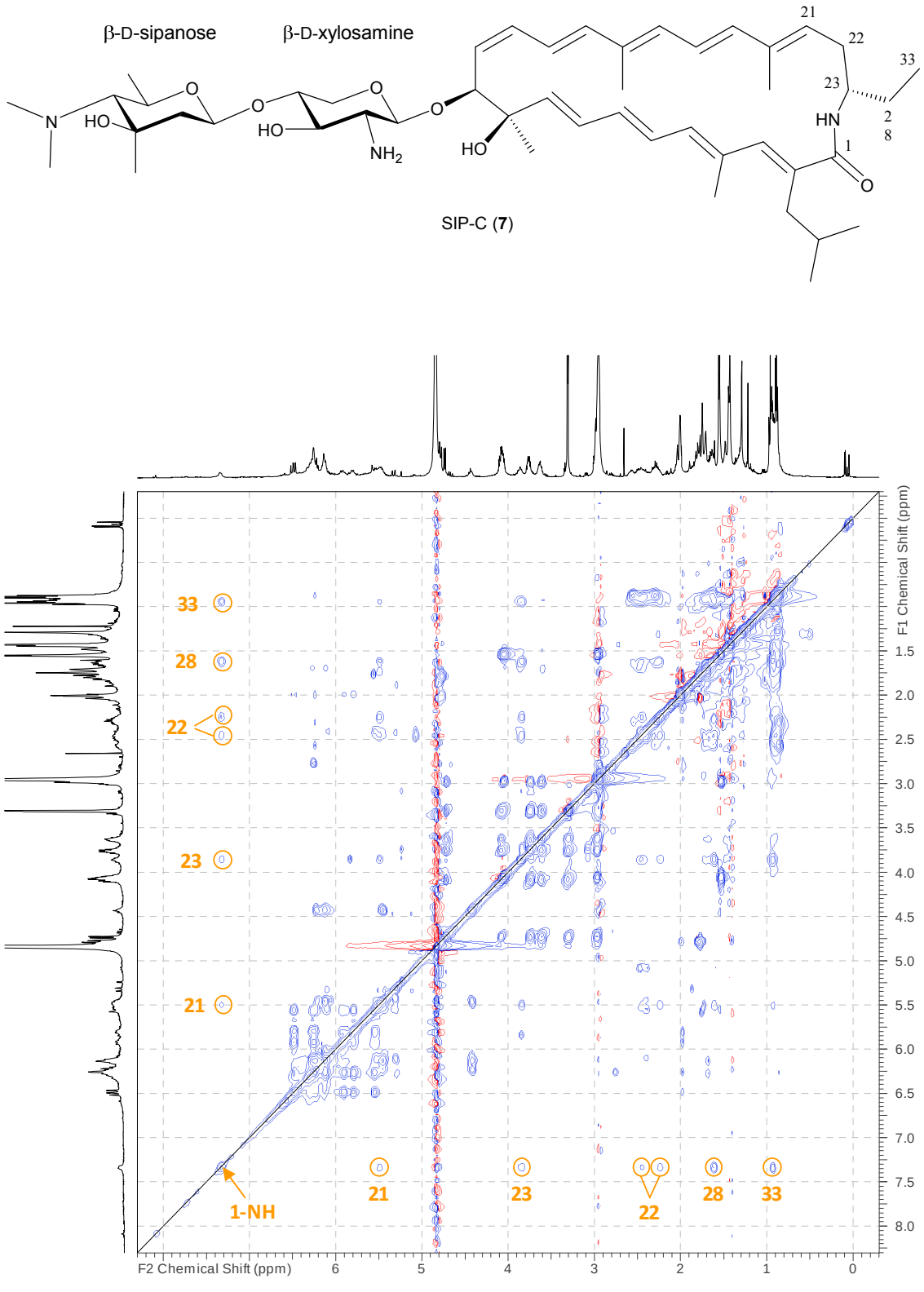

Fig. S68. TOCSY spectrum of SIP-C (**7**). Key correlations of the spin system involving the new ethyl substituent at C-23 are highlighted. The corresponding proton signal at the diagonal is indicated by an arrow.

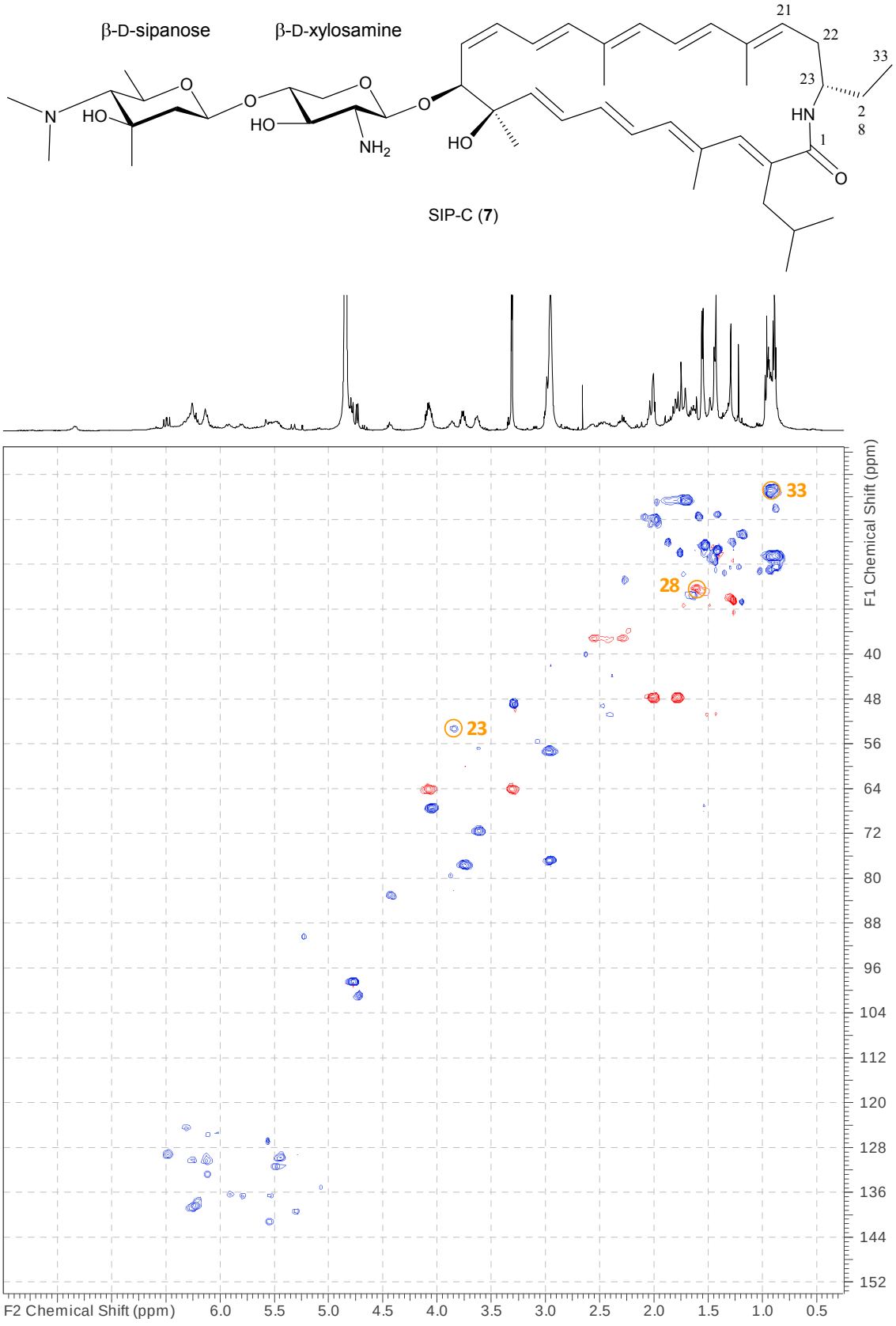

Fig. S69. Edited HSQC spectrum of SIP-C (**7**). Key correlations related with the new ethyl substituent at C-23 are highlighted.

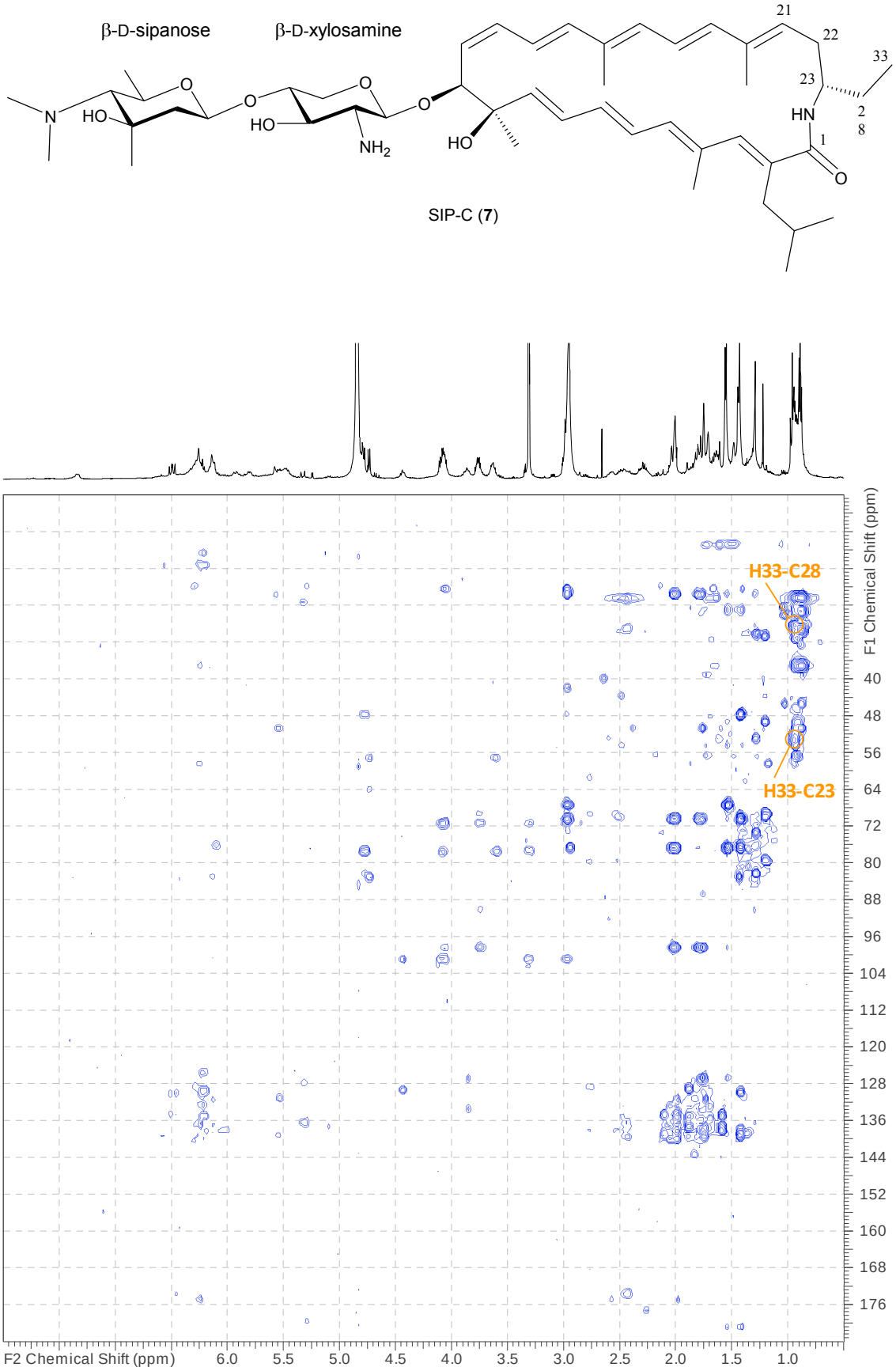

Fig. S70. HMBC spectrum of SIP-C (**7**). Key correlations related with the new ethyl substituent at C-23 are highlighted.

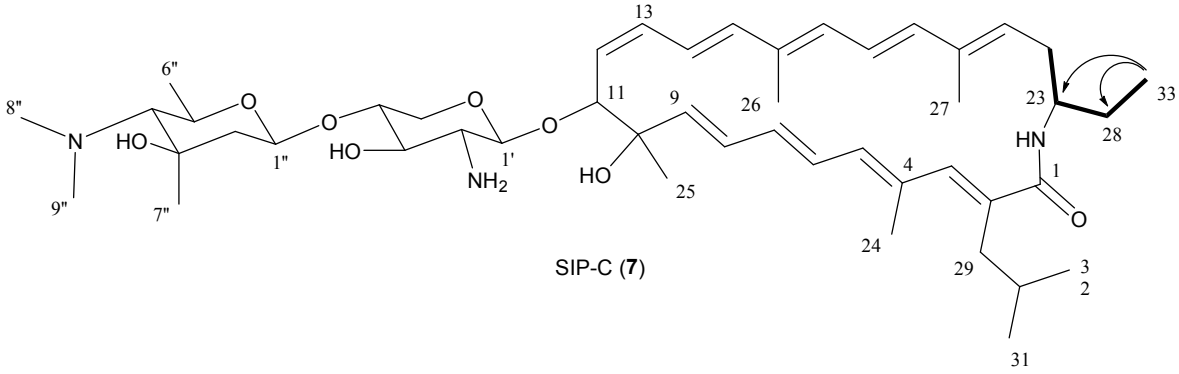

Fig. S71. Gross structure of SIP-C (**7**) determined by 2D NMR and comparisons with the NMR data of SIP-A. Only the COSY/TOCSY correlations (shown as bold bonds) of the spin system containing the new ethyl substituent at C-23 are displayed. The key HMBC correlations arising from the H-33 methyl protons are indicated by arrows.

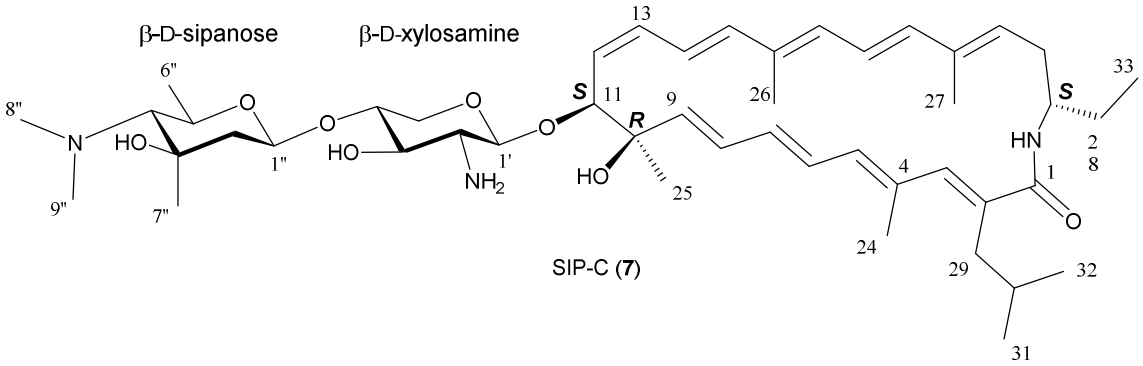

Fig. S72. Structure of SIP-C (**7**).

Table S7. ^{1}H and ^{13}C NMR data for SIP-C (**7**) in CD_3OD at 24 °C.

Position	δ_C, type	δ_H (*J* in Hz)	Position	δ_C, type	δ_H (*J* in Hz)
1	174.2, C	-	1'	100.9, CH	4.73, d (7.8)
2	n.d., C	-	2'	57.4, CH	2.99, m
3	138.6, CH	6.26, m	3'	71.6, CH	3.63, m
4	134.8, C	-	4'	77.7, CH	3.76, ddd (9.0, 8.5, 5.4)
5	136.6, CH	5.80, m	5'	64.4, CH_2	4.09, m 3.32, m
6	129.2, CH	6.49, dd (14.7, 11.5)	1"	98.5, CH	4.79,br d (9.8)
7	136.2, CH	5.91, m	2"	47.9, CH_2	2.03, br d (12.4) 1.80, m
8	130.1, CH	6.27, m	3"	n. d., C	-
9	141.2, CH	5.56, m	4"	76.9, CH	2.98, m
10	76.5, C	-	5"	67.6, CH	4.06, m
11	83.3, CH	4.42, m	6"	20.7, CH_3	1.55, m
12	129.9, CH	5.47, m	7"	21.8, CH_3	1.43, m
13	130.3, CH	6.14, m	8''	n. d., CH_3	2.65, s
14	125.8, CH	6.13, m	9''	n. d., CH_3	2.65, s
15	138.1, CH	6.24, m			
16	135.8, C	-			
17	132.8, CH	6.14, m			
18	124.4, CH	6.34, m			
19	138.6, CH	6.27, m			
20	137.5, C	-			
21	131.3, C	5.51, m			
22	36.2, CH_2	2.47, m 2.26, m			
23	53.5, CH	3.86, m			
24	16.2, CH_3	2.00, br s			
25	22.9, CH_3	1.49, br s			
26	12.8, CH_3	1.72, br s			
27	12.8, CH_3	1.76, br s			
28	28.5, CH_2	1.64, m			
29	37.2, CH_2	2.56, m 2.31, m			
30	29.5, CH	1.65, m			
31	22.5, CH_3	0.88, m			
32	22.5, CH_3	0.88, m			
33	11.3, CH_3	0.95, t (7.2)			
1-NH	-	7.35 br s*			

^{13}C chemical shifts obtained from HSQC and HMBC spectra.

* The amide proton exchanges very slowly and is clearly observed in the spectra.

Structure elucidation of sipanmycin D (8).

The UV (DAD) spectrum of **8** shows the expected sipanmycin absorbance pattern. Its molecular formula was established as $C_{48}H_{75}N_3O_8$ based on the observed ion $[M+H]^+$ at *m/z* = 822.5630 (calcd. for $C_{48}H_{76}N_3O_8^+$ = 822.5627, Δm = 0.4 ppm). This molecular formula contains one carbon atom and two hydrogen atoms more than that of SIP-C (**7**), suggesting it should correspond to the expected congener of SIP-C having a 2-methyl-1-butyl group rather than an isobutyl group as aliphatic substituent at C-2. The key in-source fragment ions at *m/z* = 172.1332 and *m/z* = 303.1915, found also in SIP-C, SIP-A and SIP-B, supports that **7** contains the same disaccharide moiety as the native sipanmycins and SIP-C. The fragment ion at *m/z* = 520.3794 indicates that the extra "CH_2", compared to SIP-C, must be localized in the macrolactam aglycon. Although the NMR spectra (1D ^{1}H and HSQC) quality was poor for the sample used, comparison of the HSQC spectrum of **8** with those of SIP-C and SIP-B unambiguously confirmed the expected structure, identical to SIP-C but having a 2-methyl-1-butyl group substituent at C-2 (as found in SIP-B).

Compound **8** was trivially designated as sipanmycin D (SIP-D).

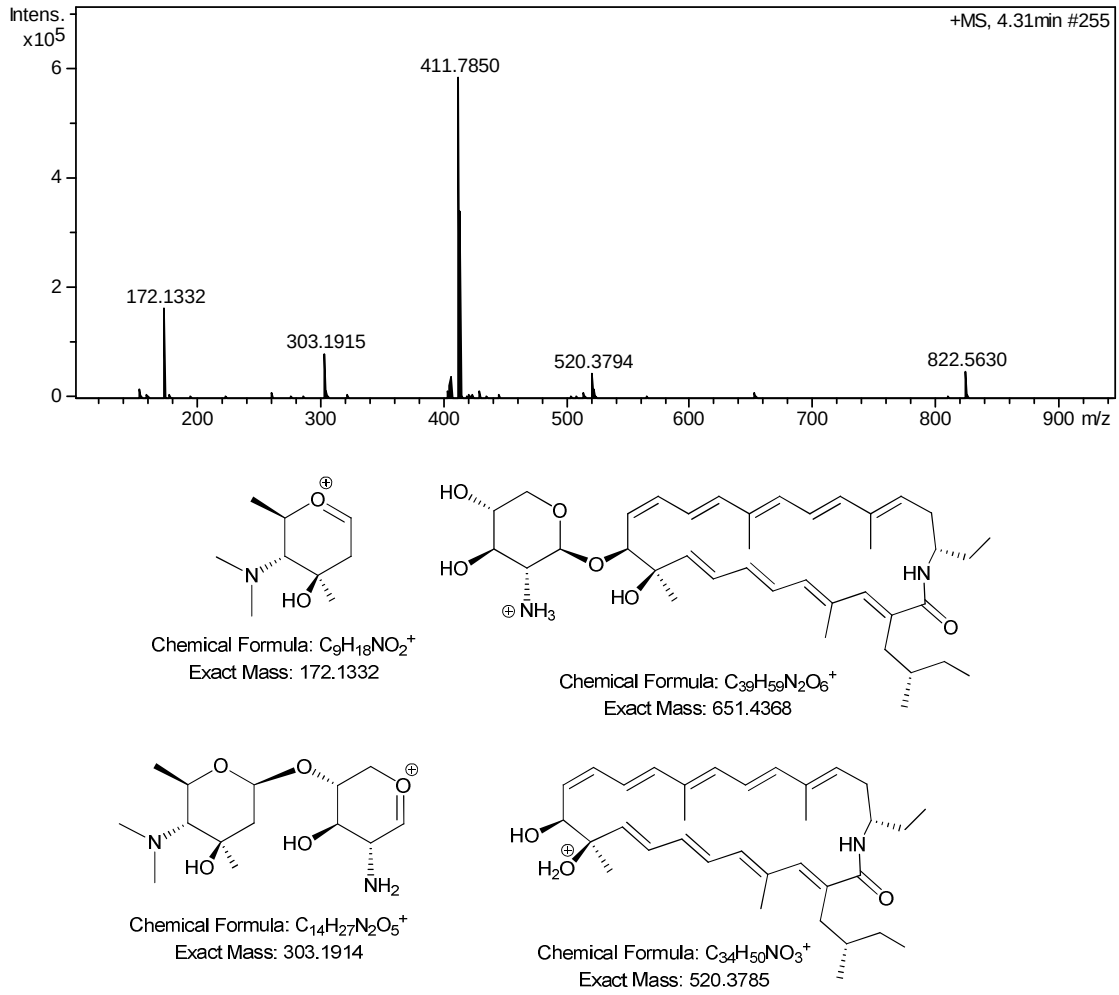

Fig. S73. HRMS spectrum of SIP-D (**8**) and identification of the key in-source fragment ions.

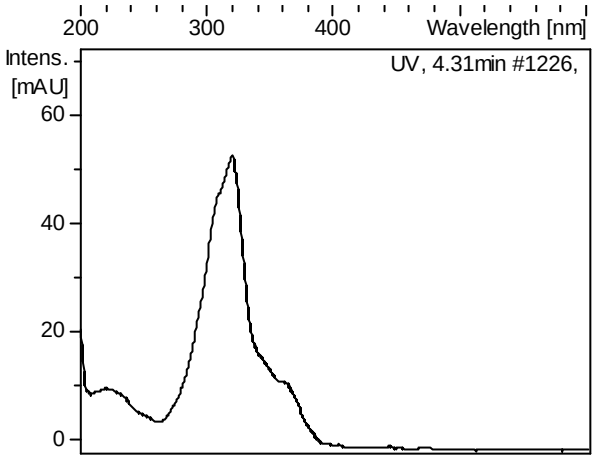

Fig. S74. UV-vis (DAD) spectrum of SIP-D (**8**)

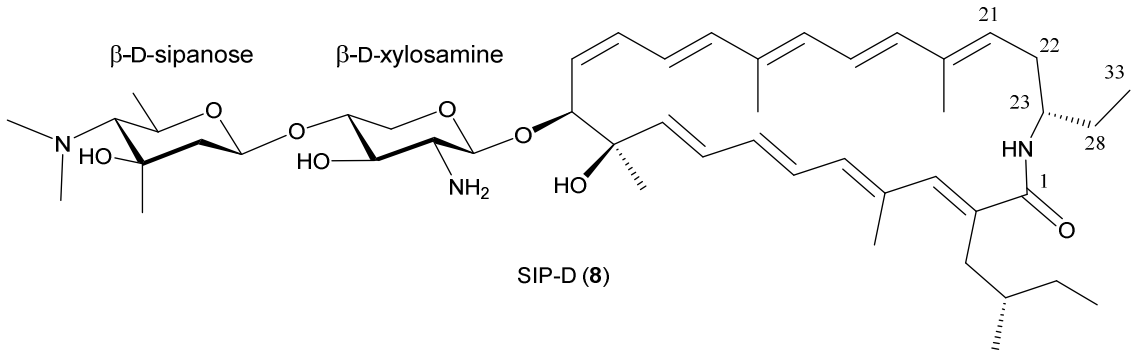

SIP-D (**8**)

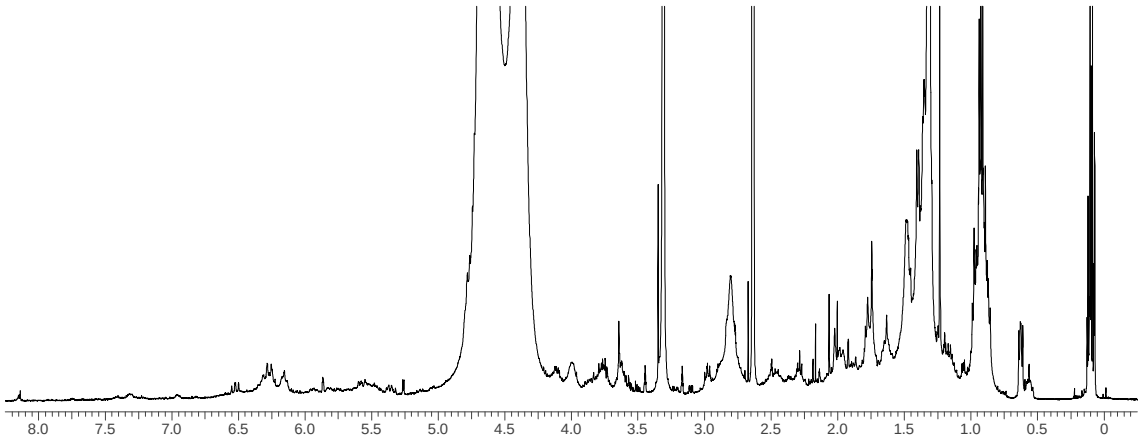

Fig. S75. ^{1}H NMR spectrum (CD_3OD, 500 MHz) of SIP-D (**8**).

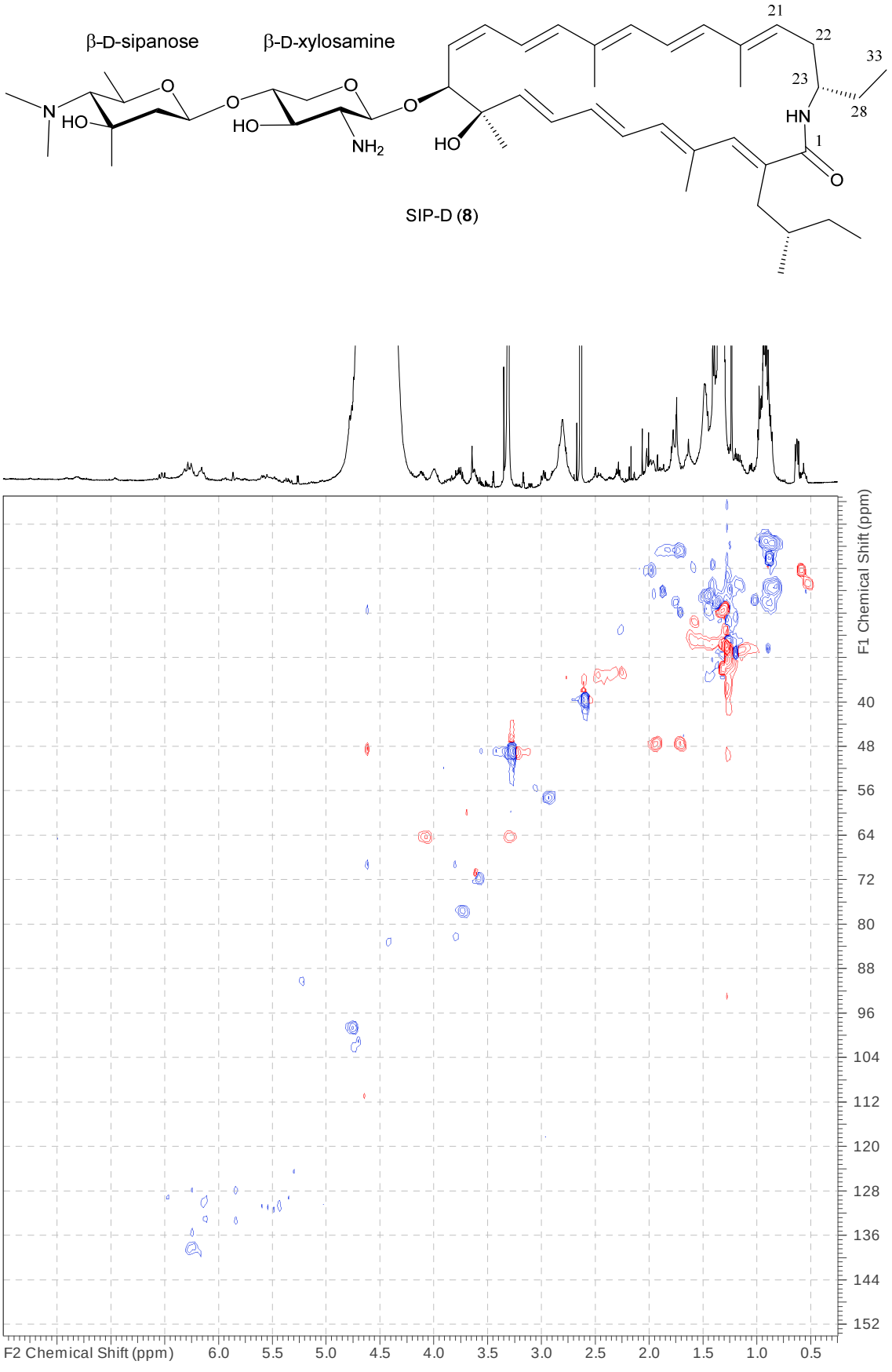

Fig. S76. Edited HSQC spectrum of SIP-D (**7**).

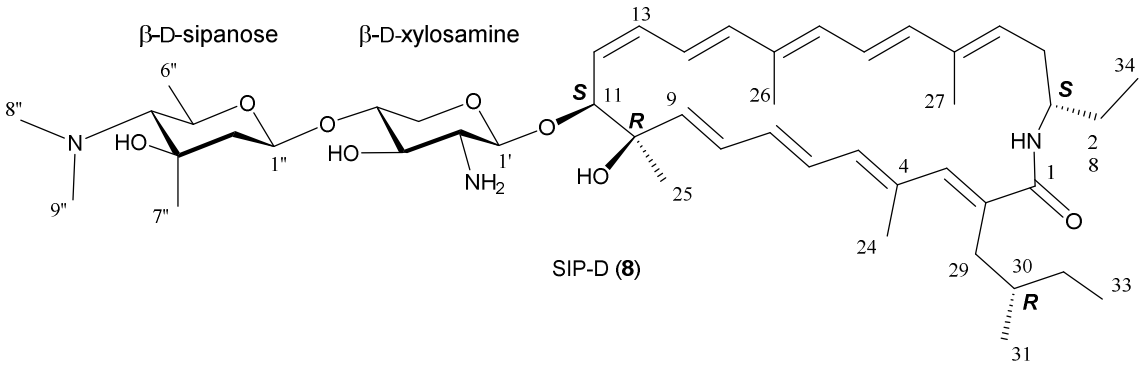

Fig. S77. Structure of SIP-D (**8**).

Table S8. ^{1}H and ^{13}C NMR data for SIP-D (**8**) in CD_3OD at 24 °C.

Position	δ_C, type	δ_H	Position	δ_C, type	δ_H
1	n.d., C	-	1'	100.9, CH	4.73
2	n.d., C	-	2'	57.4, CH	2.99
3	138.6, CH	6.26	3'	71.6, CH	3.63
4	n.d., C	-	4'	77.7, CH	3.76
5	136.6, CH	5.80	5'	64.4, CH_2	4.09 3.32
6	129.2, CH	6.49	1"	98.5, CH	4.79
7	136.2, CH	5.91	2"	47.9, CH_2	2.03 1.80
8	130.1, CH	6.27	3"	n. d., C	-
9	141.2, CH	5.56	4"	76.9, CH	2.98
10	n.d., C	-	5"	67.6, CH	4.06
11	83.3, CH	4.42	6"	20.7, CH_3	1.55
12	129.9, CH	5.47	7"	21.8, CH_3	1.43
13	130.3, CH	6.14	8''	n. d., CH_3	2.65
14	125.8, CH	6.13	9''	n. d., CH_3	2.65
15	138.1, CH	6.24			
16	n.d., C	-			
17	132.8, CH	6.14			
18	124.4, CH	6.34			
19	138.6, CH	6.27			
20	n.d., C	-			
21	n.d., C	5.51			
22	36.2, CH_2	2.47 2.26			
23	53.5, CH	3.86			
24	16.2, CH_3	2.00			
25	22.9, CH_3	1.49			
26	12.8, CH_3	1.72			
27	12.8, CH_3	1.76			
28	28.5, CH_2	1.64			
29	35.3, CH_2	2.49 2.42			
30	35.8, CH	1.42			
31	19.0, CH_3	0.84			
32	30.0, CH_2	1.12			
33	11.4, CH_3	0.87			
34	11.3, CH_3	0.95			
1-NH	-	7.34			

^{13}C chemical shifts obtained from HSQC spectrum. Multiplicities not included due to the poor spectra quality.

Fig. S78. Alignment of the sequences of the structurally characterized spinosyn forosamiyltransferase SpnP [14] with the sequences of SipS14, SipS9 and their respective homologs IdnS14 and IdnS9. The key residues H13, D356 and E357 (highlighted in the red boxes) from SpnP are only found in SipS14 and IdnS14 but not SpnS9 and IdnS9 which thus have no native glycosyl transferase activity but are mere GT auxiliary proteins.

References

1. Malmierca MG, Pérez-Victoria I, Martín J, Reyes F, Méndez C, Olano C, Salas JA. 2018. Cooperative involvement of glycosyltransferases in the transfer of amino sugars during the biosynthesis of the macrolactam sipanmycin by *Streptomyces* sp. strain CS149. Appl Environ Microbiol 84(18):e01462-18. doi: 10.1128/AEM.01462-18.

2. Olano C, Gómez C, Pérez M, Palomino M, Pineda-Lucena A, Carbajo RJ, Braña AF, Méndez C, Salas JA. 2009. Deciphering biosynthesis of the RNA polymerase inhibitor streptolydigin and generation of glycosylated derivatives. Chem Biol 16(10):1031-44. doi: 10.1016/j.chembiol.2009.09.015.

3. Malmierca MG, González-Montes L, Pérez-Victoria I, Sialer C, Braña AF, García Salcedo R, Martín J, Reyes F, Méndez C, Olano C, Salas JA. 2018. Searching for glycosylated natural products in Actinomycetes and identification of novel macrolactams and angucyclines. Front Microbiol 30: 9-39. doi: 10.3389/fmicb.2018.00039.

4. Rix U, Fischer C, Remsing LL, Rohr J. 2002. Modification of post-PKS tailoring steps through combinatorial biosynthesis. Nat Prod Rep 19(5):542-580. doi:10.1039/B103920M.

5. Gheysen K, Mihai C, Conrath K, Martins JC. 2008. Rapid identification of common hexapyranose monosaccharide units by a simple TOCSY matching approach. Chemistry 14: 8869-8878. doi: 10.1002/chem.200801081.

6. Hayakawa Y, Adachi K, Iwakiri T, Imamura K, Furihata K, Seto H, Ōtake N. 1987. Kerriamycins A, B and C, new isotetracenone antibiotics. Agric. Biol. Chem., 51(5): 1397-1405. doi:10.1080/00021369.1987.10868190.

7. Murakami R, Tomikawa T, Shin-ya K, Shinozaki J, Kajiura T, Seto H, Hayakawa Y. 2001. Ammocidin, a new apoptosis inducer in ras-dependent cells from Saccharothrix sp. II. Physico-chemical properties and structure elucidation. J. Antibiot. 54(9): 714-717. doi: 10.7164/antibiotics.54.714.

8. Murakami R, Shinozaki J, Kajiura T, Kozone I, Takagi M, Shin-Ya K, Seto H, Hayakawa Y. 2009. Ammocidins B, C and D, new cytotoxic 20-membered macrolides from Saccharothrix sp. AJ9571. J. Antibiot. 62(3): 123-127. doi: 10.1038/ja.2008.23.

9. Wyche TP, Piotrowski JS, Hou Y, Braun D, Deshpande R, McIlwain S, Ong IM, Myers CL, Guzei IA, Westler WM, Andes DR, Bugni TS. 2014. Forazoline A: marine-derived polyketide with antifungal in vivo efficacy. Angew Chem Int Ed Engl. 54(43): 11583-11586. doi: 10.1002/anie.201405990.

10. Alam P, Barber J, Brennan RJ, Kennedy K, Hassan M, Tehrani H. 1995. ^{1}H and ^{13}C NMR spectra of spiramycin I in organic and aqueous solutions. Magn. Reson. Chem. 33(3): 228-231. doi: 10.1002/mrc.1260330313.

11. Futamura Y, Sawa R, Umezawa Y, Igarashi M, Nakamura H, Hasegawa K, Yamasaki M, Tashiro E, Takahashi Y, Akamatsu Y, Imoto M. 2008. Discovery of incednine as a potent modulator of the anti-apoptotic function of Bcl-xL from microbial origin. J. Am. Chem. Soc. 130(6): 1822-1823. doi: 10.1021/ja710124p.

12. Takaishi M, Kudo F, Eguchi T. 2013. Identification of the incednine biosynthetic gene cluster: characterization of novel β-glutamate-β-decarboxylase IdnL3. J. Antibiot. 66(12): 691-699. doi: 10.1038/ja.2013.76.

13. Cieślak J, Miyanaga A, Takaku R, Takaishi M, Amagai K, Kudo F, Eguchi T. 2017. Biochemical characterization and structural insight into aliphatic β-amino acid adenylation enzymes IdnL1 and CmiS6. Proteins 85(7): 1238-1247. doi: 10.1002/prot.25284.

14. Isiorho EA, Jeon BS, Kim NH, Liu HW, Keatinge-Clay AT. 2014. Structural studies of the spinosyn forosaminyltransferase, SpnP. Biochemistry 54(26): 4292-4301. doi: 10.1021/bi5003629.